1980-03

Stark cell stabilization of a CO(2) laser

Knolhoff, Larry Edward

Monterey, California; Naval Postgraduate School

NAVAL POSTGRADUATE SCHOOL
Monterey, California

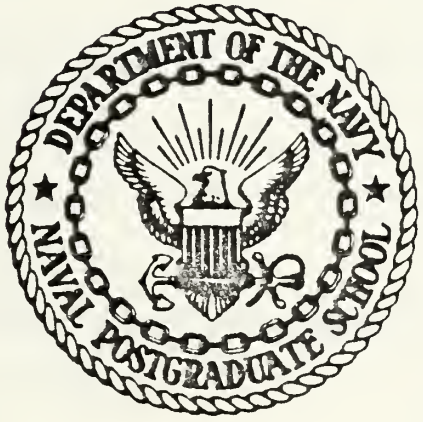

THESIS

STARK CELL STABILIZATION

OF A CO_2 LASER

by

Larry Edward Knolhoff

March 1980

Thesis Advisor: A. W. Cooper

Approved for public release; distribution unlimited.

SECURITY CLASSIFICATION OF THIS PAGE (When Data Entered)

REPORT DOCUMENTATION PAGE

READ INSTRUCTIONS BEFORE COMPLETING FORM

1. REPORT NUMBER

2. GOVT ACCESSION NO.

3. RECIPIENT'S CATALOG NUMBER

4. TITLE (and Subtitle)

STARK CELL STABILIZATION OF A CO_2 LASER

5. TYPE OF REPORT & PERIOD COVERED

Master's Thesis; March 1980

6. PERFORMING ORG. REPORT NUMBER

7. AUTHOR(s)

Larry Edward Knolhoff

8. CONTRACT OR GRANT NUMBER(s)

9. PERFORMING ORGANIZATION NAME AND ADDRESS

Naval Postgraduate School
Monterey, California 93940

10. PROGRAM ELEMENT, PROJECT, TASK AREA & WORK UNIT NUMBERS

11. CONTROLLING OFFICE NAME AND ADDRESS

Naval Postgraduate School
Monterey, California 93940

12. REPORT DATE

March 1980

13. NUMBER OF PAGES

114

14. MONITORING AGENCY NAME & ADDRESS(if different from Controlling Office)

Naval Postgraduate School
Monterey, California 93940

15. SECURITY CLASS. (of this report)

Unclassified

15a. DECLASSIFICATION/DOWNGRADING SCHEDULE

16. DISTRIBUTION STATEMENT (of this Report)

Approved for public release; distribution unlimited.

17. DISTRIBUTION STATEMENT (of the abstract entered in Block 20, if different from Report)

18. SUPPLEMENTARY NOTES

19. KEY WORDS (Continue on reverse side if necessary and identify by block number)

Laser
Stabilization
Stark

20. ABSTRACT (Continue on reverse side if necessary and identify by block number)

Studies have been conducted of the frequency stabilization of the output from a Sylvania 941 Carbon Dioxide laser by active comparison with a Stark-tuned NH_2D line center in an absorption cell. A dithered Stark voltage gave a peak-detection correction signal fed back to a PZT mounted laser resonator mirror to control the cavity optical length. Operation of an integrator incorporated in the feedback

DD FORM 1 JAN 73 1473 EDITION OF 1 NOV 68 IS OBSOLETE
S/N 0102-014-6601

SECURITY CLASSIFICATION OF THIS PAGE (When Data Entered)

loop to improve the system stability has been investigated. A method was demonstrated of using the integrator to locate the desired laser vibronic transition by scanning the laser through its spectral signature prior to initiation of servo operation. An unexpected discontinuity in the absorption lineshape of a Stark-tunable cell was discovered which made the cell unsuitable for generation of the feedback signal. A new and more versatile Stark cell was designed for test and evaluation of cell plate configuration and fabrication.

Approved for public release; distribution unlimited.

STARK CELL STABILIZATION OF A CO_2 LASER

by

Larry Edward Knolhoff
Lieutenant, United States Navy
B.S., Valparaiso Univ., 1972

Submitted in partial fulfillment of the
requirements for the degree of

MASTER OF SCIENCE IN PHYSICS

from the

NAVAL POSTGRADUATE SCHOOL
March 1980

ABSTRACT

Studies have been conducted of the frequency stabilization of the output from a Sylvania 941 Carbon Dioxide laser by active comparison with a Stark-tuned NH_2D line center in an absorption cell. A dithered Stark voltage gave a peak-detection correction signal fed back to a PZT mounted laser resonator mirror to control the cavity optical length. Operation of an integrator incorporated in the feedback loop to improve the system stability has been investigated. A method was demonstrated of using the integrator to locate the desired laser vibronic transition by scanning the laser through its spectral signature prior to initiation of servo operation. An unexpected discontinuity in the absorption lineshape of a Stark-tunable cell was discovered which made the cell unsuitable for generation of the feedback signal. A new and more versatile Stark cell was designed for test and evaluation of cell plate configuration and fabrication.

TABLE OF CONTENTS

I. INTRODUCTION

The Sylvania Model 941 CO_2 Laser to be used in atmospheric extinction studies was determined to have poor beam quality and frequency stability of the laser output. Since the chance of oscillation on a specific vibrational-rotational line is dependent on whether a cavity mode is in resonance with a vibrational-rotational peak, the mechanism used in frequency tuning a CO_2 laser involves varying the cavity mode spacing by changing the cavity length. As the laser is tuned in frequency by changing the mirror separation, competition effects occur and oscillation can switch from one rotational level to another. The fitting of a piezoelectric driver to one of the laser cavity mirrors has made possible the use of active feedback control to frequency stabilize the output.

The use of active stabilization to minimize frequency drift has been approached in a number of ways. It requires a comparison of the laser output frequency with a suitable frequency standard, generating a correction signal to be fed back to the piezoelectric transducer to adjust the laser cavity optical length. Such a signal may be obtained by passing a fraction of the laser output intensity to a suitable detector through an absorption cell containing a suitable absorbing gas. The Stark effect permits tuning an absorption line of NH_2D to oscillate about the desired laser vibronic transition frequency. The detector then

gives a sign-dependent error signal. The ability to generate a discriminant voltage without impressing any modulation on the output and the voltage control of the frequency reference make the Stark cell stabilization technique attractive as a control system.

This thesis describes the continuation of studies of the operation of Stark cell modulation, and the technical requirements for stabilization of a carbon dioxide laser.

II. THEORETICAL

A. CARBON DIOXIDE LASER

1. Lasing States and Spectra of Carbon Dioxide

The quantum states and energy levels on which molecular lasers operate originate from three contributions: i) electronic energy, due to the electronic charge cloud surrounding the nuclei; ii) vibrational energy, due to the motion (vibrations) of the nuclei about their equilibrium positions; and iii) rotational energy, due to the rotational motion of the molecule about various axes in space. Each of these components is quantized. Each widely spaced electronic level is split into a series of more closely spaced vibrational levels. This energy level scheme is shown in Figure 1. Molecular gas lasers exploit transitions between the vibrational-rotational levels of a molecule.

In general, an N-particle system has 3N degrees of freedom. The motion of the center of gravity and the orientation of the axis of a linear XY_2 molecule can be specified in terms of five degrees of freedom, leaving (3N - 5 = 4) four vibrational degrees of freedom. For a linear triatomic symmetric molecule such as CO_2, there are three distinct normal modes of vibration. The four vibrations correspond to the symmetric stretch mode, the doubly degenerate bending mode and the asymmetric stretching mode. These modes are shown in Figure 2. In a) the symmetric stretch mode, the oxygen atoms vibrate along the internuclear axis

GENERAL STRUCTURE OF MOLECULAR ENERGY LEVELS

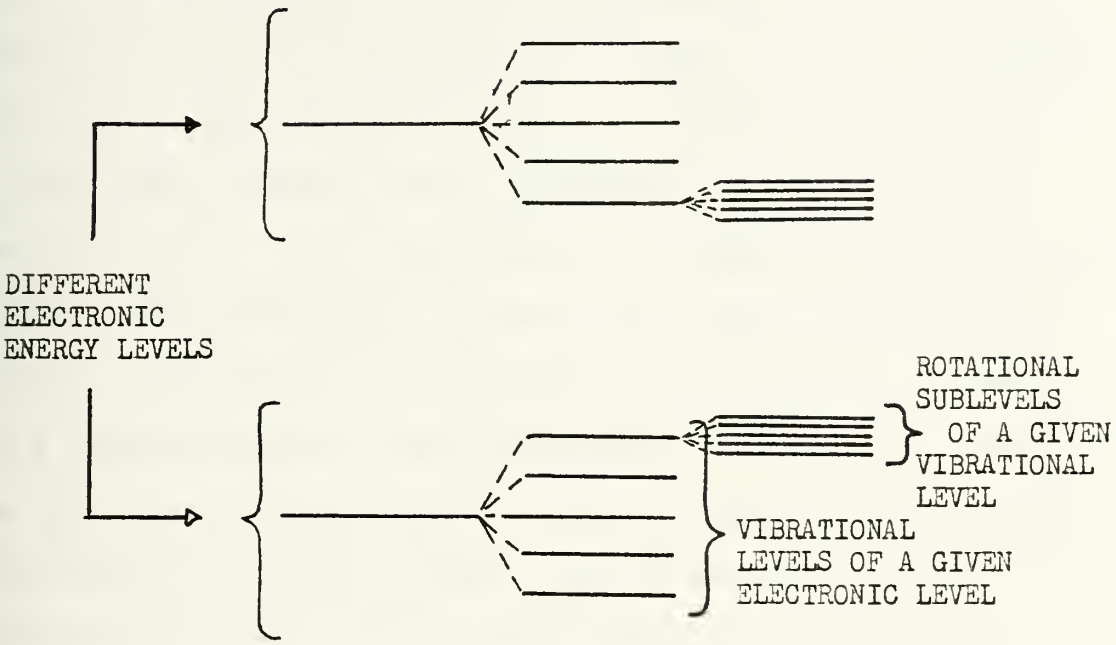

FIGURE 1

VIBRATIONAL MOTIONS OF THE CO_2 MOLECULE

a) 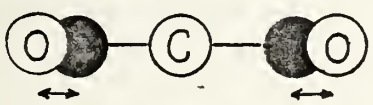 $\tilde{\nu}_1 = 1337\ cm^{-1}$ v_1 SYMMETRIC NO ELECTRIC DIPOLE MOMENT

b)  $\tilde{\nu}_2 = 667\ cm^{-1}$ v_2^{ℓ} ASYMMETRIC DIPOLE MOMENT TWOFOLD DEGENERATE I.R. ACTIVE

c) 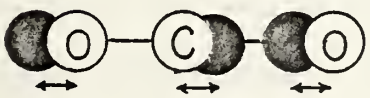 $\tilde{\nu}_3 = 2349\ cm^{-1}$ v_3 ASYMMETRIC DIPOLE MOMENT I.R. ACTIVE

TOTAL QUANTUM NUMBER $[v_1, v_2^{\ell}, v_3]$

FIGURE 2

in a symmetric manner. In b) the bending mode, the atoms vibrate symmetrically in a direction perpendicular to the internuclear axis. The bending mode has a two-fold degeneracy which arises from the equivalence of vibration in either of two orthogonal planes whose intersection lies along the molecular axis. In c) the asymmetric mode, the atoms vibrate asymmetrically along the internuclear axis. Since carbon dioxide is symmetrical in its equilibrium state it does not have a dipole moment. The symmetrical stretching vibration does not create a net electric dipole moment and therefore is not active in the infrared. The asymmetric normal vibrations produce a dipole moment and are I.R. active. The stretching vibrations have higher frequencies than the bending vibrations since the restoring force is greater in stretching a molecule than in bending.

The CO_2 molecule vibrational quantum state can be described by a set of quantum numbers written as

$$\left[v_1,\ v_2^{\ell},\ v_3\right]$$

where v is the degree of excitation of each of the three individual normal modes. The degenerate bending vibration mode for CO_2 has an associated angular momentum which depends upon the excitation and relative phase of the orthogonal vibrations. This angular momentum is denoted by the quantum number ℓ appearing above v_2. The superscript ℓ takes the value $\ell = v_2,\ v_2 - 2, \ldots,\ 1,\ 0$, with each giving rise to a sublevel.

Assuming independence of the three normal modes, and the use of normal coordinates in describing the molecular vibrations, allows the separation of the Schrödinger equation into as many separate equations as there are normal modes. The eigenvalues for each of the separate equations are given by

$$E_i = (v_i + \tfrac{1}{2})\ hc\tilde{\nu}_i \qquad (1)$$

where v_i is the quantum number associated with the i^{th} mode, and the total vibrational energy associated with an $\left[v_1,\ v_2^{\ell},\ v_3\right]$ state is approximately

$$E_v = (v_1 + \tfrac{1}{2})\ hc\tilde{\nu}_1 + (v_2 + \tfrac{1}{2})\ hc\tilde{\nu}_2 + (v_3 + \tfrac{1}{2})\ hc\tilde{\nu}_3 \qquad (2)$$

where $\tilde{\nu}$ is the frequency in wave number units associated with the normal modes of vibration.

The carbon dioxide vibrational energy levels of principal interest in laser action with their modes and frequencies are

1)	$\left[00^{0}1\right]$	Asymmetric Stretch, Σ_u^+	2349.3 cm^{-1}
2)	$\left[10^{0}0\right]$	Symmetric Stretch	1388.3 cm^{-1}
3)	$\left[02^{0}0\right]$	Bending, Σ_g^+	1285.5 cm^{-1}
4)	$\left[01^{1}0\right]$	Bending	667.3 cm^{-1}

The two vibrational levels $[10^{\circ}0]$ and $[02^{\circ}0]$ belonging to different vibrational modes have nearly the same energy and are in Fermi resonance. When the interaction between them is included as a perturbation, the wave functions are mixed and the resulting pair of mixed levels are repelled, so that the level separation is greater than expected.

The lower vibrational energy level diagram for the CO_2 molecule in conjunction with the N_2 molecule is shown in Figure 3. The dashed lines indicate radiative transitions that are allowed by electric dipole considerations. The Σ and Π notation represents the electronic-vibrational angular momentum of the molecule ($\Sigma=0, \Pi=1$), giving the value of the vector sum of the electronic orbital angular momentum and vibrational angular momentum about the internuclear axis. The + superscript implies that the vibronic eigenfunction is unchanged when reflected at any plane containing all the nuclei. the subscripts indicate whether the state is u, antisymmetric (odd symmetry) or g, symmetric (even symmetry) with respect to vibrational motion. [Ref. 1]

For every vibrational state there exists a distinct set of rotational levels with slightly different spacing for different vibrational levels. The CO_2 molecule can rotate about any axis normal to the internuclear axis. From quantum theory of rotational spectra and angular momentum the energy level due to rotational motion is given by

$$E_R(J) = BJ(J+1) = \frac{h}{8\pi^2 cI} J(J+1) \qquad (3)$$

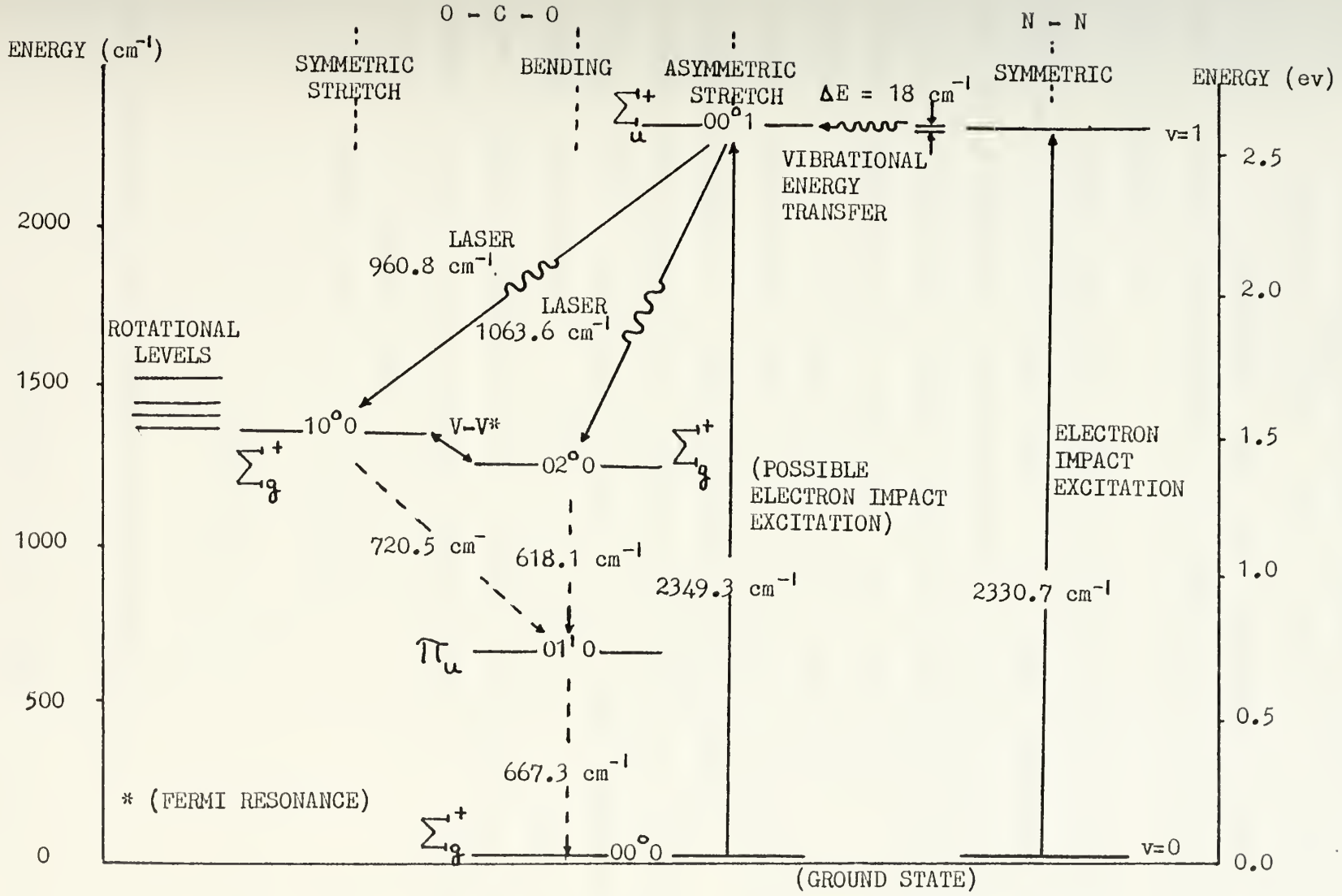

FIGURE 3 LOWEST VIBRATIONAL LEVELS OF CO_2 AND N_2

where J is the angular momentum quantum number (J = 1, 2,...), I is the moment of inertia, and B is called the rotational constant. The selection rule for J for dipole transitions of CO_2 allows only transitions between rotational levels for which $\Delta J = \pm 1$.

Laser action for carbon dioxide occurs on transitions between two vibrational levels of the same electronic state or more precisely, transitions between rotational levels of the two vibrational states (vibration-rotational transitions). These transitions are classified into "branches" by the change in J. Transitions between two vibrational levels v and v' with account taken for the rotational splitting are shown in Figure 4. The transition, in the absence of rotational energy, would consist of a single line centered at ν_o, called the Q branch where $\Delta J = 0$. Including rotational energy the transition actually consists of two groups of lines: the P branch corresponding to a change in rotational quantum number of $\Delta J = +1$ and R branch corresponding to a change in rotational quantum number of $\Delta J = -1$.

Solving for ν in the equation

$$\Delta E = h\nu \tag{4}$$

and defining ν_o as the band center frequency or

$$\nu_o = \frac{1}{h} \left[E_v\ (0) - E_{v'}(0)\right] \tag{5}$$

the transition frequencies can be written as

$$\begin{aligned} \nu &\cong \nu_o - (2B/h)J && P(J+1)\ \text{Branch} \\ \nu_o &\cong \nu_o && Q\ \text{Branch} \\ \nu &\cong \nu_o + (2B/h)J && R(J-1)\ \text{Branch} \end{aligned} \qquad (6)$$

where J is the rotational quantum number of the lower level. The rotational levels of a linear molecule are positive or negative depending on whether the sign of the total eigenfunction

$$\psi_T = \psi_e \psi_r \psi_v \qquad (7)$$

remains unchanged or changed upon an inversion.

The infrared selection rules for the vibrational-rotational transitions relevant to CO_2 are [Ref. 2]

$$\begin{aligned} &\Delta v = \pm 1 \\ &\Delta \ell = 0, \pm 1; \quad g \not\leftrightarrow g; \quad u \not\leftrightarrow u \\ &\Delta J = 0, \pm 1; \quad + \leftrightarrow +; \quad s \not\leftrightarrow a \quad (J=0) \not\leftrightarrow (J=0) \end{aligned} \qquad (8)$$

where s and a designate the symmetric and antisymmetric total rotational eigenfunction ψ_r and the symbols $\leftrightarrow$ and $\not\leftrightarrow$ represent allowed and not allowed respectively. In all symmetric excited vibrational levels (Σ^+) the even rotational levels are positive and the odd are negative with respect to inversion along the molecular axis while the converse is true for the antisymmetric levels (Σ^-). For the Π, Δ ... doubly

degenerate vibrational levels, for each J there is a positive and negative level with alternating order (+-, -+, +-, -+,... or -+, +-, -+, +-,...).

Because CO_2 is exactly symmetric and is without nuclear spin the Q branch or $\Delta J = 0$ transition is strictly forbidden by symmetry restrictions ($\Sigma \longleftrightarrow \Sigma$, $\Delta J \neq 0$). J to $J \pm 1$ transitions within a single vibrational energy level are also forbidden. Since the two oxygen atoms are spinless, symmetrically located indistinguishable particles and the CO_2 wave function remains unchanged, the system obeys Bose-Einstein statistics. Therefore all CO_2 g states have rotational levels with even J values only, while all u states have only odd J values. The absence of alternating rotational levels causes the spacing between adjacent lines to be twice that expected on the basis of the size of the molecular rotational constant B. This spacing is 4B instead of 2B. Experimental evidence shows that only the even J values appear in CO_2 P- and R-branch spectra. The $^{12}C^{16}O_2$ system can oscillate on approximately one hundred transitions spanning the wavelength range from 9.1 to 10.7μm. They occur on the P(J) and R(J) branches of both the $00^{\circ}1 \longleftrightarrow 10^{\circ}0$ and $00^{\circ}1 \longleftrightarrow 02^{\circ}0$ rotational-vibrational bands. A detailed laser transition diagram for the $00^{\circ}1$ - $10^{\circ}0$ and $00^{\circ}1$ - $02^{\circ}0$ bands including some rotational levels is shown in Figure 5 and some of the P- and R-branch transitions for the $00^{\circ}1$ - $10^{\circ}0$ vibration-rotation levels with their corresponding transition wavelengths and frequencies are given in Table I. [Ref. 3]

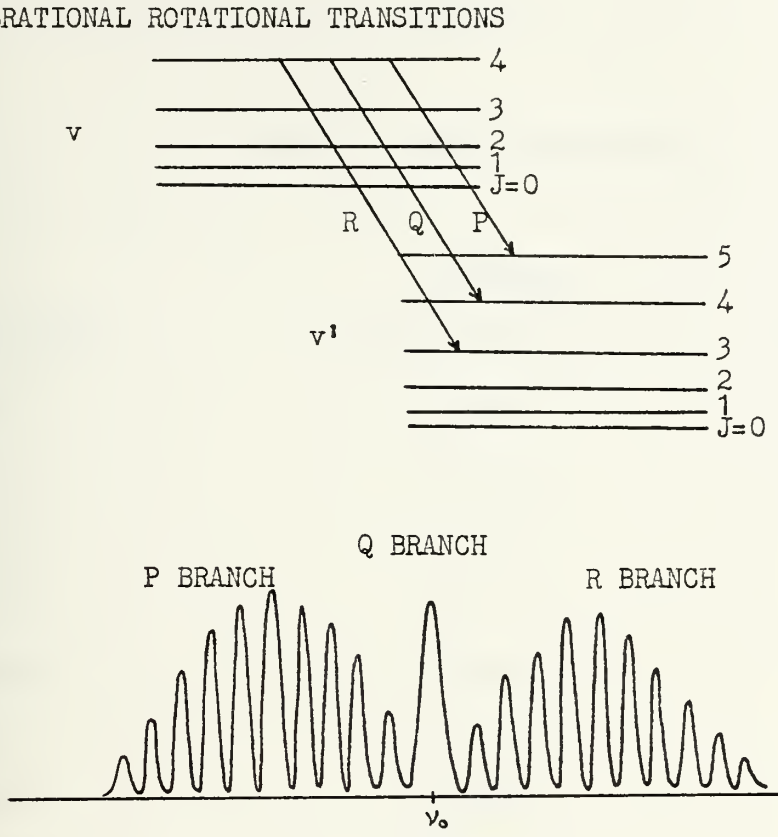

FIGURE 4

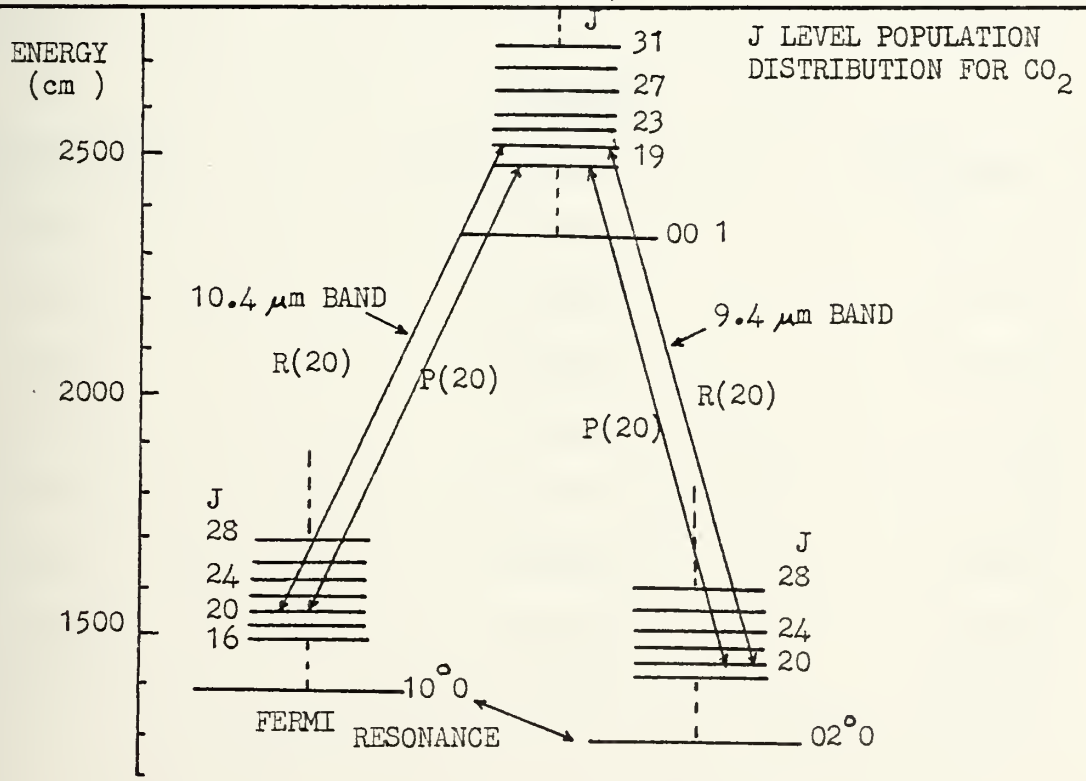

FIGURE 5

TABLE I

$00^{\circ}1 - 10^{\circ}0$ TRANSITION

P BRANCH

TRANSITION	WAVELENGTH (m)	FREQUENCY (cm^{-1})
P(14)	10.5326	949.43
P(16)	10.5518	947.70
P(18)	10.5713	945.96
P(20)	10.5912	944.18
P(22)	10.6118	942.35
P(24)	10.6324	940.52
P(26)	10.6534	938.67
P(28)	10.6748	936.78

R BRANCH

TRANSITION	WAVELENGTH (m)	FREQUENCY (cm^{-1})
R(14)	10.2860	971.91
R(16)	10.2855	972.24
R(18)	10.2605	974.61
R(20)	10.2470	975.90
R(22)	10.2335	977.18
R(24)	10.2200	978.47
R(26)	10.2075	979.67
R(28)	10.1950	980.87

2. Excitation Mechanism

Electrical pumping in a gas laser is achieved by allowing a current to pass through the gas producing ions and free electrons. The average electron energy and the ability of an electron to excite a neutral molecule by collision is much greater than the ion energy. The equilibrium condition established among the electrons can be described by an effective electron temperature T_e. Assuming a Maxwellian energy distribution, and that for each collision some fraction δ of the electron energy is lost, the effective electron temperature is given by [Ref. 4]

$$T_e = \frac{e}{(2\delta)^{1/2} k} (E\ell) \qquad (9)$$

where E is the applied electric field, k is Boltzmann's constant, e is the elementary charge on an electron, and ℓ is the electron mean free path. Since the mean free path is

$$\ell = \frac{kT}{\sqrt{2}\pi\sigma^2 P} \qquad (10)$$

with $\pi\sigma^2$ the collision cross section and P the pressure, T_e can be given as a function of the ratio E/P. The ratio of applied electric field to pressure is used as a parameter in describing the discharge condition.

The primary electrical pumping mechanisms for a gas are: i) excitation by electron impact or a collision of the first king represented by the equation

$$A + (e + KE) \longrightarrow A^* + e \qquad (11)$$

where * represents the excited state of A, and KE the translational kinetic energy converted to excitation energy. ii) Excitation by collision between atoms or molecules of different species (resonant energy transfer) characterized by the equation

$$A + B^* \longrightarrow A^* + B + KE \qquad (12)$$

where A* and B* are the excited states. This type of excitation process is called a collision of the second kind.

Selective excitation of polyatomic molecules through vibrational energy transfer from a diatomic molecule has been used effectively in the production of population inversion on vibrational-rotational transitions of the polyatomic molecule. For the N_2 - CO_2 system shown in Figure 3, the $[00^{\circ}1]$ level of carbon dioxide is chiefly excited by a resonant energy transfer via collisions of the second kind between CO_2 molecules in the ground state and N_2 molecules in the excited state. As a result of these resonant collisions the populations of certain sets of levels are very strongly coupled so that they act essentially as a single level. The vibrationally excited N_2 molecules in the ground electronic state N_2^* (v = 1) are produced primarily by indirect electron impact excitation. The pump rate R_p of the upper state is

$$R_p = N_e \langle v\sigma \rangle \qquad (13)$$

where

$$\langle v\sigma \rangle = \int v\,\sigma(E)\,f(E)\,dE \qquad (14)$$

N_e is the electron density, V is the electron velocity, f(E) is the electron energy distribution and $\sigma(E)$ is electron excitation cross section. [Ref. 5] The cross section for electron impact excitation of N_2 in the ground state is very high making substantial population densities of N_2^* (v =1) achievable. Figure 6 shows the total electron excitation cross section of the N_2 levels as a function of electron energy with the cross section reaching a maximum value of approximately 3 X $10^{-16}cm^2$ at an electron energy of 2.3ev. [Ref. 6] The vibrationally excited nitrogen molecule in the ground electronic state cannot decay through electric dipole radiation back to the ground state (v = 1 to v = 0) since N_2 is a diatomic homonuclear molecule with no permanent dipole moment. The energy difference E between the N_2^* (v = 1) and CO_2 $[00^o1]$ energy levels is about $18cm^{-1}$. This is negligible in comparison with the average thermal energy kT at room temperature of $210cm^{-1}$. The near resonance molecule - molecule collision leading to energy transfer can be written as

$$N_2^* (v=1) + CO_2 [00^o0] \text{ --- } N_2 (v=0) + CO_2 [00^o1] - 18cm^{-1} \qquad (15)$$

This resonance transfer produces a mixed state in which the combined populations of N_2^* (v = 1) and CO_2 $[00^\circ 1]$ are essentially in equilibrium: this effect increases the effective lifetime of CO_2 $[00^\circ 1]$. The transfer cross section is largely due to the negligible difference between the energy levels. The level $[10^\circ 0]$ (or $[02^\circ 0]$) is more than $900cm^{-1}$ from N_2^* (v = 1) and the transfer cross section is small compared to that for the reaction in (15).

To a lesser degree excitation can occur by direct electron impact on the ground state CO_2 molecule $[00^\circ 0]$ and by resonant exchange of energy between CO molecules in excited levels and CO_2 in the ground state. Electron impact on the ground state CO_2 molecules results in excitation of the CO_2 molecule to the $[00^\circ 1]$ level since the transition to Σ_u^+ $[00^\circ 1]$ is optically connected to the ground state Σ_g^+ $[00^\circ 0]$ and is given by

$$CO_2\left[\Sigma_g^+,\ 00^\circ 0\right] + (e + KE) \text{ --- } CO_2\left[\Sigma_u^+,\ 00^\circ 1\right] + e \qquad (16)$$

The cross section for vibrational excitation of CO_2 by electron impact is shown in Figure 7. [Ref. 7]

A substantial amount of CO (10% of CO_2 pressure) can be produced as a result of dissociation of CO_2 in a discharge. The electron excitation cross sections for CO are reported in Reference 8 to be similar in form to that of N_2 but shifted to lower energies with the peak value for the total cross section being approximately $8 \times 10^{-16} cm^2$

at 1.8 ev. The difference between the first CO vibrational energy level and the upper laser level of CO_2 is given as $170cm^{-1}$. These final two mechanisms account for the possibility of producing a population inversion in a pure CO_2 laser.

Normally the CO_2 oscillator functions with a plasma that consists of a CO_2 - N_2 - He mixture. The helium component plays two important roles. The first is related to the increased rate of relaxation of the $[01^10]$ level. By reducing the bending mode population which in turn reflects itself in a reduction of the lower laser level populations the gain is increased. Helium also reduces the kinetic and rotational temperature of the CO_2 in the plasma. This will also increase the gain, since the same total upper-state population is now distributed among fewer levels.

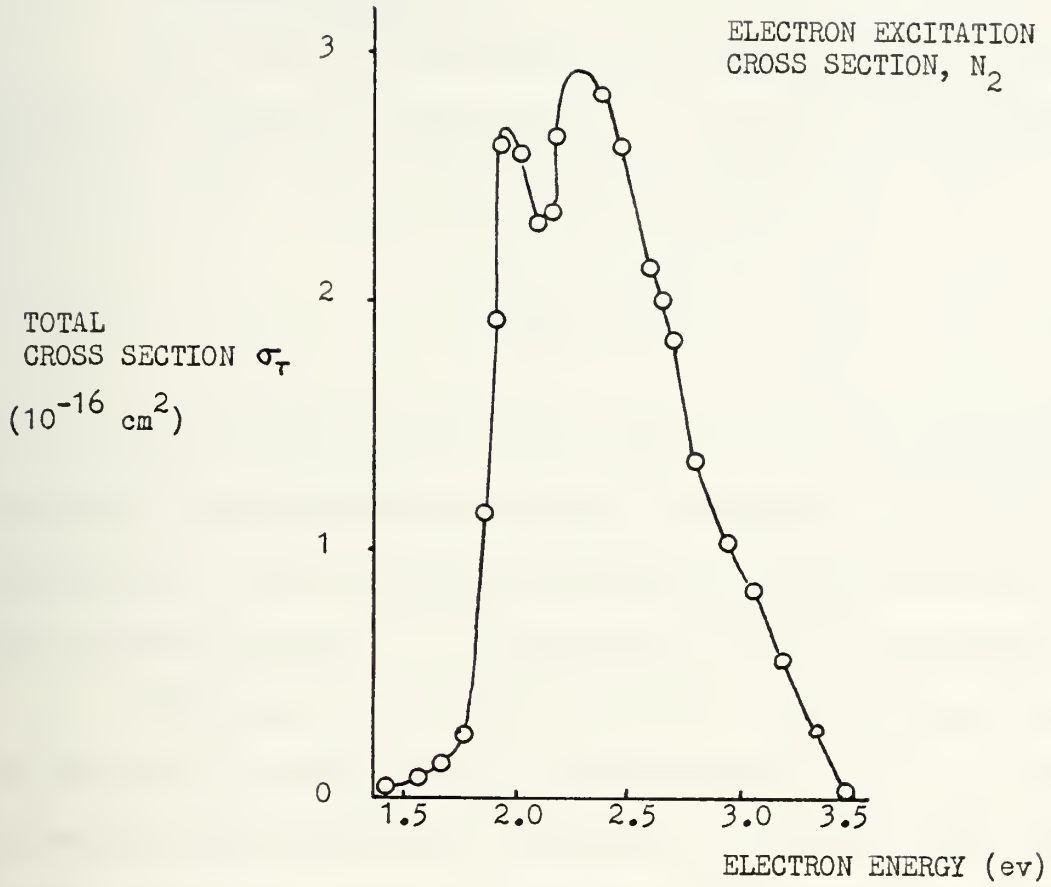

FIGURE 6

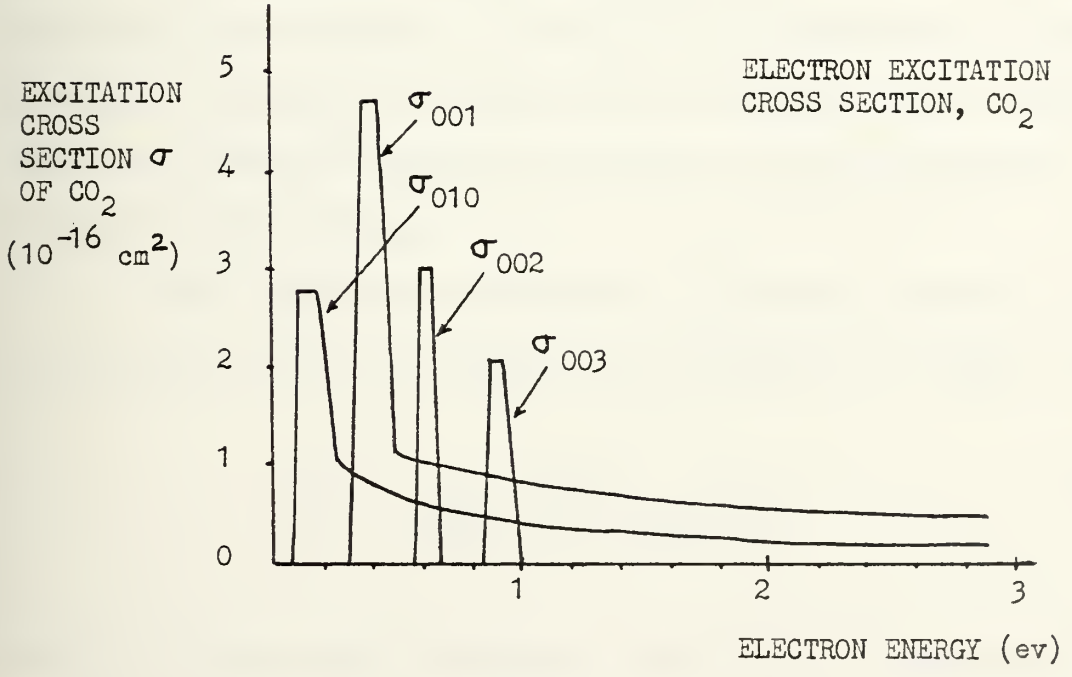

FIGURE 7

3. Lineshape Function

The function describing the distribution of emitted intensity versus the frequency, ν, is called the lineshape function, $g(\nu)$ and is normalized according to

$$\int_{-\infty}^{\infty} g(\nu)\, d\nu = 1 \qquad (17)$$

The frequency spectrum and $g(\nu)$ are the same for purposes of spontaneous emission, stimulated emission and absorption. Line broadening mechanisms may be divided into two classifications: i) homogeneous and ii) inhomogeneous.

Homogeneous broadening involves the spectral spread of the whole system caused by the broadening of the spectrum of each indistinguishable molecule. It is due most often to the finite collisional lifetime of excited molecules and the consequent interruption of the radiative process. The result of frequent collisions is the presence of many truncated radiative or absorptive processes with a line-width of radiation greater than that of an individual uninterrupted process.

The normalized Lorentzian lineshape function which is characteristic of homogeneous broadening is [Ref. 9]

$$g(\nu) = \frac{\Delta\nu_L}{2\pi\left[(\nu-\nu_0)^2 + (\Delta\nu_L/2)^2\right]} \qquad (18)$$

Here ν_0 is the center frequency and $\Delta\nu_L$ is the separation between the two frequencies at which the Lorentzian is down to half

its peak value, or the full width at half maximum.

The linewidth $\Delta\nu_L$ is related to the finite lifetime τ of the emitting state by

$$\Delta\nu_L = \frac{1}{\pi\tau} = \frac{1}{\pi g(\nu_0)} \tag{19}$$

The Lorentzian linewidth is pressure dependent since the frequency of collisions is proportional to the density of the gas. The time interval between collisions can be approximated by the ratio of the mean free path (10) to the mean thermal velocity $\bar{v}$

$$\bar{v} = \left(\frac{8kT}{\pi M} \right)^{\frac{1}{2}} \tag{20}$$

and

$$\tau_c \cong \frac{(MkT)^{\frac{1}{2}}}{(16\pi)^{\frac{1}{2}} Pa} \tag{21}$$

where M is the mass of the molecule. Since τ_c is inversely proportional to the pressure P, the linewidth $\Delta\nu$ is proportional to the pressure.

Inhomogeneous broadening is due to the spread in the individual transition frequencies of the molecules and not the broadening of the lines of the individual molecules. The thermal motion of the gaseous molecules is the cause of Doppler broadening. The transition frequency ν is Doppler shifted due to the finite velocity of the molecule.

Using the Maxwell velocity distribution function of a gas, the normalized Doppler broadened lineshape function for inhomogeneous broadening is Gaussian and given in Reference 10 as

$$g(\nu) = \frac{c}{\nu_o} \frac{M}{2\pi kT}^{\frac{1}{2}} \exp\left[-(M/2kT)(c^2/\nu_o^2)(\nu - \nu_o)^2\right] \qquad (22)$$

where M is the molecular mass at equilibrium at temperature T, and ν_o is the resonant frequency.

The linewidth obtained from (22) is

$$\Delta\nu_D = 2\nu_o \left[2kT \ln 2 / Mc^2\right]^{\frac{1}{2}} \qquad (23)$$

and reexpressing $g(\nu)$ in terms of $\Delta\nu_D$ gives

$$g(\nu) = \frac{2(\ln 2)^{\frac{1}{2}}}{\pi^{\frac{1}{2}} \Delta\nu_D} \operatorname{Exp}\left[-4(\ln 2)(\nu-\nu_o)^2 / \Delta\nu_D^2\right] \qquad (24)$$

For a carbon dioxide laser Doppler broadening dominates at low pressure giving a Gaussian line, and pressure (collisional) broadening dominates at high pressures giving a Lorentzian line. In general, the overall broadening is due to a combination of effects and mechanisms and is given by a convolution of the various processes. The overall lineshape (g_o) of two broadening mechanisms, one homogeneous (g_1) and the other inhomogeneous (g_2), may be written as

$$g_o(\nu) = \int_{-\infty}^{\infty} g_1(\nu-\nu') g_2(\nu')\, d\nu' \qquad (25)$$

The convolution of a single Lorentzian line with a single Gaussian in (25) gives a Voigt profile. [Ref. 11] If both Doppler and collision widths are appreciable, the total line width can be approximated by [Ref. 12]

$$\Delta\nu \cong \left[\Delta\nu^2_{\text{Doppler}} + \Delta\nu^2_{\text{collision}}\right]^{\frac{1}{2}} \qquad (26)$$

Figure 8 (a) and 8 (b) shows a general comparison of Lorentzian, Gaussian, and Voigt lineshapes. In 8 (b) the lineshapes were normalized so that $g(o) = 1$ and in 8 (a) the curves were drawn with equal linewidths. The Voigt profile was calculated numerically on a Hewlett-Packard 9810A calculator using (18) and (24) in (25). The program used was a slightly modified version of the one found in Reference 13.

COMPARISON OF THE LORENTZIAN, GAUSSIAN AND VOIGT LINESHAPE FUNCTIONS

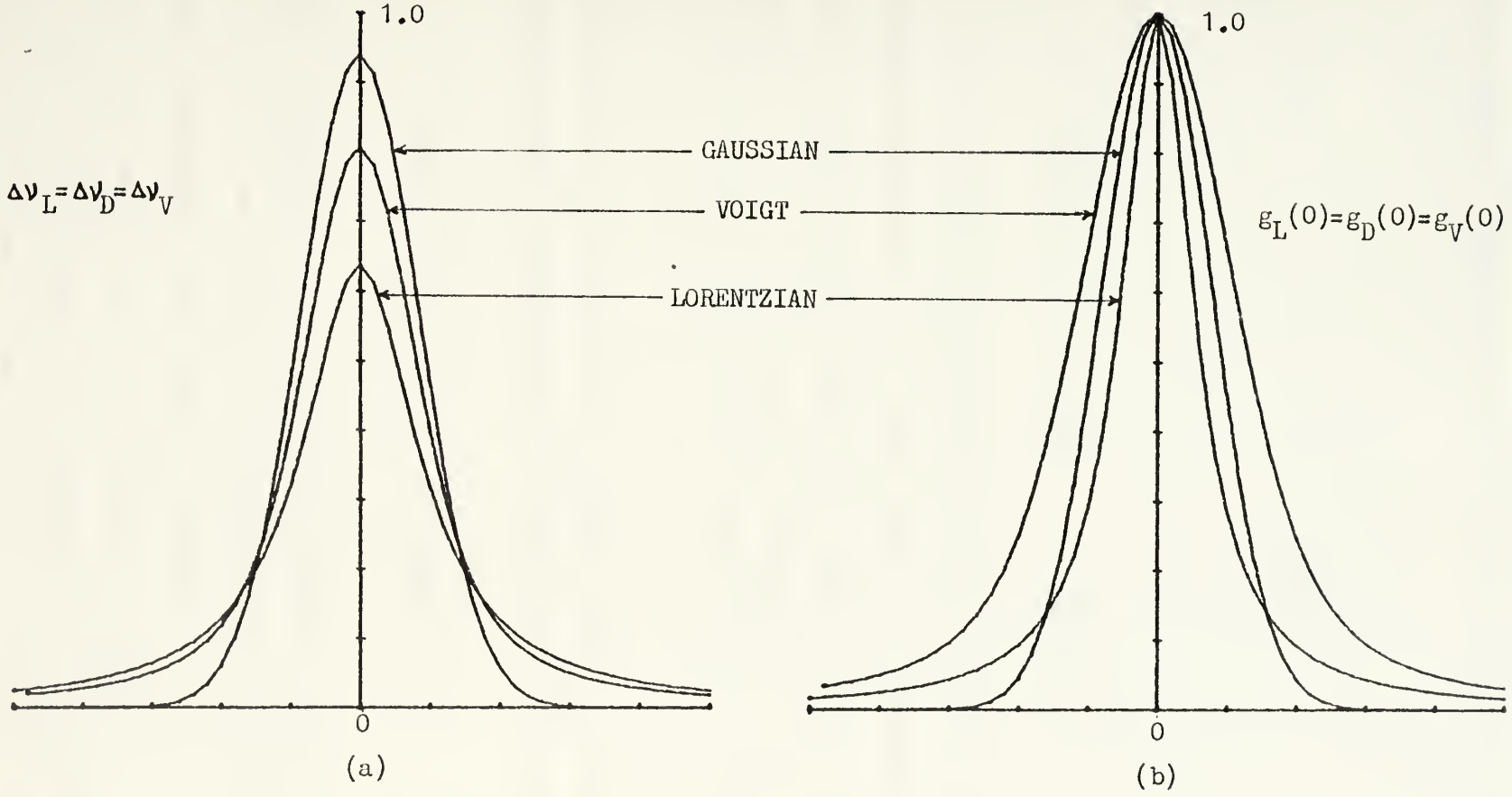

FIGURE 8

4. Laser Modes and Spacing

The general expression for a laser resonator cavity resonant frequency is given by

$$\nu_{q\ell m} = q + (1 + \ell + m)\, f\, \frac{c}{2L\eta} \qquad (27)$$

where

$$f = \frac{1}{\pi} \cos^{-1} \left[\left(1 - \frac{L}{R_1}\right) \left(1 - \frac{L}{R_2}\right) \right]^{\frac{1}{2}}$$

R_1 and R_2 are the radii of curvature of the two laser mirrors separated by a distance L, η is the index of refraction of the medium, ℓ and m are the transverse mode numbers with values of 0, 1, 2,..., and q is the longitudinal mode number which is equal to the number of half wavelengths in the distance L.

From (27) the separation between laser oscillation frequencies in the longitudinal (or Axial) mode for $\Delta q=1$ is

$$\Delta\nu_q = \nu_{(q+1)} - \nu_q = c/2\eta L \qquad (28)$$

If the gain linewidth of the medium is greater than or equal to the axial mode frequency spacing $\Delta\nu_q$, several longitudinal modes may oscillate at a time.

For each value of q but different values of $\ell + m$ there is a set of transverse mode frequencies falling between those which result from a change of the longitudinal mode

index q. The frequency separation between adjacent transverse modes is

$$\Delta\nu_{\ell+m} = \nu_{\ell+m+1} - \nu_{\ell+m} = f\,\frac{c}{2\eta L} \qquad (29)$$

In most applications of gas lasers, operation in the lowest order ($\ell = m = 0$) or fundamental transverse mode is desired. This can be accomplished by inserting into the laser cavity a circular aperture of size such that it passes the fundamental mode with little loss but blocks much of higher order transverse modes which extend further from the optic axis. Typical gas lasers tend to operate in the fundamental transverse mode because of the aperture represented by the discharge tube.

For the case of a resonator with mirror reflectivities ρ_1 and ρ_2, an average distributed loss constant α and the average loss per pass equal to $\alpha L - \ln(\rho_1 \rho_2)^{\frac{1}{2}}$ the passive resonator linewidth is given by [Ref. 14]

$$\Delta\nu_c = \frac{c\left[\alpha - \frac{1}{L}\ln(\rho_1 \rho_2)^{\frac{1}{2}}\right]}{2\pi\eta} = \frac{c\,(1 - R)}{2\pi\eta\, L} \qquad (30)$$

where in the approximation $R = (\rho_1 \rho_2)^{\frac{1}{2}} \cong 1$ and $\alpha = 0$.

In general the passive cavity resonance frequency ν_c does not coincide with the molecular line center frequency ν_o, resulting in the oscillation at a frequency near ν_c but shifted slightly toward ν_o. This effect is called frequency pulling and is due to a shift in the index of

refraction near molecular resonance. The atomic dispersion "pulls" the laser oscillation frequency ν from the passive resonator value toward that of the atomic resonance ν_o. The frequency of oscillation for a high Q resonator cavity is given by

$$\nu = \nu_c - (\nu_c - \nu_o) \frac{\Delta\nu_c}{\Delta\nu} \tag{31}$$

where $\Delta\nu$ is the total molecular linewidth due to Doppler and pressure broadening.

For operation in the lowest order transverse mode where $\ell = m = 0$ (27) becomes

$$\nu_q = [q + f] \frac{c}{2\eta L} = \nu_c \tag{32}$$

Substitution of (30) and (32) into (31) gives for the frequency of oscillation

$$\nu = [q + f] \frac{c}{2\eta L} - \left[\frac{(q+f)\, c^2\, (1-R)}{4\pi\eta^2\, L^2} - \frac{\nu_o\, c\, (1-R)}{2\pi\eta\, L} \right] \frac{1}{\Delta\nu} \tag{33}$$

Equation (33) shows that the laser oscillation frequency may be tuned by changing the cavity length. This is the fundamental means of stabilization techniques using a piezoelectric driven mirror in the cavity.

5. Frequency Instabilities and Causes

The condition for stable resonator operation is given by the condition

$$0 \leq (1 - {}^{L}/_{R_1})\ (1 - {}^{L}/_{R_2}) \leq 1 \qquad (34)$$

The change in laser frequency due to the change in cavity length is given by [Ref. 15]

$$d\nu = -\nu \frac{dL}{L} \qquad (35)$$

For a system where the cavity mirrors are fixed to a cavity structure with a coefficient of expansion, α_{eff}, the change in cavity temperature ΔT can change the length of the cavity resonator and thus the laser frequency by

$$\frac{\Delta\nu}{\nu} = -\frac{dL}{L} = -\alpha_{eff}\,\Delta T \qquad (36)$$

Therefore changes in ambient temperature and acoustic vibrations in the cavity which modulate the cavity length are sources of instability which can contribute to both long and short term drifts in the cavity resonance frequency.

The oscillation frequency of a CO_2 laser can also change by varying functions in the operating parameters such as pressure and discharge current. Mocker in Reference 16 reported a 5 - 8 MHz/torr downshift in frequency due to an increase in pressure and a .5 - .9 MHz/torr upshift in

frequency due to an increase in discharge current. He concluded that the pressure dependent frequency shift is caused by a change in the overall index of refraction of the gas discharge and the current dependent frequency shift is attributed to the change in the index of refraction caused by the change in the electron density of the plasma. In a CO_2 gas discharge the refractive index η is determined by all constituents in the plasma such as the neutral molecules and electrons: [Ref. 17]

$$\eta = 1 - \tfrac{1}{2} \frac{\eta_e e^2}{M_e \epsilon_o \omega^2} + 2\pi \alpha_m \eta_m \qquad (37)$$

Where η_e and M_e are the electron density and mass respectively: η_m and α_m are the density and polarizability of the neutral molecules respectively. A significant reduction of the refractive index may arise from dissociation of CO_2 molecules into components with a smaller electric permittivity.

Therefore it is important to operate a CO_2 laser with a well regulated low ripple power supply and closely controlled gas pressure and temperature.

The frequency deviation $\Delta\nu$ from the resonant frequency ν is therefore determined by the fluctuation in the refractive index $\Delta\eta$ and cavity length ΔL and is given by

$$\frac{\Delta\nu}{\nu} = \frac{\Delta L}{L} + \frac{\Delta\eta}{\eta} \qquad (38)$$

For a sealed CO_2 laser the pressure fluctuations are negligible and the temperature and flow rate of cooling water are the dominant causes of instability in the laser.

B. FREQUENCY TUNING MECHANISM

By bringing a cavity mode into resonance with a vibrational-rotational peak a CO_2 laser can be tuned to a vibrational-rotational line. The cavity mode spacing $\delta\nu_c$ of a single mode TEM_{ooq} laser dictates the chance of oscillation on a specific rotational level and changes as the cavity mirror separation is varied. The optical length of the Model 941 laser cavity is 45 cm, short enough to ensure single axial-mode operation and give a value for $\delta\nu_c = \nu_q - \nu_{q+1} = c/2L$ of 333MHz. The cavity linewidth calculated from (30) with $\alpha = 0$ and using the reflectivities given by Sylvania for the cavity mirrors, $\rho_1 = 1.0$ and $\rho_2 = .70$ is 19MHz. Each vibrational-rotational transition is lineshape broadened with a linewidth $\Delta\nu$. From (23) the Doppler-broadened linewidth for the CO_2 transitions is approximately 50MHz. For the pressures and mixtures used in single transverse mode (small bore diameter) CO_2 lasers (15 - 20 Torr) the Lorentzian pressure broadening $\Delta\nu_L$ can exceed the Doppler broadening. The value listed by Sylvania for $\Delta\nu_L$ is 100MHz giving a total linewidth using (26) of 112MHz. The absolute frequency separation of the vibrational-rotational lines $\Delta\nu_{v-R}$ is between 52 and 57GHz depending on the J number of the transition. Figure 9, although not drawn to scale, shows three P(J) lines and a set of cavity modes showing the frequency spacing involved. The successive order of the transitions is dictated by the absolute cavity length;

they occur in an arbitrary fashion giving each laser its own spectral signature.

As a CO_2 laser is tuned in frequency by changing the cavity length, competition effects occur and oscillation switches from one rotational line to another. In the interrotational level competition region, two rotational levels compete for the total population of the same and higher vibrational levels. Mocker [Ref. 18] reported that the competition effects are due to intensity-dependent anomalous dispersion arising from index and gain saturation and that the switching from one rotational level to an adjacent level occurs over a small finite frequency interval.

While the laser oscillates on a given vibrational-rotational transition the population density or the population inversion on that particular transition is reduced by saturation effects until the single pass gain in the medium equals the single pass loss of the optical cavity. If the vibrational level lifetime (typical values 1 - 10msec) is considerably longer than the rotational relaxation time ($< 1\,\mu$sec) a Boltzmann distribution will describe the population density of the various rotational levels at the same temperature. Therefore if the gain on the oscillating transition is the highest the gain on the non-oscillating vibrational-rotational transitions starting from other rotational levels in the vibrational level will be less than the single-pass loss of the optical cavity. This means that once the laser transition starts

oscillating, the gain on the other transitions falls below that required for laser oscillation with the other rotational levels coupling (due to collisions) their stored energy into the lasing transition and only one transition oscillates. This is the situation of very strong competition effects. As the cavity mode is tuned away from the center of the lasing transition a point is reached where another transition has equal gain and a competition will be initiated. The intensity dependent dispersion represents a frequency pulling term such that a cavity resonance is pulled toward the line center frequency. Transitions of approximately equal strength have their competition region halfway between line centers, while unequal strength transitions compete closer toward the weaker transition. Figure 10 illustrates the competition between vibrational-rotational transitions and how the laser can be tuned in frequency by varying the cavity mode separation as a result of changing the cavity length. In Figure 10(a) the cavity mode at ν_{n1}, is in resonance with the $P(J_1)$ laser transition causing it to oscillate and $P(J_2)$ is between the cavity modes. In Figure 10(b) the cavity length is increased slightly and the modes at ν_{n2} and ν_{m2} are in resonance with the $P(J_1)$ and $P(J_2)$ transitions respectively and competition can occur. If the gains are mutually exclusive then only one line would survive at the expense of the other. If the gain of each line is sufficient to sustain oscillation simultaneously then both laser lines

would coexist. In Figure 10(c) the cavity mode at ν_{m3} is in resonance with the $P(J_2)$ transition causing it to oscillate while the $P(J_1)$ transition is between the cavity modes. This frequency tuning mechanism makes it possible to use a piezoelectric driver to actively control and stabilize the frequency output of the laser.

3 CO_2 LASER P(J) TRANSITIONS AND CAVITY MODES

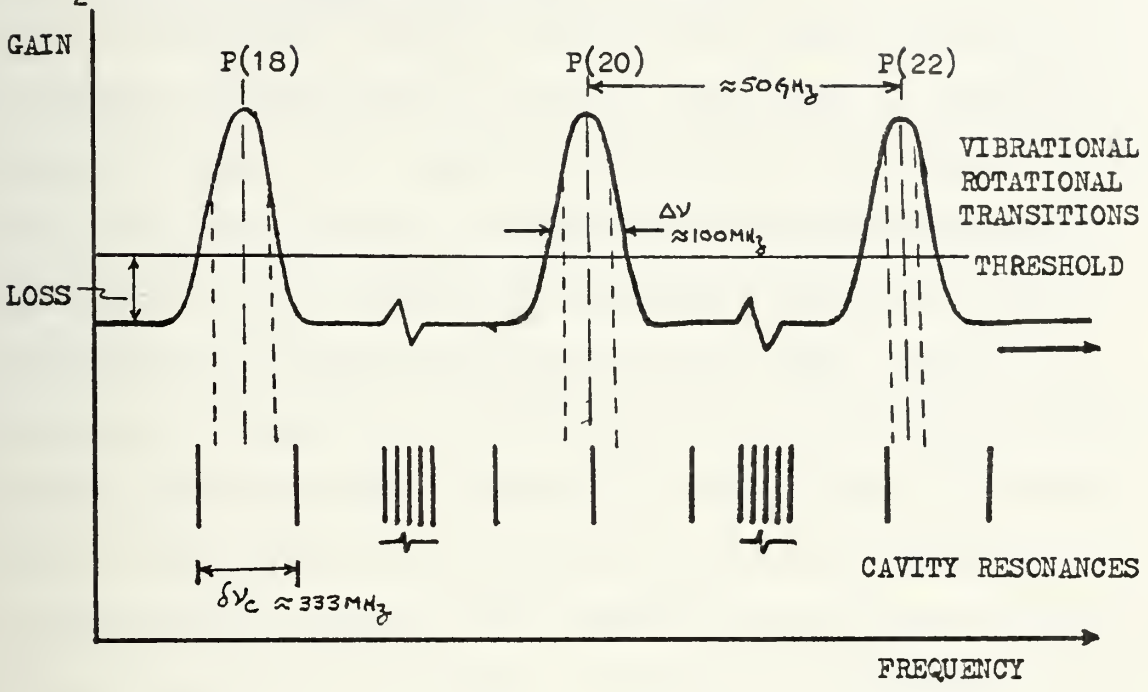

FIGURE 9

MODE COMPETITION AND FREQUENCY TUNING

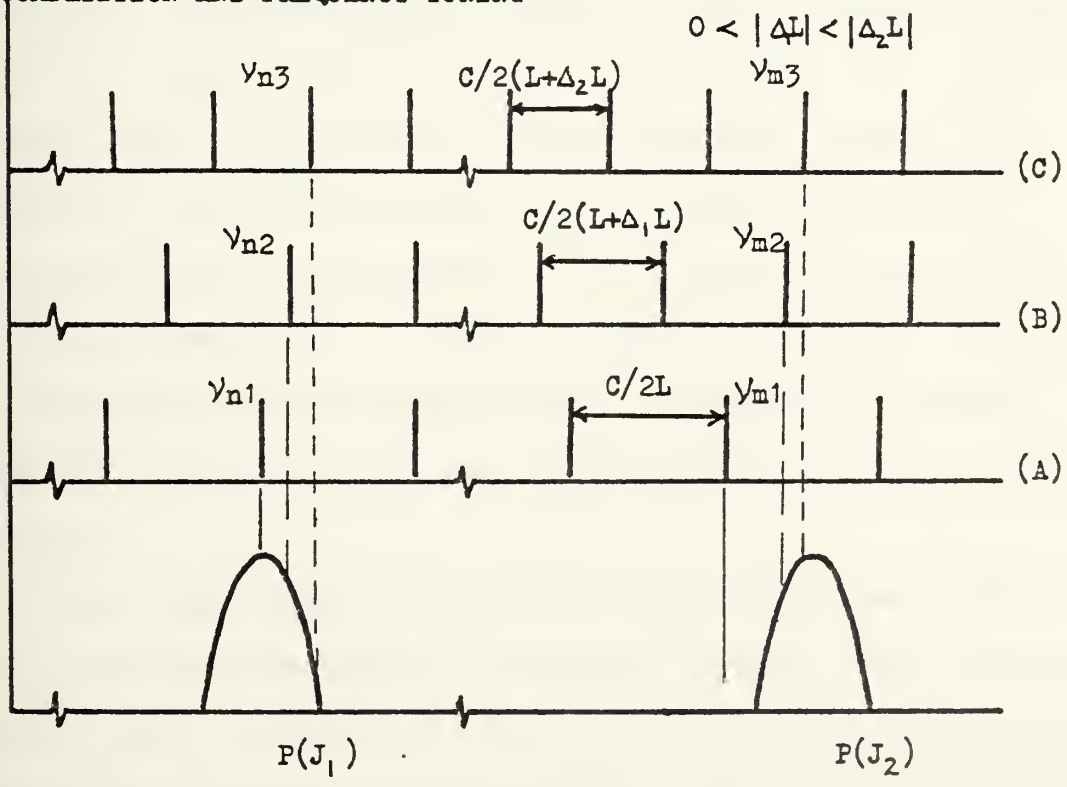

FIGURE 10

C. FREQUENCY STABILIZATION TECHNIQUES

Although many of the instabilities contributing to frequency fluctuations in the CO_2 laser can be reduced by external means (ie. control of discharge current by regulated power supply and control of system temperature with the aid of a separate temperature controlled heat exchanger) to frequency stabilize the laser actively requires the ability to change either the index of refraction of the laser medium or resonator cavity length. The laser cavity length can be accurately controlled by mounting a piezoelectric crystal which expands and contracts proportionally to an applied voltage. An error or frequency correction signal that is proportional to and indicates the direction of the required length correction can drive the piezoelectric crystal and frequency stabilize the laser. A common feature shared by a number of approaches involves the basic principle of establishing a frequency reference either internal or external to the laser to which the frequency is locked. By applying a modulation signal to the laser, causing its oscillating frequency to "dither" about a reference point, and using phase sensitive detection techniques, an error signal can be fed back to servo the laser frequency to the reference.

Another stabilization technique which has some useful advantages over the methods referred to above uses a frequency reference that is external to the laser with the discriminant obtained not by dither modulating the laser frequency about

the reference, but by modulating the reference about the laser frequency. The important advantage of this technique is that it avoids impressing modulation (AM or FM) on the laser output. A gas cell containing a molecular absorber which is tuned into resonance with the desired CO_2 laser line by a suitable D.C. electric field applied to the absorber provides the frequency reference. By superposition of an A.C. electric field, the absorption line center can be modulated about the lasing frequency and phase detected, producing the required correction signal back to the piezoelectric drive on the laser. Another advantage of this technique is the fact that it is voltage-controllable which means the laser frequency may be controllably tuned across the transition line width by programming the D.C. bias voltage applied to the Stark cell.

D. STARK CELL STABILIZATION

1. Stark Effect

Stark effects are the changes in the spectrum of a system due to an applied electric field. The rotational spectrum of a molecule which has a dipole moment is modified in an electric field, since the field exerts torques on the electric dipole moment changing its rotational motion.

The effect of an electric field on the rotational energy levels of molecules is given by quantum-mechanical perturbation theory. The Stark effect in a gas occurs when an external electric field is applied to the gas. The effect is characterized by the splitting of an absorption peak into several peaks by removing the degeneracy of the rotational energy levels. The application of the field in the absorbing gas results in the splitting of a line into $2J + 1$ lines.

The first order Stark effect which is linear with the applied electric field is produced by applying the electric field to a symmetric top molecule (molecule with three or more fold symmetry - molecule with two principal moments of inertia equal). A symmetric top molecule's principal advantage is the existence of a permanent electric dipole moment. The Stark splitting of the energy levels in molecules possessing a permanent dipole moment is given by [Ref. 19]

$$h\Delta\nu = \frac{\mu M E K}{J(J+1)} \cos\Theta \qquad (39)$$

Where μ is the molecular dipole moment and E is the electric field strength, Θ is the angle between μ and E, J is the total rotational quantum number, M is the magnetic quantum number or the component of J along a fixed direction, and K is the quantum number describing the interaction of the two principal moments of inertia. The selection rules for vibration-rotational transitions are

$\Delta J = 0, \pm 1$

$\Delta K = 0$ For Parallel Bands

$\Delta K = \pm 1$ For Perpendicular Bands

$\Delta M = 0$ For Stark Field Parallel to Laser Electric Field

$\Delta M = \pm 1$ For Stark Field Perpendicular to Laser Electric Field

For asymmetric molecules or those which do not have a permanent electric dipole moment, the expression for the Stark splitting of the energy levels is more complicated and involves second order perturbation calculations including the neighboring states $J' = J + 1$ and $J' = J - 1$. The energy splitting goes as the square of the external electric field. The second order quadratic Stark effect is usually considered negligible in Stark modulation. [Ref. 20]

For slightly asymmetric top molecules an intermediate type of Stark effect results. These molecules can have pairs of nearly degenerate levels and a first

order Stark effect can result for small molecular asymmetry and large fields.

2. Selection of Gases

Changes in absorption produced by an applied electric field on the states involved in transitions as given by the vibrational-rotational selection rules may result in a modulation of the laser intensity by a gas containing an appropriate molecule. In order to achieve an appreciable Stark effect and large modulation J should be small.

The selection of a suitable molecule for modulation of an individual laser is rather straightforward. The criteria to achieve a high modulation index are: 1) it is necessary to use molecules with a large dipole moment; 2) slightly asymmetric molecules may be used provided the Stark effect is essentially linear at the values of applied electric field used for modulation; 3) a linear Stark effect in either lower or upper state or both is suitable and the overall effect is determined by combination of the Stark effect on both states; 4) the absorbing Stark sensitive line and laser line should be within one or two Doppler widths of the absorbing gas. This requirement is not valid in the pressure broadening case where the higher pressures result in broader lines, poorer resolution and a smaller index of modulation with equivalent fields.

Investigations by Landman, Marante and Early [Ref. 21], Jensen and Tobin [Ref. 22] and most recently Martin, Corcoran and Smith [Ref. 23] have reported many gases capable of Stark modulation of a CO_2 laser. Table II lists some of

the absorbing gases used for Stark modulation and their corresponding CO_2 laser lines.

TABLE II

GASES USED IN STARK MODULATION OF $00^{\circ}1 - 10^{\circ}0$ TRANSITION

Gas	Laser Line Modulated
C_2H_3Cl	P(16), P(18), P(20), R(16), R(18), R(20)
CH_3Br	P(22)
CH_3I	P(14)
NH_3	R(14)
$C_2H_4F_2$	P(14), P(18), P(20), R(18)
$C_2H_2F_2$	P(10), P(12), P(14), P(18), P(20), P(22)
NH_2D	P(14), P(20), R(12)

3. NH_2D Rotational-Vibrational Spectra

Of the gases in Table II the microwave and infrared spectra of NH_2D have been studied extensively. Brewer et. al. in Reference 24 reported a rapid Stark tuning rate and relatively high absorption coefficient for NH_2D making it possible to obtain substantial modulation with relatively low electric field strength and short path length. Kelly, Francke and Feld [Ref. 25] observed the transitions which could be tuned into resonance with three of the 10.6μm CO_2 laser lines, namely P(20), P(14) and R(12). The NH_2D transitions were identified as belonging to the type $(v_2, J) = (0, 4) \longleftrightarrow (1, 5)$. The assigned transitions are shown in Figure 11 with the corresponding CO_2 laser lines enclosed in brackets. The lower and upper levels, the Stark shift δ_o required to bring each NH_2D transition into resonance with its respective laser line, laser line wavelength (cm^{-1}) and zero field splitting (cm^{-1}) for the three laser lines are given in Table III from Reference 24. Of primary interest in this discussion is the transition involved in absorption of the P(20) CO_2 laser line in the 10.4μm band.

The NH_2D absorption line involved belongs to the transition

$$(v, J_{K_-} J_{K_+}) = (0_a, 4_{04}) \longleftrightarrow (1_a, 5_{05})$$

This transition is nearly in coincidence with but at a slightly lower frequency than the 944.19cm^{-1} P(20) line

of the CO_2 laser. The P(20) laser frequency exceeds the zero field splitting of the $(O_a, 4_{04}) \longleftrightarrow (1_a, 5_{05})$ transition by 1720 ± 60 MHz. A relatively large and linear Stark effect results from mixing of the two nearly degenerate rotation-inversion levels $(O_a, 4_{04})$ and $(O_s, 4_{14})$ in the lower state of the transition. The subscript s(a) refers to a symmetric (antisymmetric) inversion state with respect to simultaneous exchange of all pairs of identical nuclei. The upper level $(1_a, 5_{05})$ has only a negligible second order Stark effect [Ref. 26].

RELEVANT ENERGY LEVELS OF NH_2D

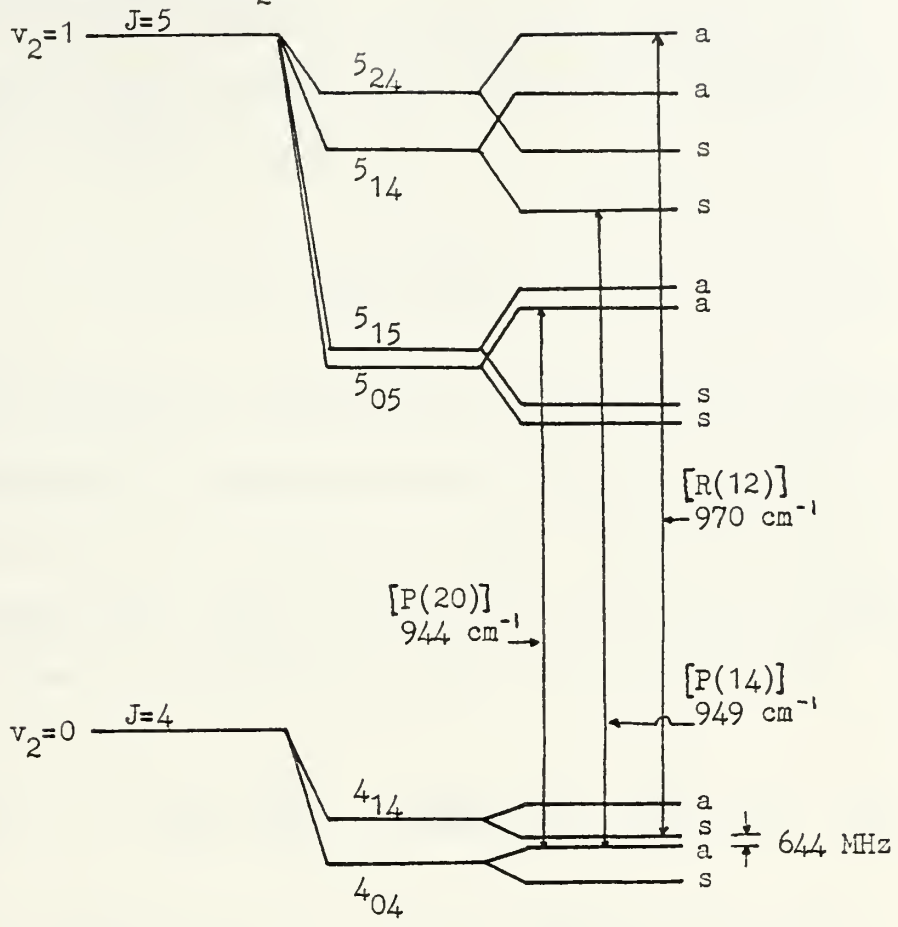

FIGURE 11

TABLE III

IDENTIFICATION OF OBSERVED NH_2D TRANSITIONS

LASER LINE	LOWER LEVEL	UPPER LEVEL	δ_o (MHz)	LASER FREQ. (cm^{-1})	ZERO FIELD SPLITTING (cm^{-1})
P(14)	0_a, 4_{04}	1_s, 5_{14}	-2300±60	949.43	949.40
P(20)	0_a, 4_{04}	1_a, 5_{05}	-1720±60	944.18	944.14
R(12)	0_a, 4_{14}	1_a, 5_{24}	+2800±100	970.55	970.64

4. Error Signal Analysis

The modulated output intensity from a Stark cell due to absorption by a single Stark component, exhibiting a linear Stark effect is given by

$$I = I_o \exp -[\gamma \ell] \tag{40}$$

Here γ is the absorption coefficient of the gas as a function of light intensity and applied electric field, I_o is the input intensity and ℓ is the cell length. The line center absorption coefficient where the line is collision-broadened in the high pressure Lorentzian region is given by [Ref. 27]

$$A(\lambda_o) = -\frac{1}{8\pi} \frac{\lambda_o^2}{\tau_{12}} \left(\frac{2}{\pi \Delta\nu_L}\right)\left(N_2 - \frac{g_2}{g_1} N_1\right) \tag{41}$$

Where λ_o is its wavelength, τ_{21} is the radiative lifetime of the vibrational-rotational transition, N_2 and N_1 are the upper- and lower-level population, respectively, g_2 and g_1 are the corresponding statistical weights and $\Delta\nu_L$ is the homogeneous linewidth as given in (19). The pressure dependence of $\Delta\nu_L$ is cancelled since N_2 and N_1 are also proportional to pressure, and $A(\lambda_o)$ is a constant.

The absorption coefficient at line center for an inhomogeneous line in the low-pressure Doppler broadened limit is given by [Ref. 27]

$$A(\lambda_o) = -\frac{1}{8\pi} \frac{\lambda_o^2}{\tau_{21}} \frac{2}{\Delta\nu_D} \left(\frac{\ln 2}{\pi}\right)^{\frac{1}{2}} \left(N_2 - \frac{g_2}{g_1} N_1\right) \tag{42}$$

Where $\Delta\nu_D$ is the inhomogeneous linewidth given by (23) and is a constant. The pressure dependence of N_2 and N_1 cause $A(\lambda_o)$ to vary linearly with pressure.

Plant and Abrams in Reference 27 plotted the line center absorption coefficient vs Stark cell pressure for NH_2D as shown in Figure 12. Using Voigt profile fits to the line shapes they were able to get a relation for the line center absorption coefficient which was an excellent fit to the experimental points. This relation is

$$A(\lambda_o) = -\frac{1}{8\pi}\frac{\lambda_o^2}{\tau_{21}}\frac{a}{\Delta\nu_L(\pi)^{1/2}}\left(N_2 - \frac{g_2}{g_1}N_1\right)(1-\text{erf}a)(\exp[a^2]) \qquad (43)$$

Where $a = (\Delta\nu_L/\Delta\nu_D)(\ell n\, 2)^{\frac{1}{2}}$ and erf is the error function.

From Figure 12 at pressures above about 5 torr one can approximate the Stark cell absorption lineshape with a Lorentzian and $A(\lambda_o) = 0.028\text{cm}^{-1}$, a constant. The modulator bandwidth reaches a limit, since the Stark effect changes character as the frequency of the perturbing field becomes comparable to the linewidth. Claspy et. al. [Ref. 28] estimated that the modulator bandwidth increased with pressure according to a pressure broadening coefficient. Therefore the broader line at higher pressures required a greater field variation for the same absorption change.

The absorption coefficient in (40) can be given by

$$\gamma = A(\lambda_o)_{MAX} \propto g(\nu) \qquad (44)$$

LINE - CENTER ABSORPTION COEFFICIENT VS STARK CELL PRESSURE

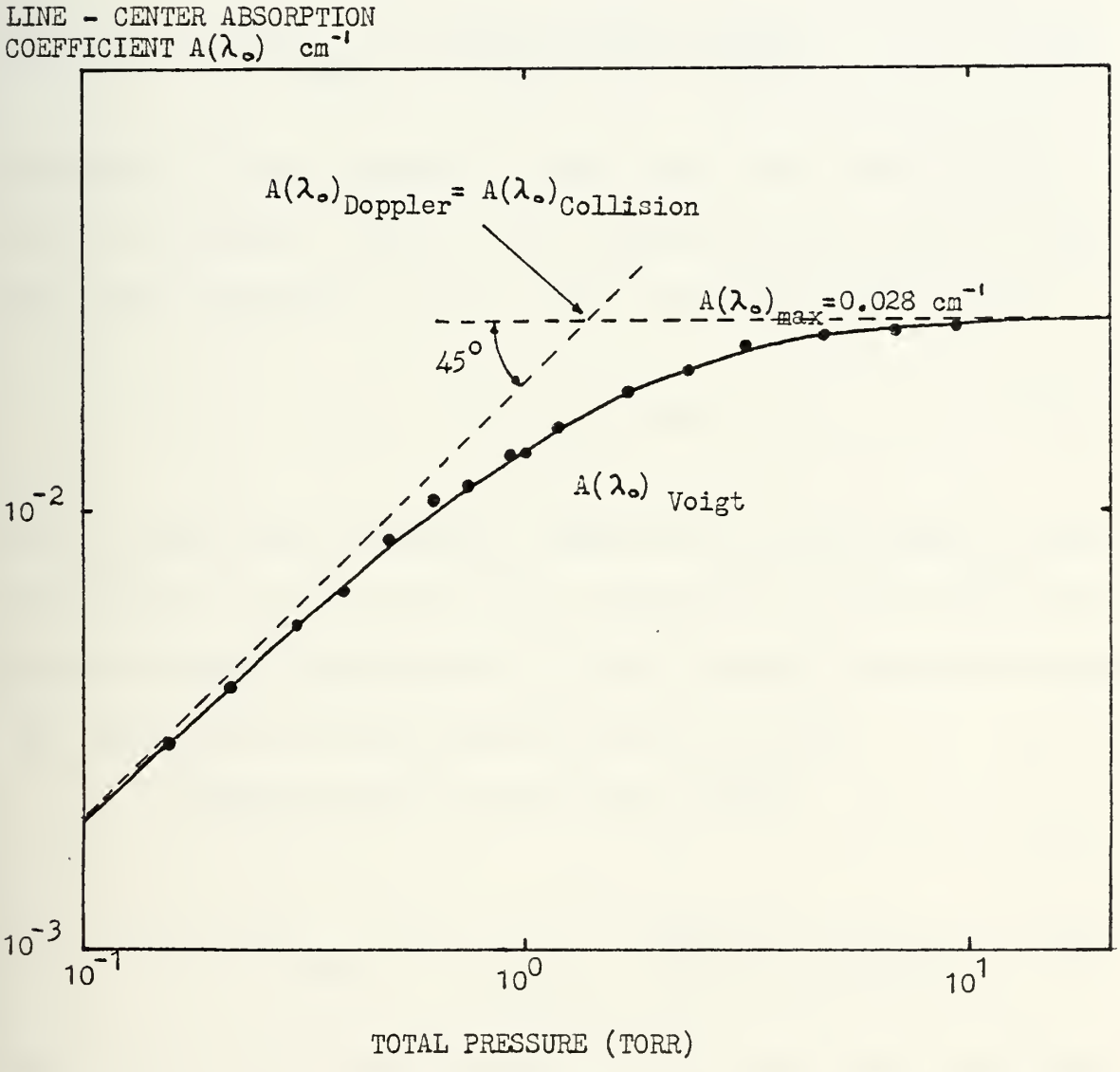

FIGURE 12

Where α is a constant dependent on gas pressure and $g(\nu)$ is the lineshape function of the absorbing gas. Assuming a Lorentzian lineshape and letting α equal the pressure broadening coefficient C, times the pressure P, (44) can be written as

$$\gamma = A(\lambda_o)_{MAX} \, CP \, \frac{\Delta\nu}{2\pi\left[(\nu-\nu_o)^2-(\Delta\nu/2)^2\right]} \tag{45}$$

where $\Delta\nu$ is the linewidth of the Stark cell, and $(\nu-\nu_o)$ is the frequency offset of the absorption line center from the laser frequency. Let $(\nu-\nu_o)$ be defined as ϵ where

$$\epsilon = \epsilon_o + SE \tag{46}$$

ϵ_o is the offset frequency dependent on the offset of the absorption line from the laser frequency at zero field and S is the Stark coefficient or Stark tuning rate which relates the line shift to the applied electric field.

Substituting (46) into (45) gives

$$\gamma = A(\lambda_o)_{MAX} \, CP \, \frac{\Delta\nu}{2\pi\left[(\epsilon_o + SE)^2 + (\Delta\nu/2)^2\right]} \tag{47}$$

Therefore, for a fixed pressure in the cell and a set laser line, γ the absorption coefficient is only dependent on the applied Field E. Impression of an A.C. voltage with an electric field in the form $E' = \Delta E \cos\omega t$ on the applied field E will give γ a time dependence by oscillating the

absorption line shape about the line center frequency which will act as a dither mechanism about ν . A schematic of the dither mechanism for a Stark cell modulator is shown in Figure 13. The remainder of the work described in this thesis will refer to the P(20) - NH_2D combination.

Nussmeier and Abrams [Ref. 26] give the frequency offset between the absorption line center of NH_2D and the P(20) 10.6 μm line center as a function of applied voltage as

$$\epsilon = \epsilon_o + SE = -2042 + 0.143|M|E \qquad (48)$$

Where ϵ is given in MHz, M is the z component of the rotational quantum number J and has integer values from -4 to 4, and E is the applied electric field in $^{V}/_{cm}$. Setting $\epsilon = 0$ and $M = \pm 4$ in (48) shows that an electric field of 3570 $^{V}/_{cm}$ is needed to bring one component of NH_2D absorption into resonance with the P(20) transition. The values reported in the literature for the Stark tuning rate, S, for the P(20) CO_2 line and NH_2D with $M = \pm 4$ are consistent with Nussmeier and Abrams value of .572 MHz $^{cm}/_{V}$.

DITHER MECHANISM

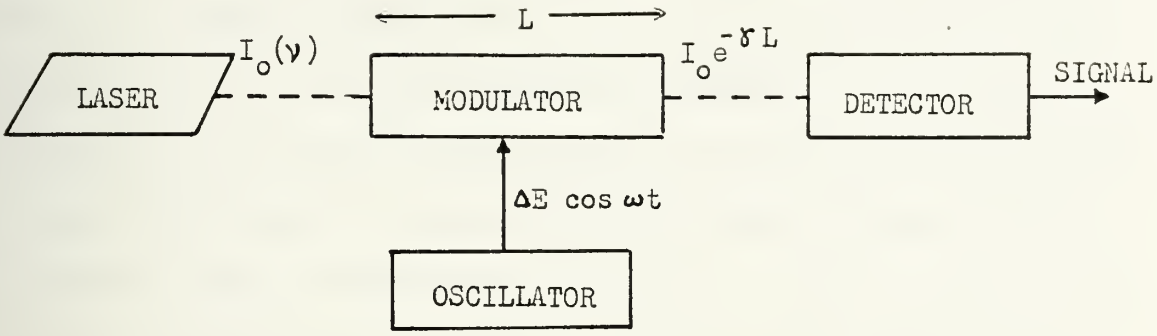

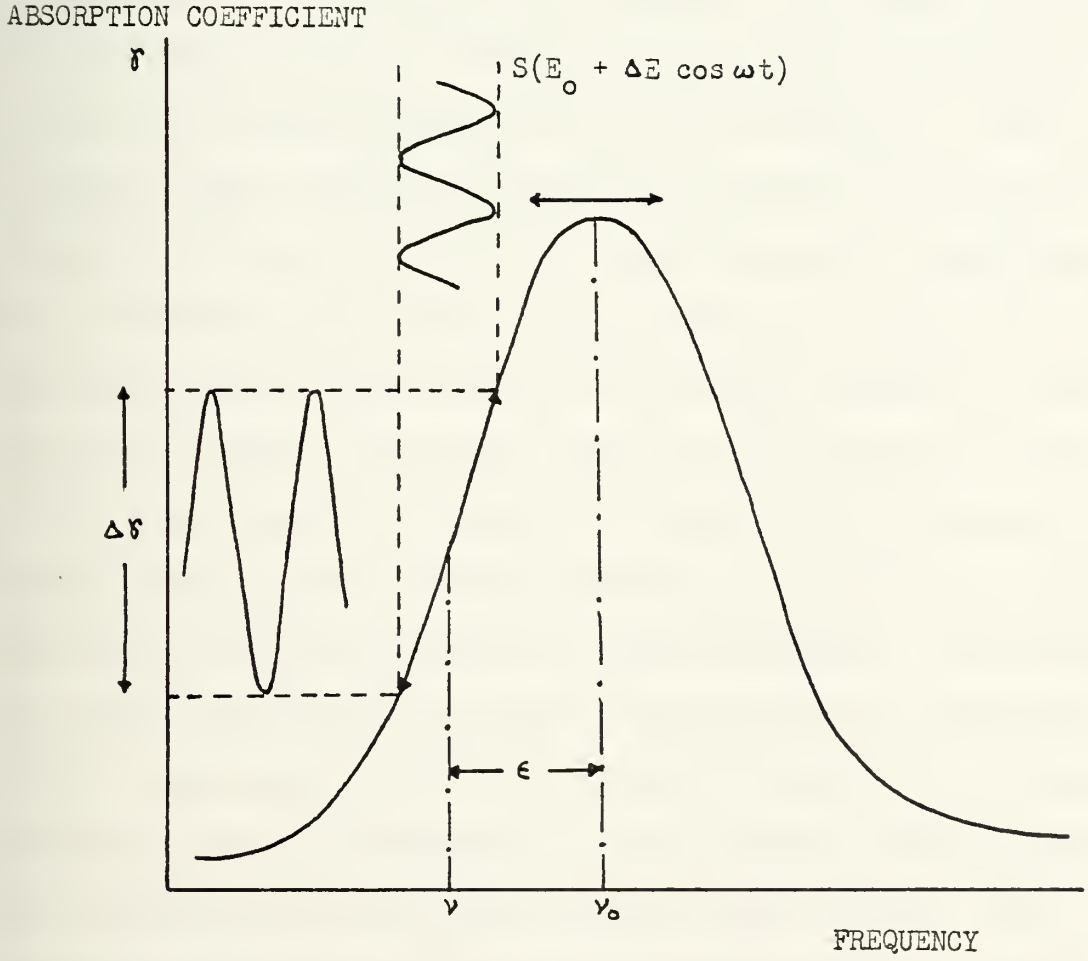

FIGURE 13

5. Stark Cell Stabilization System

A schematic of a laser stabilization system is shown in Figure 14 and is a somewhat simplified version of the one given in Reference 29. A small percentage (less than $^{1w}/cm^2$ to avoid saturation effects) of the laser output is directed into the Stark cell via a beam splitter and plane mirror. The basic Stark cell consists of two parallel metal electrodes in a vacuum tight container with an entrance and exit window. A precision high-voltage power supply biases one Stark electrode to bring an absorption line in NH_2D into resonance with the P(20) line center. An A.C. voltage from an audio oscillator drives the second electrode at a set frequency. The cell contains NH_2D formed by mixing one part NH_3 with ND_3 to a desired pressure in the cell. The exchange of hydrogen and deuterium is reported in Reference 30 to be rapid with an equilibrium concentration to 45% NH_2D reached in less than one minute. When the laser is oscillating on the P(20) line the Stark effect will produce a sinusoidal modulation in the intensity through the cell which can be detected by a pyroelectric or HgCdTe detector. The signal is phase sensitively detected relative to the reference audio oscillator waveform in a lock-in amplifier. The detected phase is dependent on the relative frequencies of the absorption line center and the laser output. The magnitude and sign of the lock-in amplifier D.C. output which is proportional to the phase difference between the

laser frequency and the Stark-shifted reference will produce a suitable error signal. After this error signal is appropriately phased, integrated and amplified it is fed back to the piezoelectric mounted laser cavity mirror to tune out the frequency difference and the frequency control feedback system is complete. Because the laser is capable of oscillating on a number of vibrational-rotational laser transitions dependent on the resonator cavity length, a linear ramp voltage applied to the piezoelectric drive will cause the laser to scan through its spectral signature profile until the P(20) transition is reached at which time the servo stabilization technique can be initiated.

SCHEMATIC DIAGRAM OF STABILIZATION SYSTEM

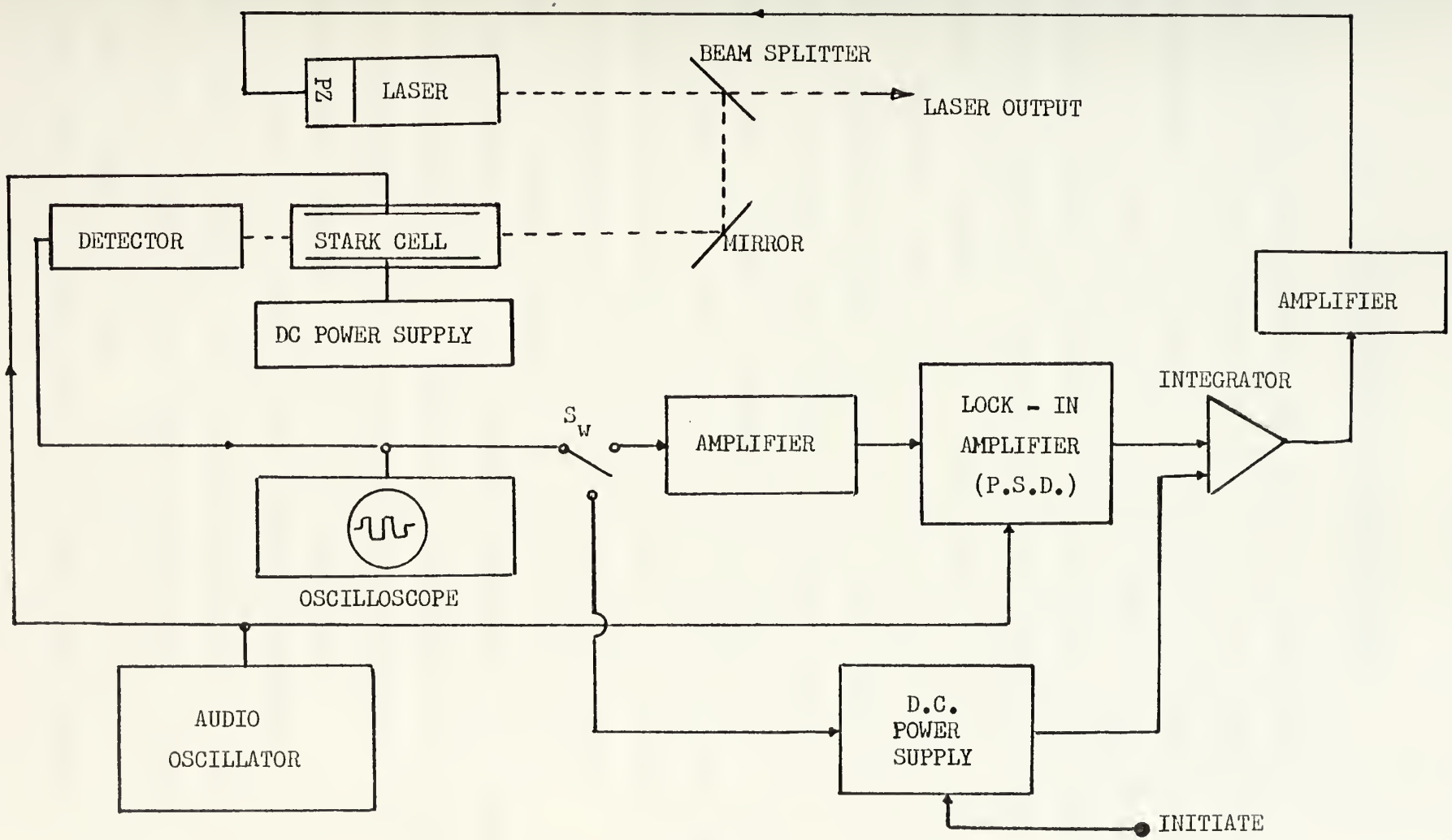

FIGURE 14

III. EXPERIMENTAL INVESTIGATION

Preliminary engineering work done in Reference 13 studied the characteristics of the Sylvania CO_2 Model 941 Laser pertinent to the design of a Stark cell stabilized system. The instabilities of the laser due to fluctuations in discharge current caused by an unregulated, unfiltered laser power supply and system temperature variations were measured and discussed. The piezoelectric parameter and thermal expansion coefficient also were determined for the laser. Computer analysis demonstrated the feasibility of producing a suitable error signal for phase sensitive detection with available equipment and the need for a servo loop integrator. A vacuum tight Stark cell was constructed and tested to 3000 volts with no evidence of breakdown.

The parameters for the Sylvania 941 piezoelectric tunable and linearly polarized CO_2 laser used in the following discussion of experimental procedures and results are given in Appendix A. Appendix B discusses the optical design and specifications of the optical engineering CO_2 laser spectrum analyzer used in the experiments.

To prevent the instabilities caused by changes in discharge current a stable high voltage power supply (Sylvania 941S) which in turn was run from a stable line regulator was used to power the laser. The use of a circulation pump minimized flow rate fluctuations and the system usually

reached an equilibrium temperature condition after a few minutes. The current to the laser from the 941S power supply could not be controlled manually and was preset for optimum performance of the laser.

A. SERVO LOOP INTEGRATOR

In order to provide optimum frequency stabilization of the CO_2 laser the P(20) line should be maintained in coincidence with the center absorption frequency of a Stark shifted NH_2D transition as accurately as possible. The two transitions in coincidence will produce a zero error signal. As the P(20) line drifts in frequency the magnitude and sign of error signal will be proportional to the change in frequency, and direction of the drift, respectively. If a proportional correction signal is supplied directly to the piezoelectric driver the magnitude of the error signal will decrease to an equilibrium condition at a nonzero value for ϵ. The equilibrium condition exists when the PZ voltage producing a frequency difference ϵ is equal to the PZ voltage supplied by the correction signal.

Integration of the error signal will produce a correction signal that will drive the piezoelectric crystal in a manner proportional to the total time integral of the error signal. This integration will allow the error signal to return to zero at the required PZ voltage. The integrated signal will continue to increase until the frequency difference (error signal) is zero. At $\epsilon = 0$ the integrator maintains the voltage at a constant D.C. value until a nonzero error signal indicates the need for a change.

The integrator shown in Figure 14 serves a dual purpose: i) integration of the error signal supplied by phase detection in the lock-in amplifier when the stabilization feedback

control system is in operation. ii) Integration of a selectable D.C. voltage to provide a linear ramp voltage to the laser piezoelectric driver in order to search for the required laser transition before the servo stabilization procedure can be initiated.

The integrator described in Appendix C was designed to respond to both slow and rapid changes in frequency of the P(20) line from the Stark shifted NH_2D absorption center frequency. The gain was designed to be equal to one to make the integrator output equal to the integral of the input.

A diagram of the apparatus used to examine the characteristics of the integrator is shown in Figure 15.

The input to the integrator was provided by a regulated 0 - 25 V D.C. supply which was set at a constant voltage . A three way reversing polarity switch S: was used to provide positive or negative values of V_i to the integrator or to isolate the integrator from the input voltage. The input voltage to the integrator was fed into channel A of a time base plotter and the output of the integrator into channel B. Figure 16 shows the integrator output as a function of a step input with $V_i = \pm 2$ volts. The graphical output indicates that integration of a 2 volt input for approximately 10 seconds gives an integration output of 20 volts and slope of 1.95 $^{V}/_{sec}$. Thus the integrator output equals the integral of the input. Figures 17 a & b respectively show typical operation and response of the integrator to step inputs of ±4V and ±6V. Since the

integrator is part of the feedback control system that drives the piezoelectric crystal, differences between the analog integration of the input signal and the exact mathmetical values are not critical and can be compensated for in the proportionality constant associated with amplification of the correction signal. In other words, the integrator is concerned primarily with the manner in which the piezoelectric crystal is driven rather than the magnitude of the correction signal.

The integrator saturates at a voltage of ±14 volts; therefore if the P(20) line consistently drifts in the same direction the integrator may saturate. By ganging a polarity reversing switch to the input and output of the integrator, saturation can be controlled by reversing the sign of the signal in magnitude while maintaining sign of the proper correction signal to tune out the frequency difference. Minor drift in steady state voltage output inherent in analog integrations can be controlled by a voltage offset null on the integrator. This possible integrator-induced long term instability will cause the laser frequency to drift slightly but it can be corrected for in the feedback control system like any other instabilities in the system.

The incorporation of an integrator should improve the ability of the feedback control system to frequency stabilize the laser and produce a system suitable for laboratory or field use.

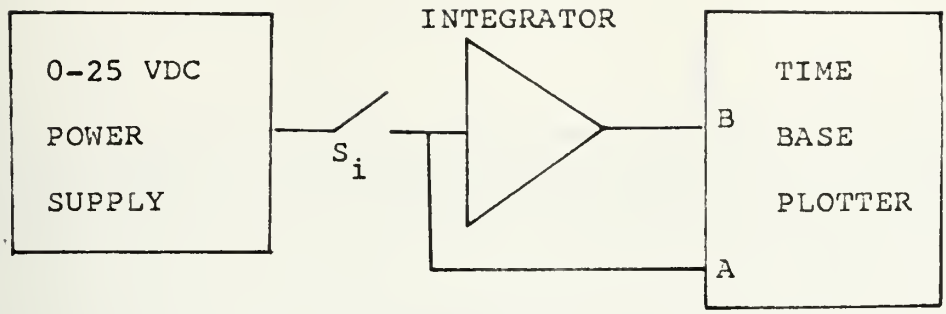

FIGURE 15

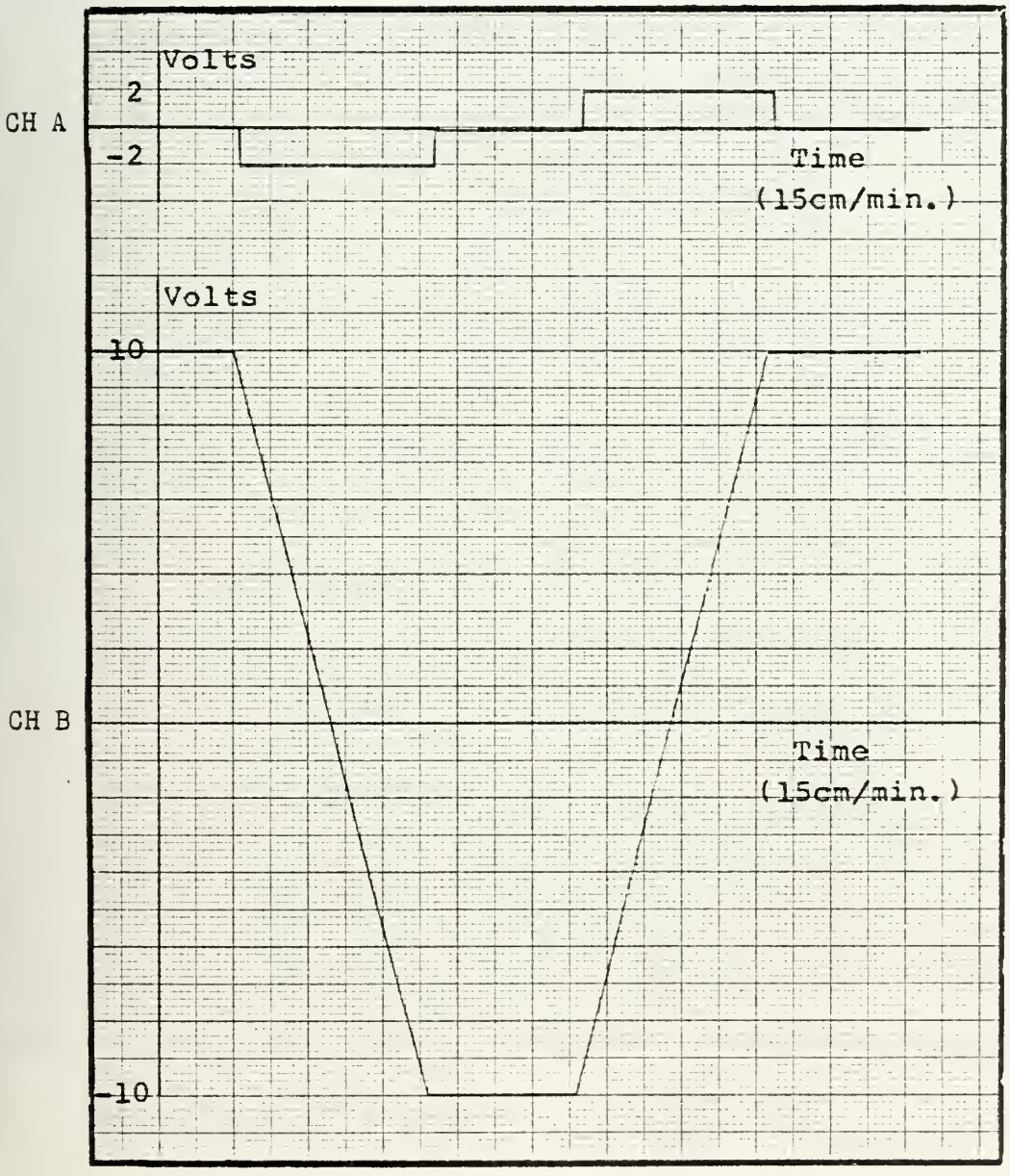

FIGURE 16

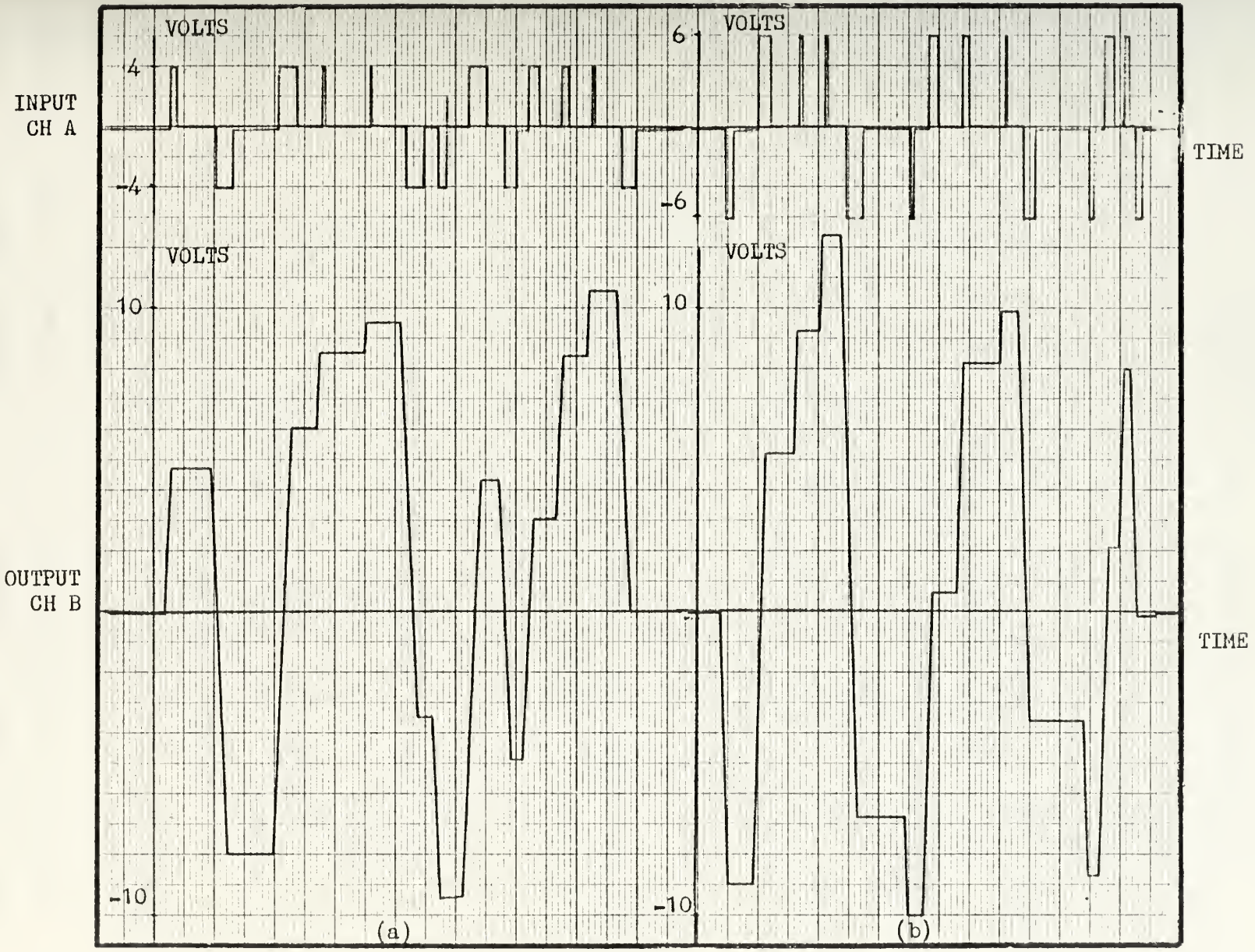
VOLTS
4
-4
INPUT
CH A
VOLTS
10
-10
OUTPUT
CH B
(a)
VOLTS
6
-6
TIME
VOLTS
10
-10
TIME
(b)

FIGURE 17

B. LASER SPECTRAL SIGNATURE

The laser is capable of oscillation on a number of transitions other than the P(20) as the resonator optical length varies. This capability adds to the versatility of the laser as well as satisfying a need to search for and find the desired transition before the feedback stabilization system can be initiated. If the cavity length of a CO_2 laser is slowly increased a certain sequence of lines will appear. After changing the cavity length approximately one half wavelength the sequence will repeat itself. The output profile obtained by changing the laser mirrors separation is called the laser signature.

A schematic of the experiment to determine the spectral signature of the laser is shown in Figure 18. The spectral signature was produced by plotting the relative intensity of the laser as a function of applied voltage to the piezoelectric driver (PZ voltage). The PZ voltage was supplied by a Kepco model ABC regulated D.C. supply with a range of 0 - 1500 volts. It was operated in the voltage-programmable mode with a positive ground. It was programmed to operate at a voltage ratio of 100:1 output to input. Using the integrator described in Appendix C to supply a linear ramp voltage as the input to the programmable power supply, the laser could be scanned through a free spectral range. The scan rate was controlled by the magnitude of the input voltage to the integrator since the slope of the integrator output voltage is directly proportional

SCHEMATIC OF LASER SPECTRAL SIGNATURE EXPERIMENT

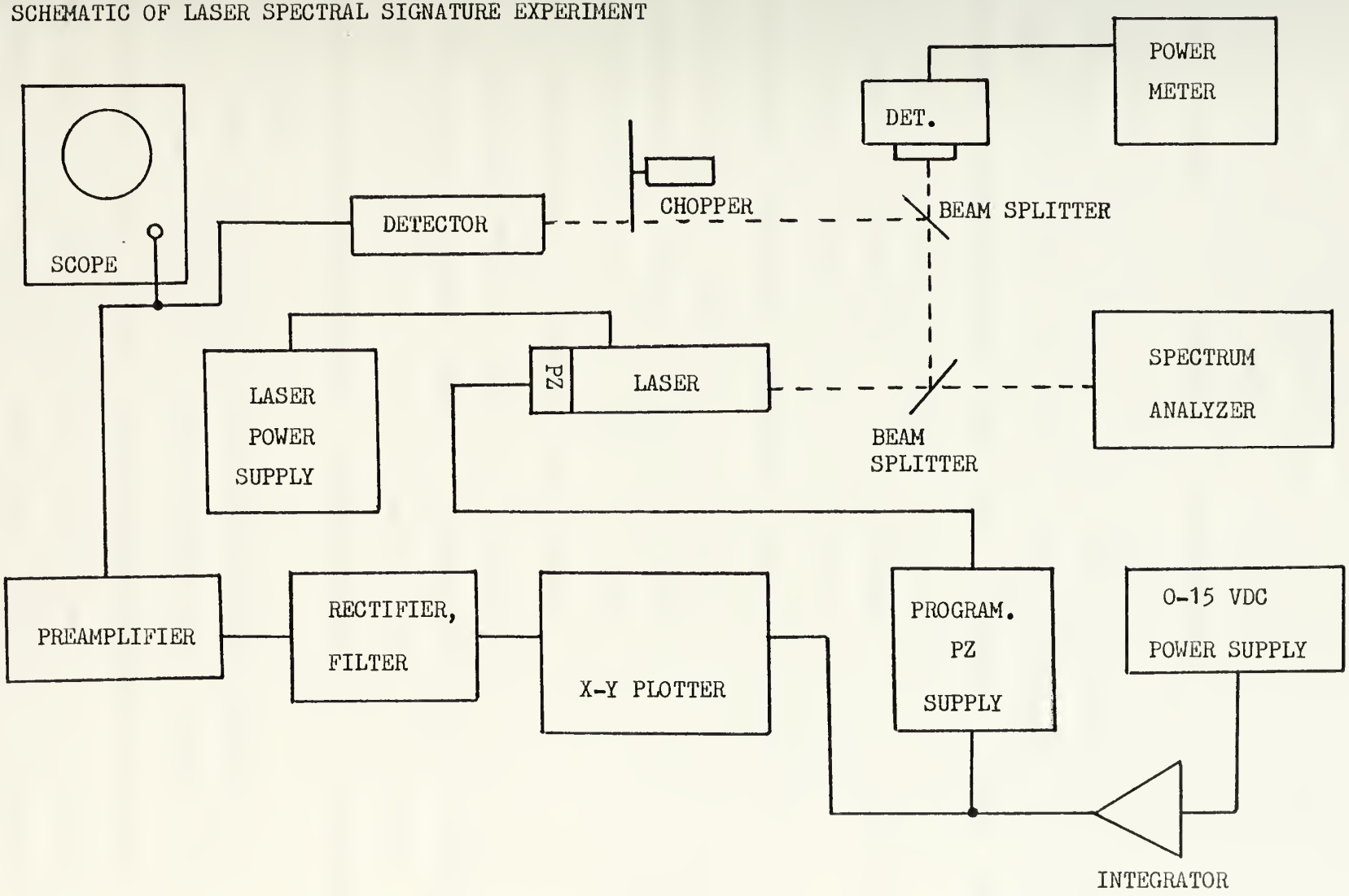

FIGURE 18

to the input voltage. The direction of scan was controlled by a 3 position reversing polarity switch that changed the sign of the slope as a result of changing the sign of the input voltage. The output of the integrator which was directly proportional to the PZ voltage was supplied to the x axis of an x - y plotter. The relative intensity of the chopped laser output was obtained from a pyroelectric detector signal that was amplified, filtered and rectified. The relative intensity signal was then supplied to the y channel of the plotter. The frequency of the laser for a given PZ voltage could not be monitored, but the vibrational-rotational transition could be identified using an Optical Engineering CO_2 spectrum analyzer described in Appendix B. Typical results are shown in Figure 19 for an increasing PZ voltage scan (0 - 1500 V D.C.) and Figure 20 for a decreasing PZ voltage scan (1500 - 0 V D.C.).

The power meter in Figure 18 monitored the operation of the laser. It was used as a comparison with the results shown in Figures 19 & 20. Figures 21 & 22 give typical results for relative power output as a function of applied PZ voltage.

In each set of plots the scan direction appears to have caused a hysteresis effect [Ref. 24]. Differences in the traces appear to be caused by hysteresis effects and nonlinearity of the piezoelectric element. If the dipoles (whatever their nature: electronic, ionic or polyatomic) resist the change of the electric field the electric

displacement (strain) will lag the electric field (stress). A lag in the displacement relative to the voltage change results in a hysteresis effect and the scan direction will shift the laser signature in the direction of scan, independent of the scan rate. From Figures 19 - 22 nine laser lines were obtained in the laser signature and the free spectral range of the laser is approximately 1.4 kv which agrees with the value found in Reference 13.

Looking at the shape of the laser signature it is apparent that none of the lines are allowed to lase over their full width before the neighboring line begins to oscillate. The mode competition or the fact that the oscillations at various transition frequencies compete for the available gain are quite prevalent in a CO_2 laser and help to insure single wavelength operation. Throughout the experiment only one vibrational-rotational line was observed to lase at a time. The laser oscillated in the lowest order transverse mode TEM_{00} throughout the full range of the PZ voltage.

The method of scanning through the laser signature can be used in the stabilization system shown in Figure 14 to find the required P(20) transition prior to initiating the feedback control.

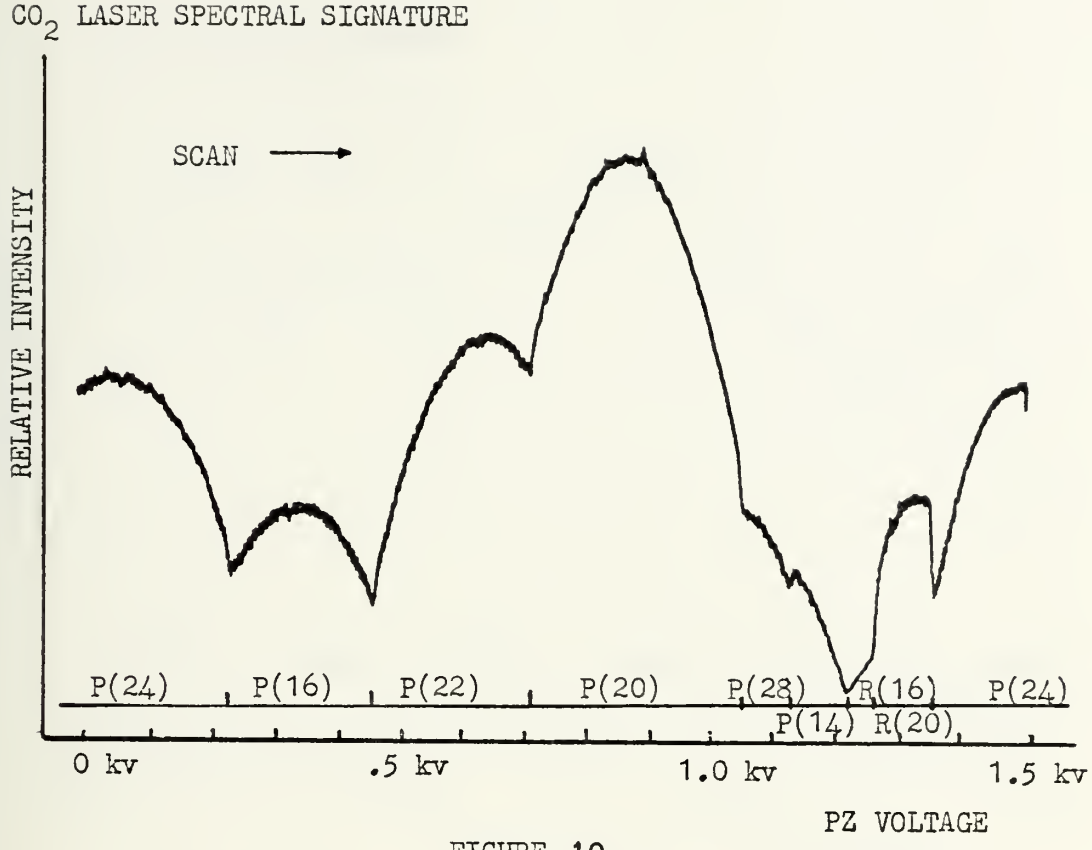

FIGURE 19

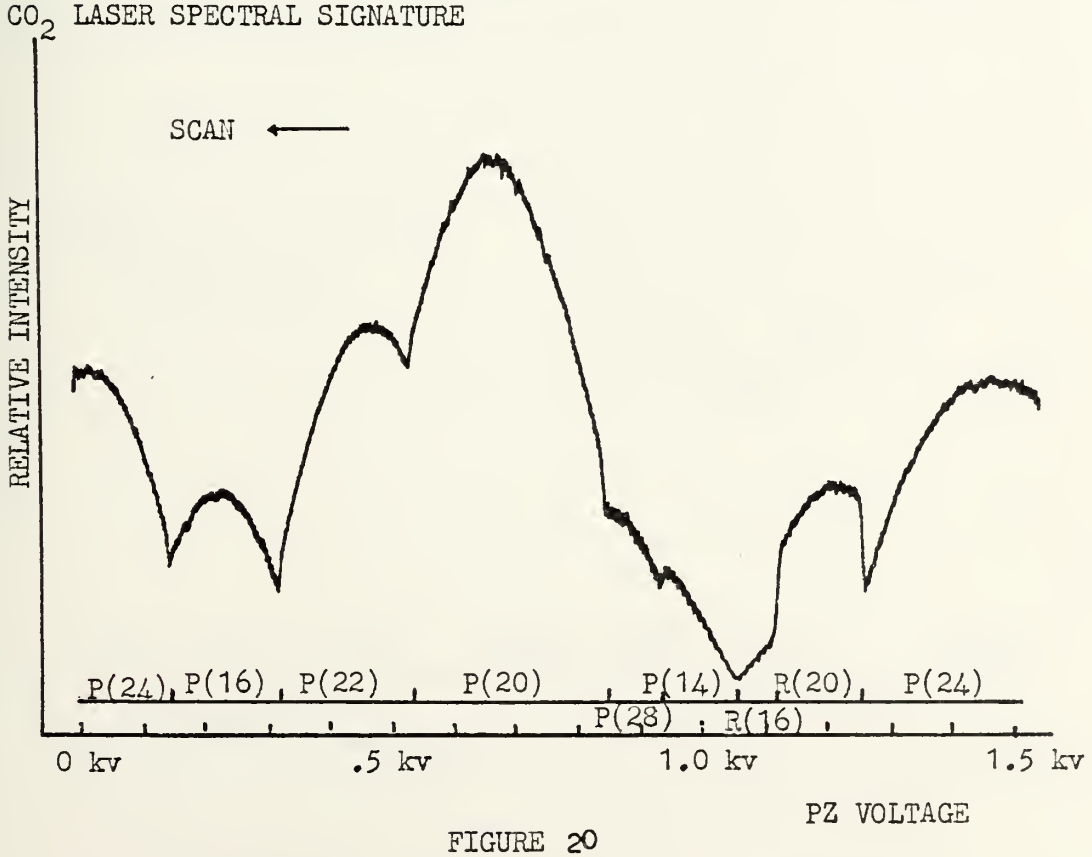

FIGURE 20

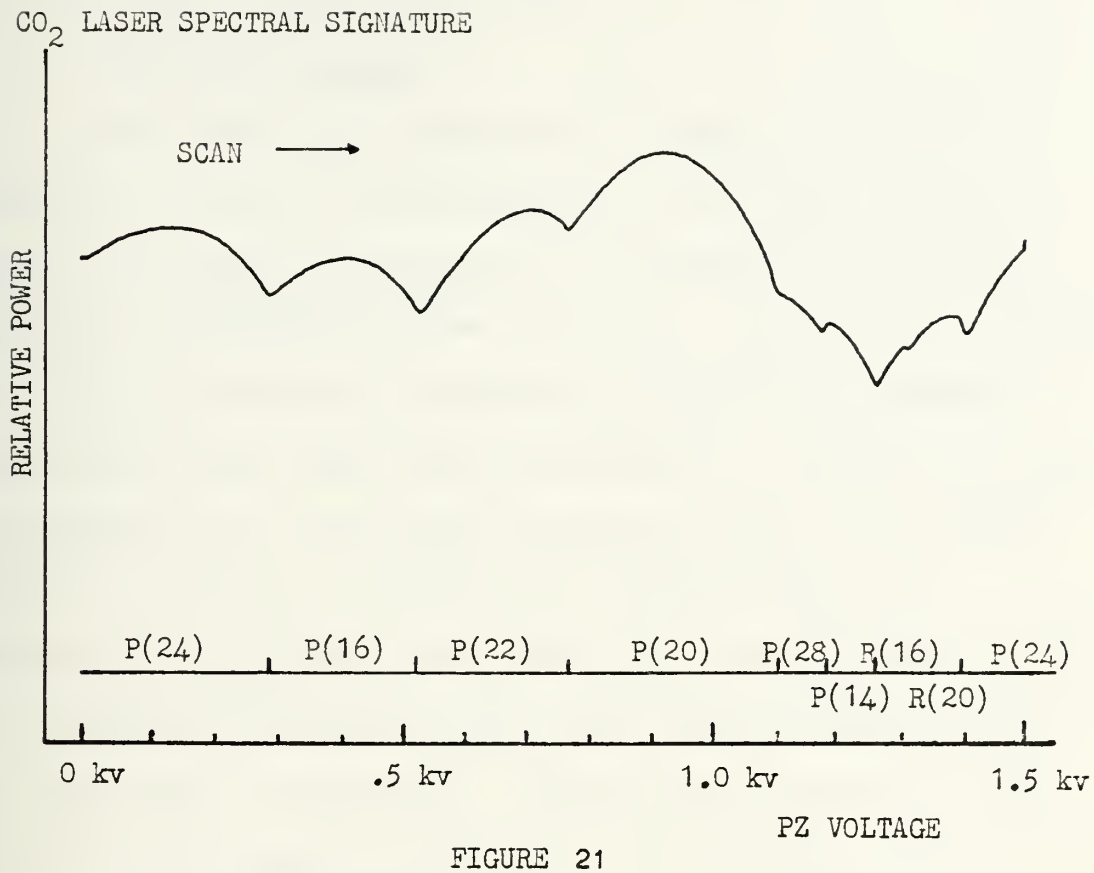

FIGURE 21

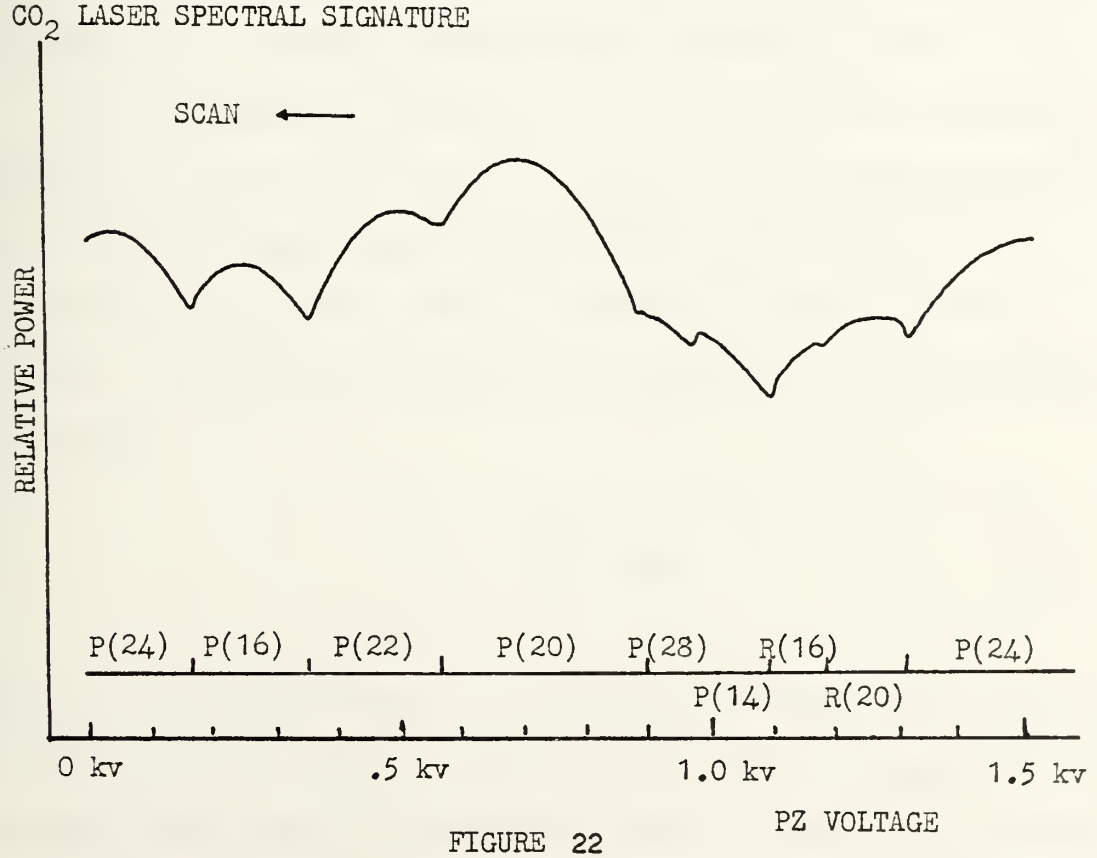

FIGURE 22

C. STARK CELL OPERATION AND TEST

1. Stark Cell Design

The Stark cell described in Reference 13 was expected to operate satisfactorily in the stabilization system. The cell was designed to eliminate a persistent problem of breakdown in previous cells. All metal surfaces were isolated from the low pressure gas filled channel through which the laser beam would pass. The cell was made to accomodate one inch NaCl windows at each end and had a single port used to fill the cell with the NH_2D gas. Fabrication of the cell resulted in an uneven plate separation of approximately 7mm with 1mm of plexiglass between each plate and the channel. The cell was tested to 3000 volts with no breakdown and held a good vacuum. Figure 23 shows the cell design with pertinent specifications.

As discussed in Section II. D. 3 the rest frequency of the $(0, 4_{04}\ 1M = 41) \longrightarrow (1, 5_{05}\ 1M = 51)$ transition of NH_2D is shifted approximately 1700 MHz into coincidence with the 10.6 μm P(20) line by applying a Stark field of 3570 V/cm. The voltage required to produce the Stark field is given by

$$V = - \int \vec{E} \cdot d\vec{\ell} \qquad (49)$$

where V is the difference in potential between the plates, E is the electric field strength between the plates and d represents the path of integration taken between the plates.

STARK CELL AND SPECIFICATIONS

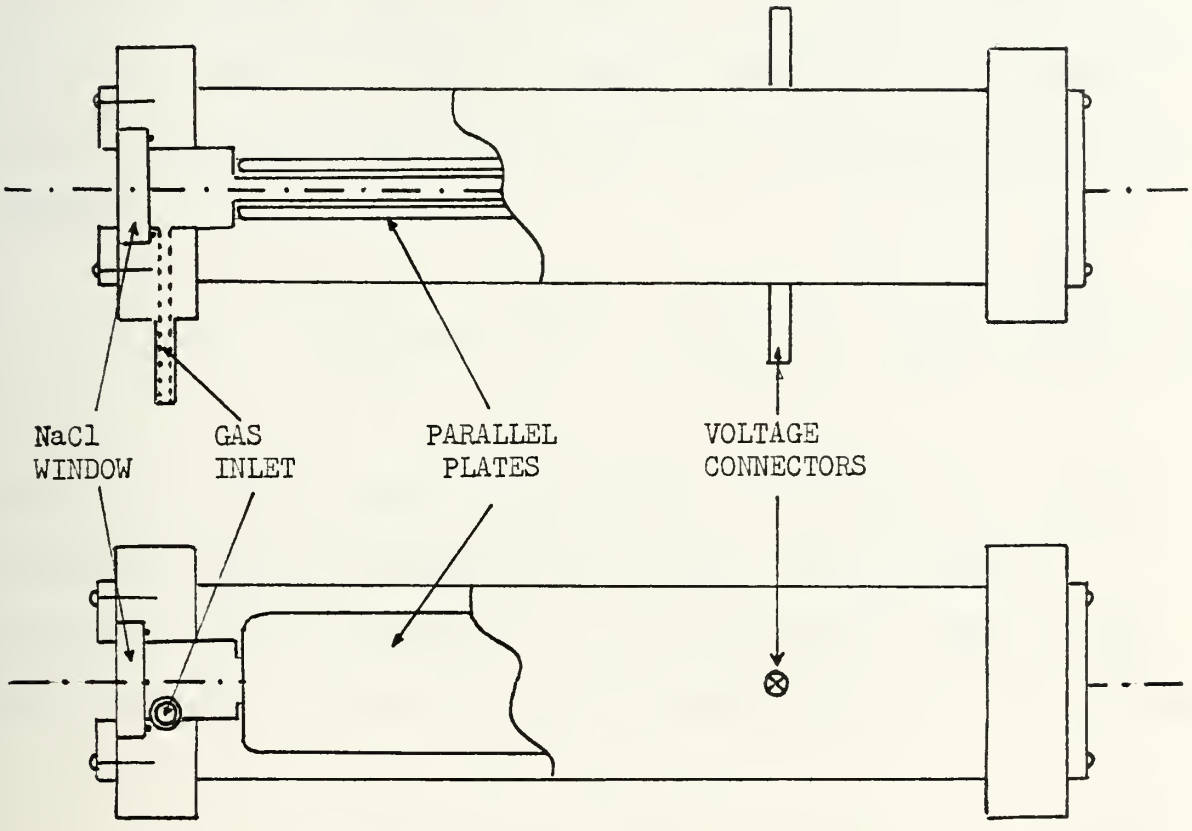

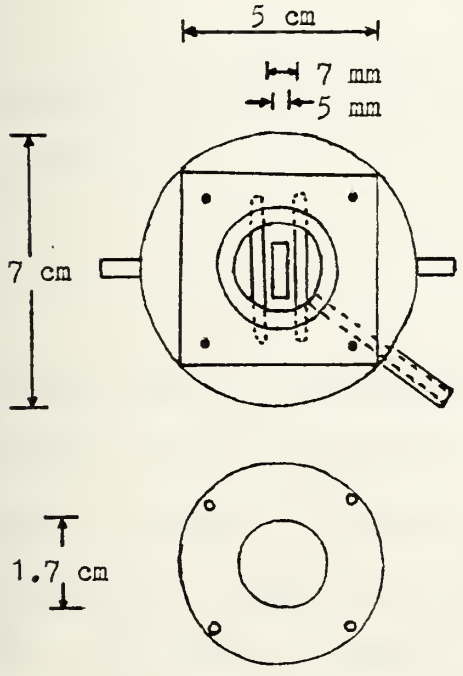

SPECIFICATIONS

PLATES:

MATERIAL	STAINLESS STEEL
LENGTH	20.3 cm
WIDTH	3.6 cm
SEPARATION	7.0 mm

CELL:

MATERIAL	PLEXIGLAS

FIGURE 23

Although the simplest path between the plates is a perpendicular straight line the electrostatic force is path independent since each plate is an equipotential surface. Applying (49) to Figure 24 for a straight perpendicular path from the lower plate (L) to the upper plate (u) yields.

$$V = -\int_L^u E \cdot d = -\int_L^u E \cos 180^\circ \, d = \int_L^u E \, d\ell = E_o[d-(a+b)]+E[a+b] \qquad (50)$$

Where E_o is the electric field with no dielectric, d is the separation between plates, a and b are the dielectric thickness at the plates and E is the electric field inside the dielectric. Since E can be related to E_o by the relation

$$E = E_o/\kappa \qquad (51)$$

where κ is called the dielectric constant, (50) can be written as

$$V = E_o\left[d - (a+b)\right] + E_o\left(\frac{a+b}{\kappa}\right) \qquad (52)$$

Substituting in the values for the Stark cell shown in Figure 21 and letting $E_o = 3570$ V/cm. The approximate Stark cell voltage to bring one component of the center absorption frequency of NH_2D into resonance with the P(20) line is V = 2030 volts. Here d = 7mm, a = b = 1mm and κ = 2.7 - 3.2 for plexiglass (methyl methacrylate). Although this is a

relatively high applied D.C. voltage, it is within the breakdown limits specified for the cell.

PLATE CONFIGURATION IN STARK CELL

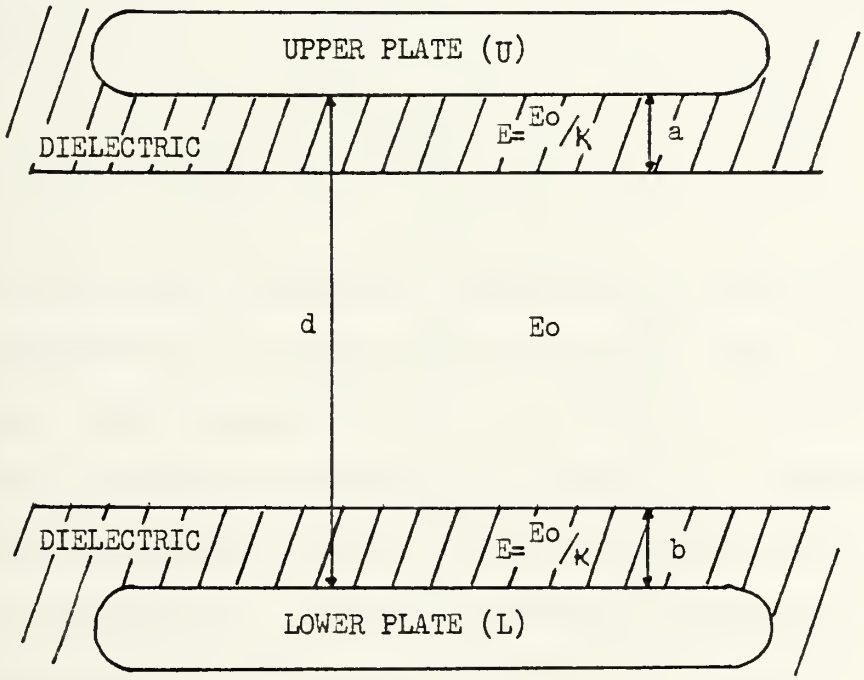

FOR THE STARK CELL IN FIGURE 21

d = 7mm

a = b = 1mm

$\kappa \cong 2.7 - 3.2$ FOR PLEXIGLAS (METHYL METHACRYLATE)

Figure 24

2. Stark Cell Absorption Lineshape

Experimentation to determine the absorption lineshape and modulator performance as a function of pressure began by measuring the relative intensity out of the Stark cell as a function of pressure with no electric field across the plates. The attenuation of monochromatic radiation follows Beer's law

$$\frac{d}{dx} I(\nu) = - \mu(\nu) \; I(\nu) \tag{53}$$

from which

$$I_x = I_o \; e^{-\mu x} \tag{54}$$

where μ is a linear extinction coefficient which is the sum of the coefficients of total absorption and total nonforward scattering. The relative value of μ depends strongly on the density and molecular composition of the gas. Absorption is of greatest importance in the infrared (particularly in the 8 - 14 μm wavelength). Rayleigh scattering because of its strong dependence on wavelength should be unimportant for wavelengths longer than the visible range and no Mie scattering should be present. Since the density is proportional to the pressure of the gas μ is dependent on the pressure.

The experimental arrangement is schematically represented in Figure 25. The laser was tuned and maintained at the center of the P(20) transition by keeping the power meter at its maximum value and monitoring the spectrum

SCHEMATIC OF LINE SHAPE FUNCTION EXPERIMENT

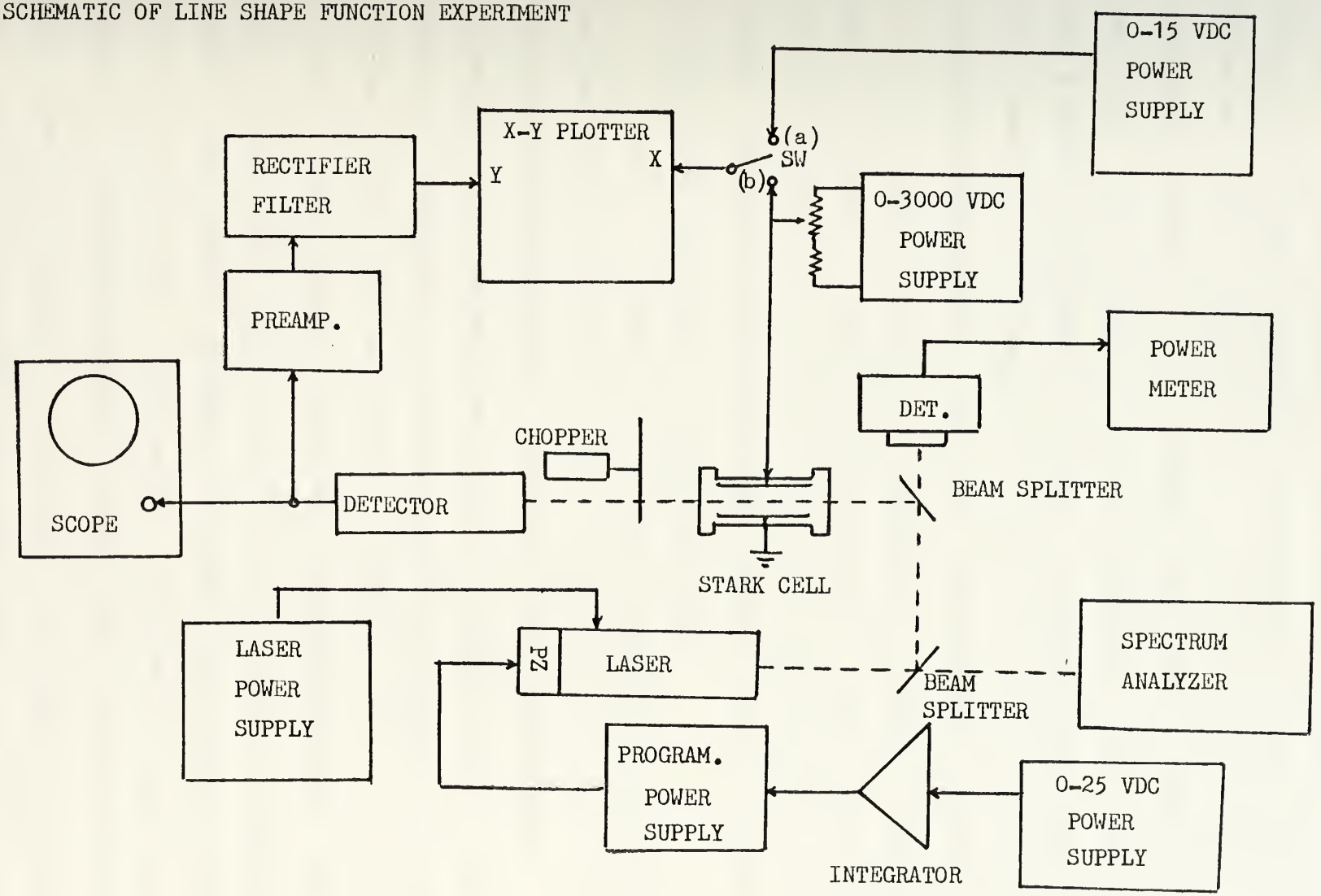

FIGURE 25

analyzer for the P(20) line. The cell was evacuated to 2×10^{-5} torr and used as a zero pressure reference. The Stark cell output intensity was measured by the pyroelectric detector. The y axis of the x - y plotter sampled the relative intensity of the chopped Stark cell output via the detector, amplifier and filtered rectifier. The x-axis of the plotter was manually set to a voltage proportional to the pressure of the NH_2D gas in the cell with the switch closed to position (a). NH_2D gas was obtained by mixing a 1 to 1 ratio of NH_3 and a commercially prepared sample of ND_3 in the cell. The gas was allowed to reach an equilibrium condition before the relative intensity measurements were taken. Figure 26 shows the experimental relative intensity of the P(20) transition vs NH_2D pressure.

An x - y plot of the relative modulated intensity vs the applied Stark cell bias voltage should provide the Stark shifted absorption lineshape. The experimental arrangement is the same as Figure 23 except that the D.C. Stark cell voltage is voltage-divided and fed to the x axis of the plotter with the switch in position (b). The laser is set to oscillate on the P(20) line and monitored. The NH_2D in the Stark cell is mixed in a 1:1 ratio as described above. The applied voltage to the cell was manually scanned from 0 - 3000 volts. Figures 27 - 34 show the experimental relative intensity vs applied Stark cell voltage for several NH_2D pressures and scan directions. An unexpected discontinuity evident on the graphs and while monitoring the pyroelectric detector output directly on an oscilloscope showed up at

RELATIVE INTENSITY vs NH_2D PRESSURE IN STARK CELL

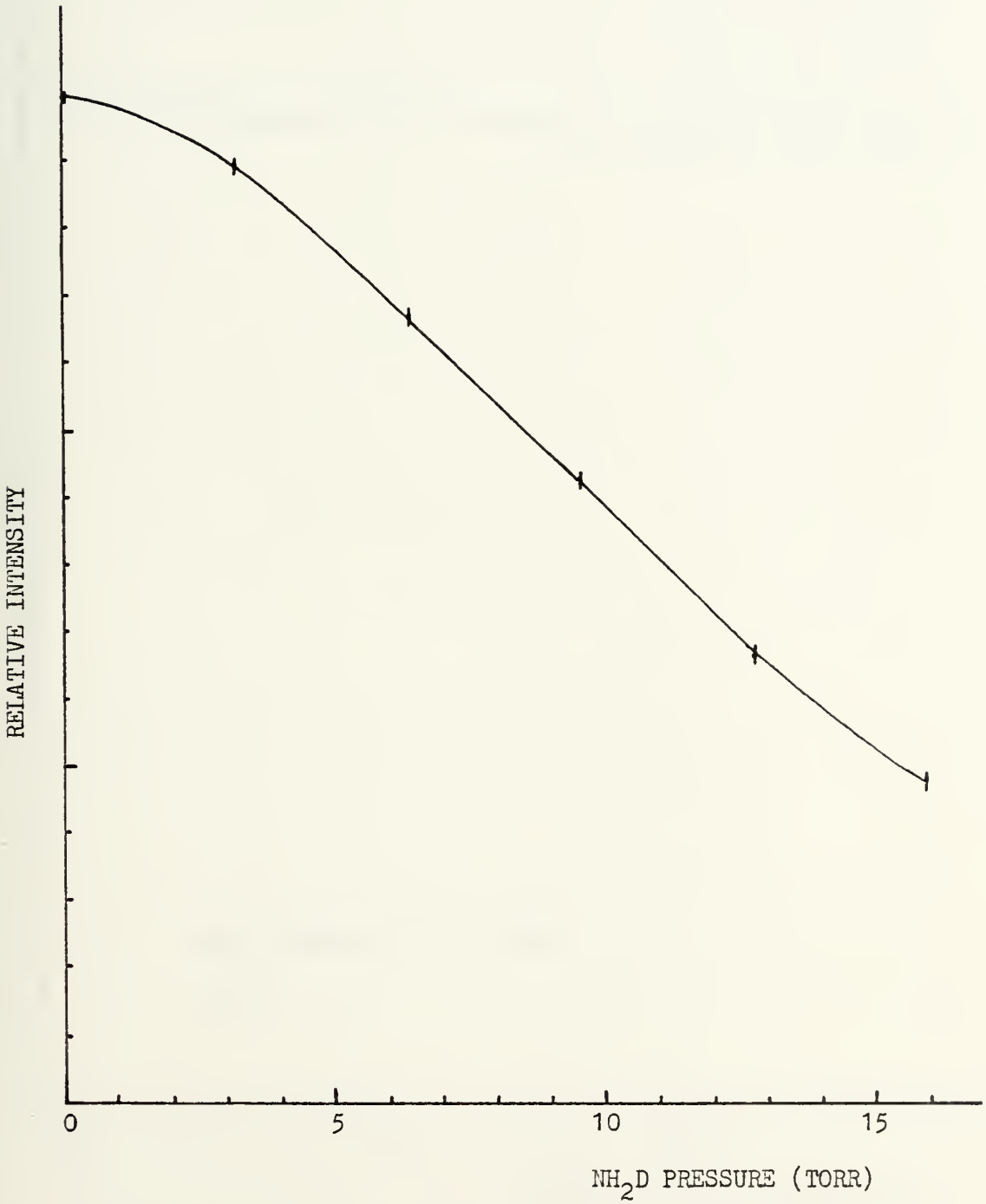

FIGURE 26

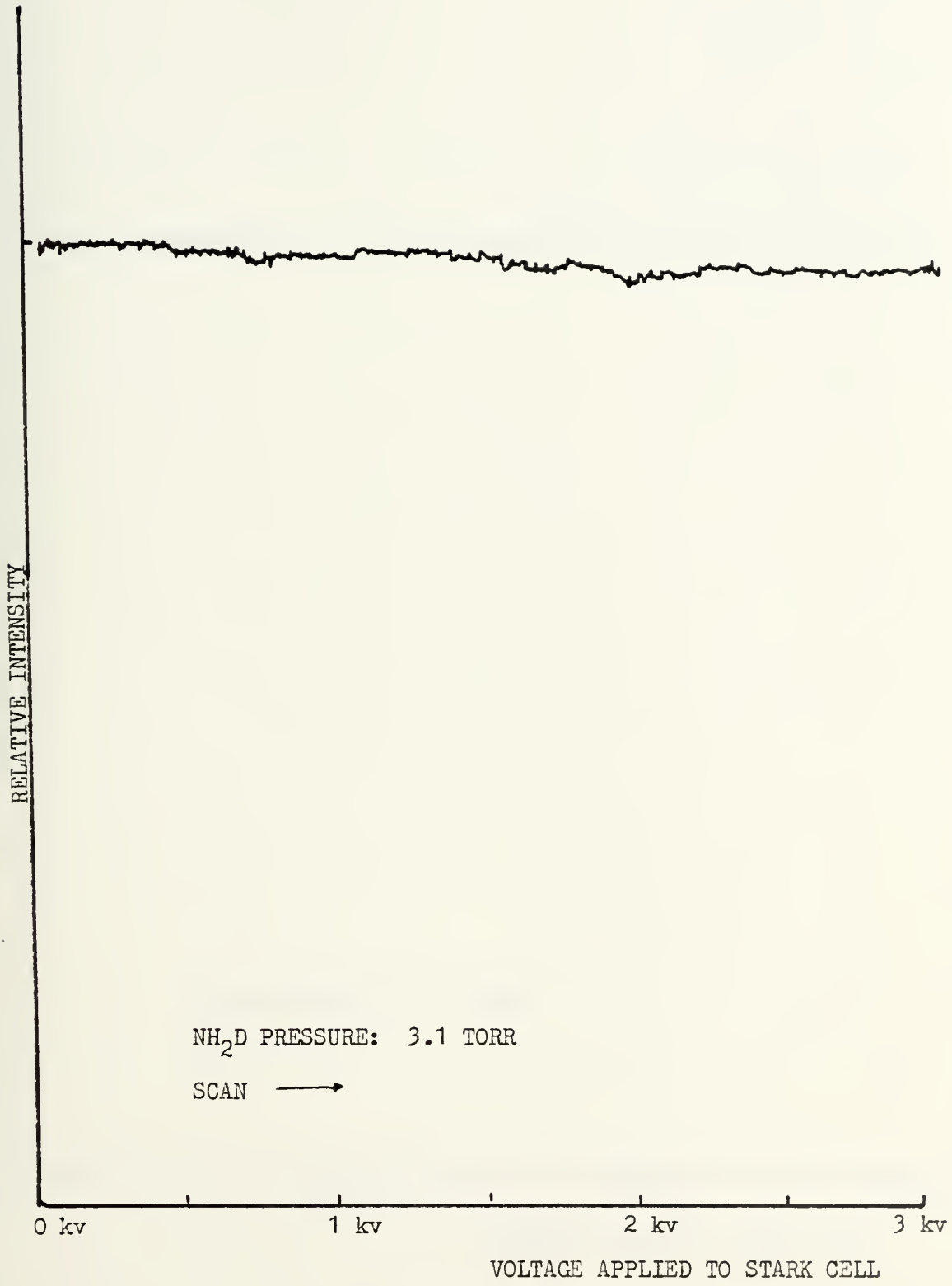
RELATIVE INTENSITY
NH2D PRESSURE: 3.1 TORR
SCAN
0 kv
1 kv
2 kv
3 kv
VOLTAGE APPLIED TO STARK CELL

FIGURE 27

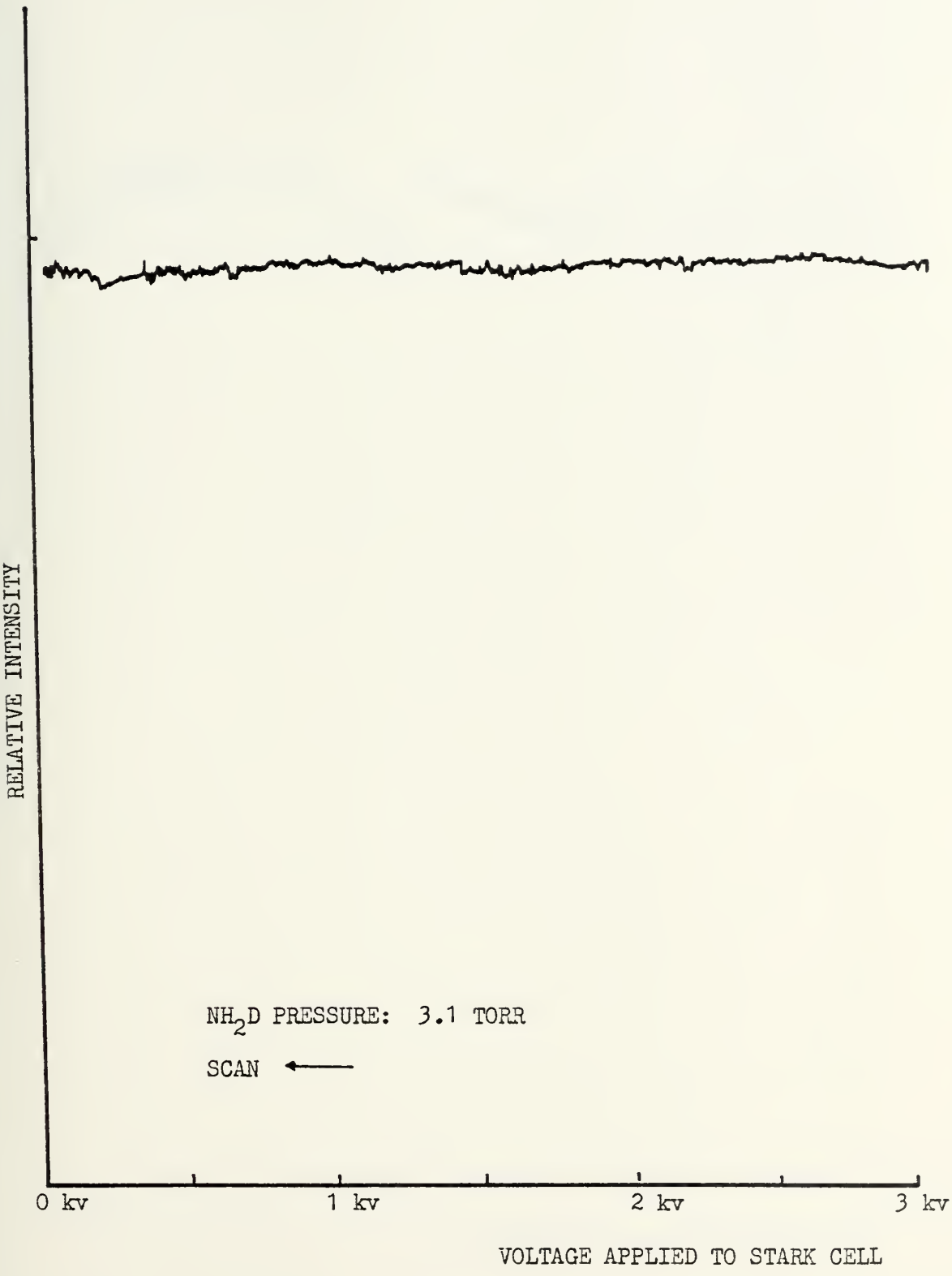
RELATIVE INTENSITY
NH_2D PRESSURE: 3.1 TORR
SCAN
0 kv
1 kv
2 kv
3 kv
VOLTAGE APPLIED TO STARK CELL

FIGURE 28

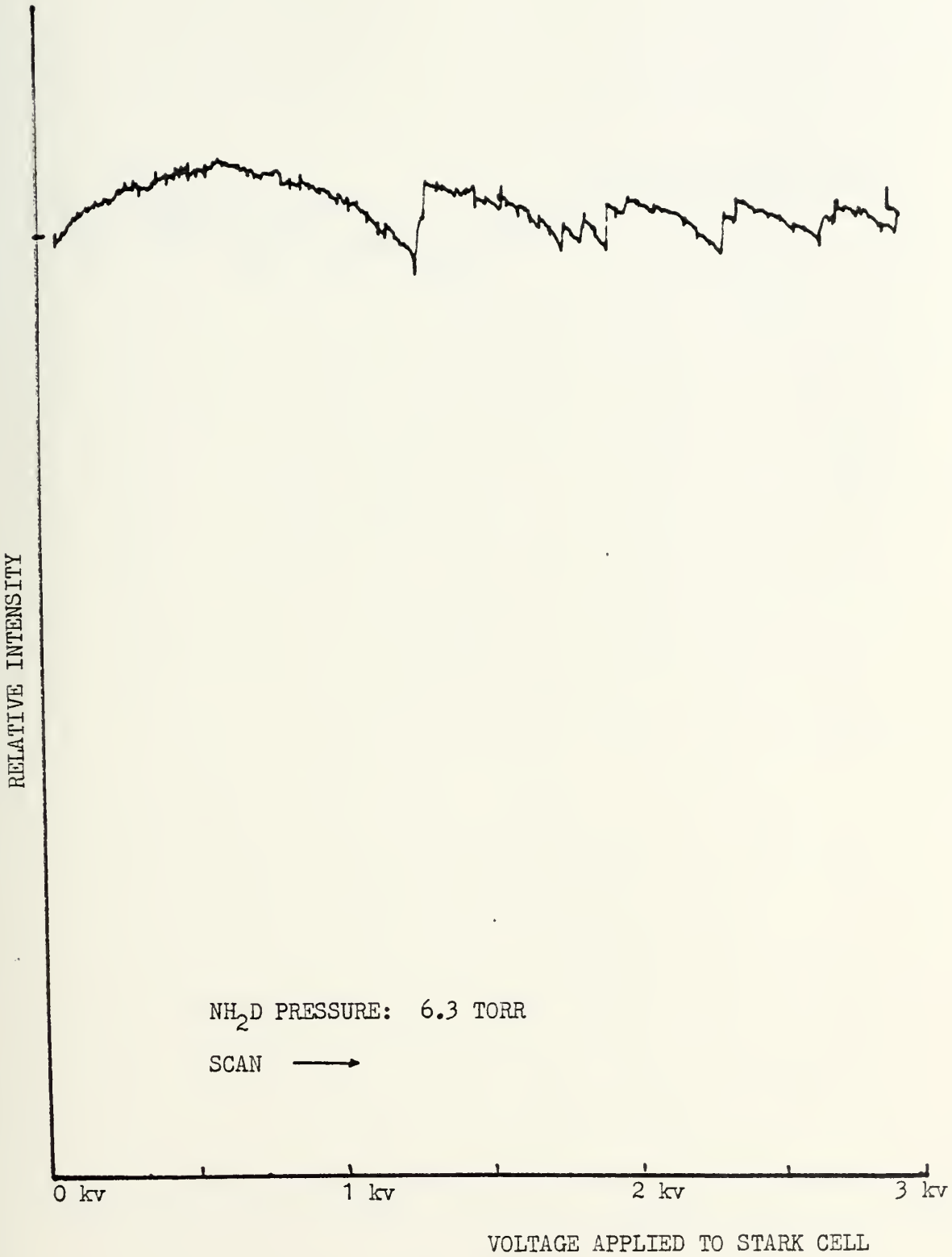
RELATIVE INTENSITY
NH_2D PRESSURE: 6.3 TORR
SCAN
0 kv
1 kv
2 kv
3 kv
VOLTAGE APPLIED TO STARK CELL

FIGURE 29

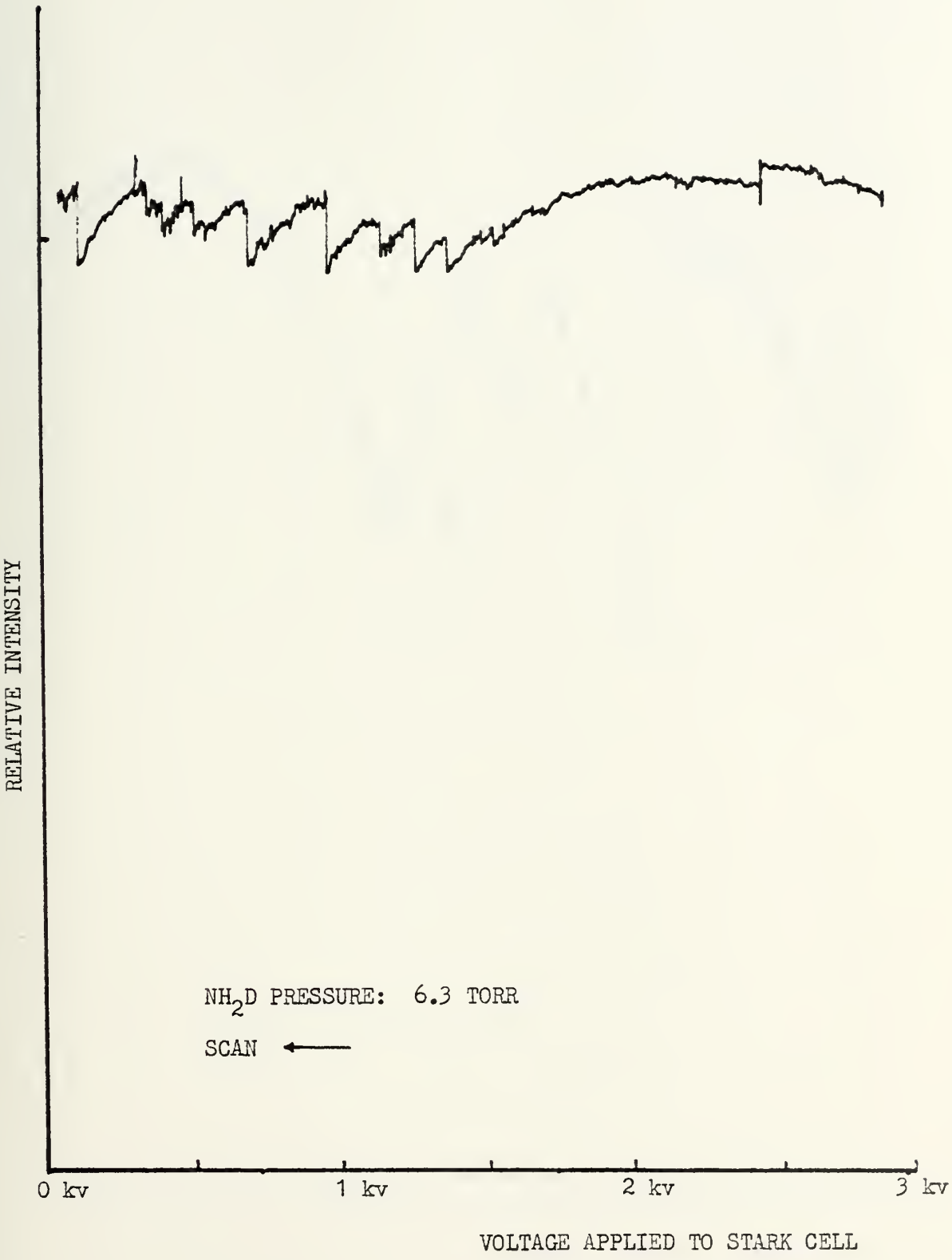
RELATIVE INTENSITY
NH_2D PRESSURE: 6.3 TORR
SCAN ←
0 kv
1 kv
2 kv
3 kv
VOLTAGE APPLIED TO STARK CELL

FIGURE 30

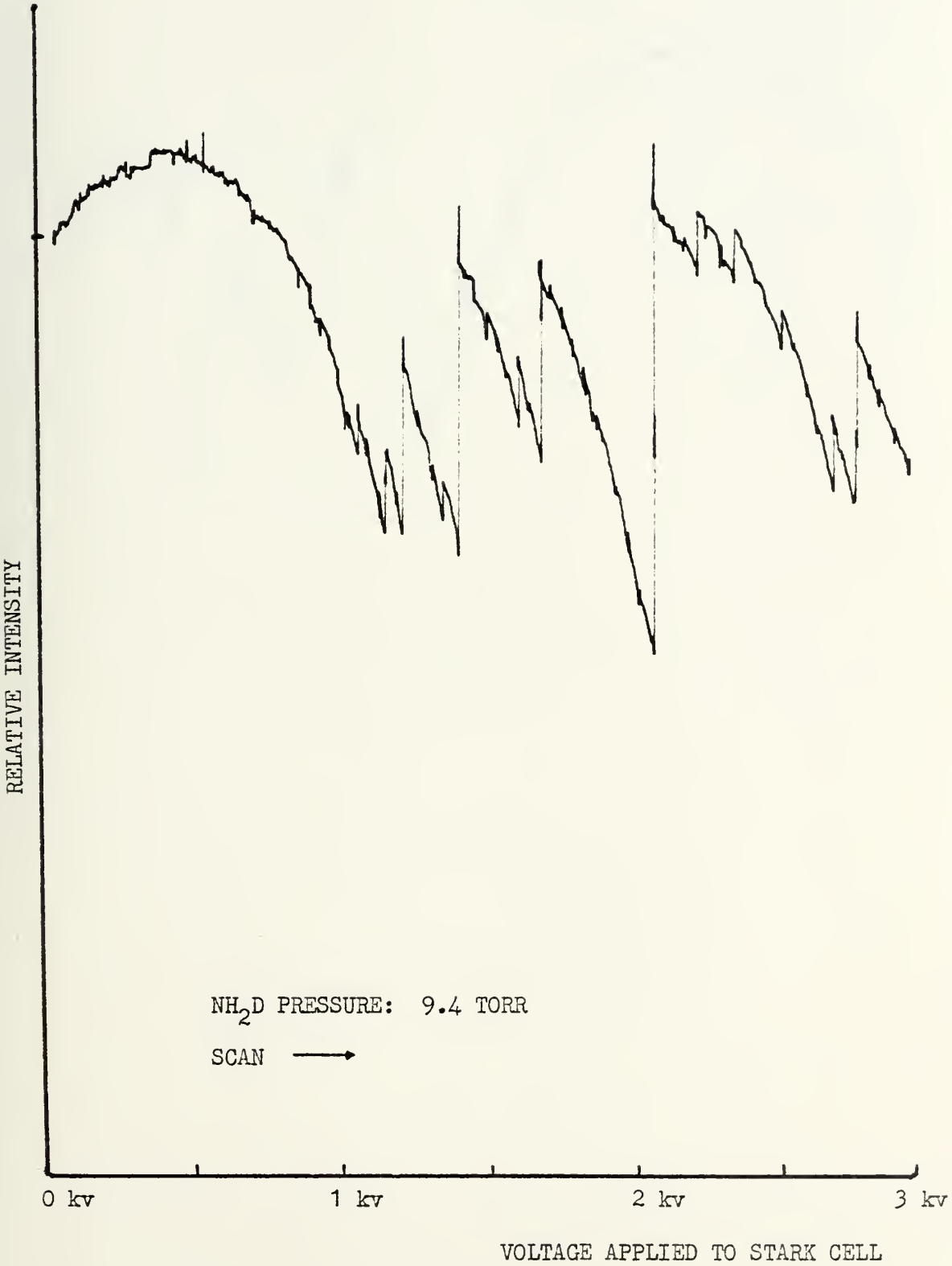
RELATIVE INTENSITY
NH_2D PRESSURE: 9.4 TORR
SCAN ⟶
0 kv
1 kv
2 kv
3 kv
VOLTAGE APPLIED TO STARK CELL

FIGURE 31

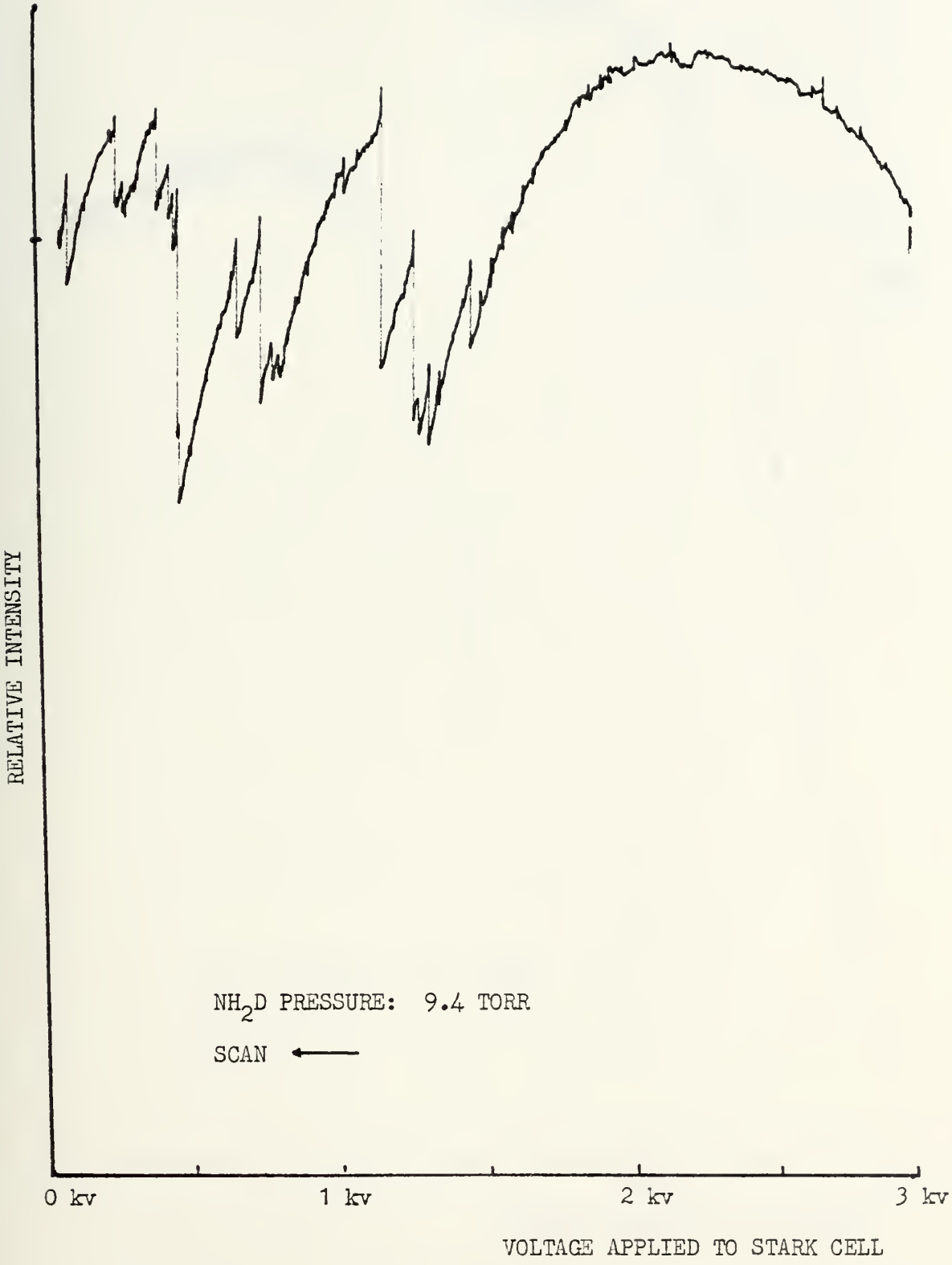
RELATIVE INTENSITY
NH_2D PRESSURE: 9.4 TORR
SCAN
0 kv
1 kv
2 kv
3 kv
VOLTAGE APPLIED TO STARK CELL

FIGURE 32

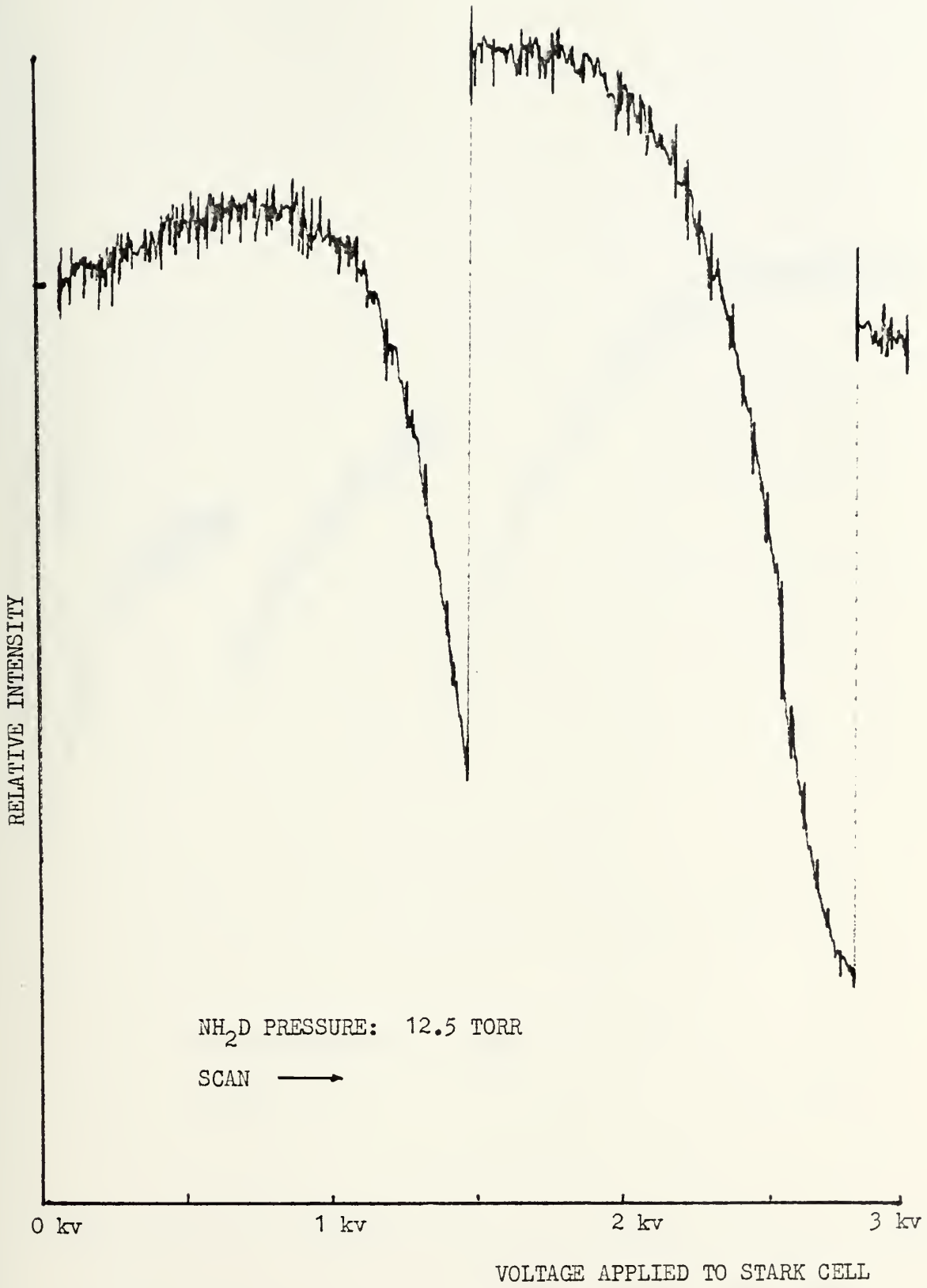
RELATIVE INTENSITY
NH_2D PRESSURE: 12.5 TORR
SCAN
0 kv
1 kv
2 kv
3 kv
VOLTAGE APPLIED TO STARK CELL

FIGURE 33

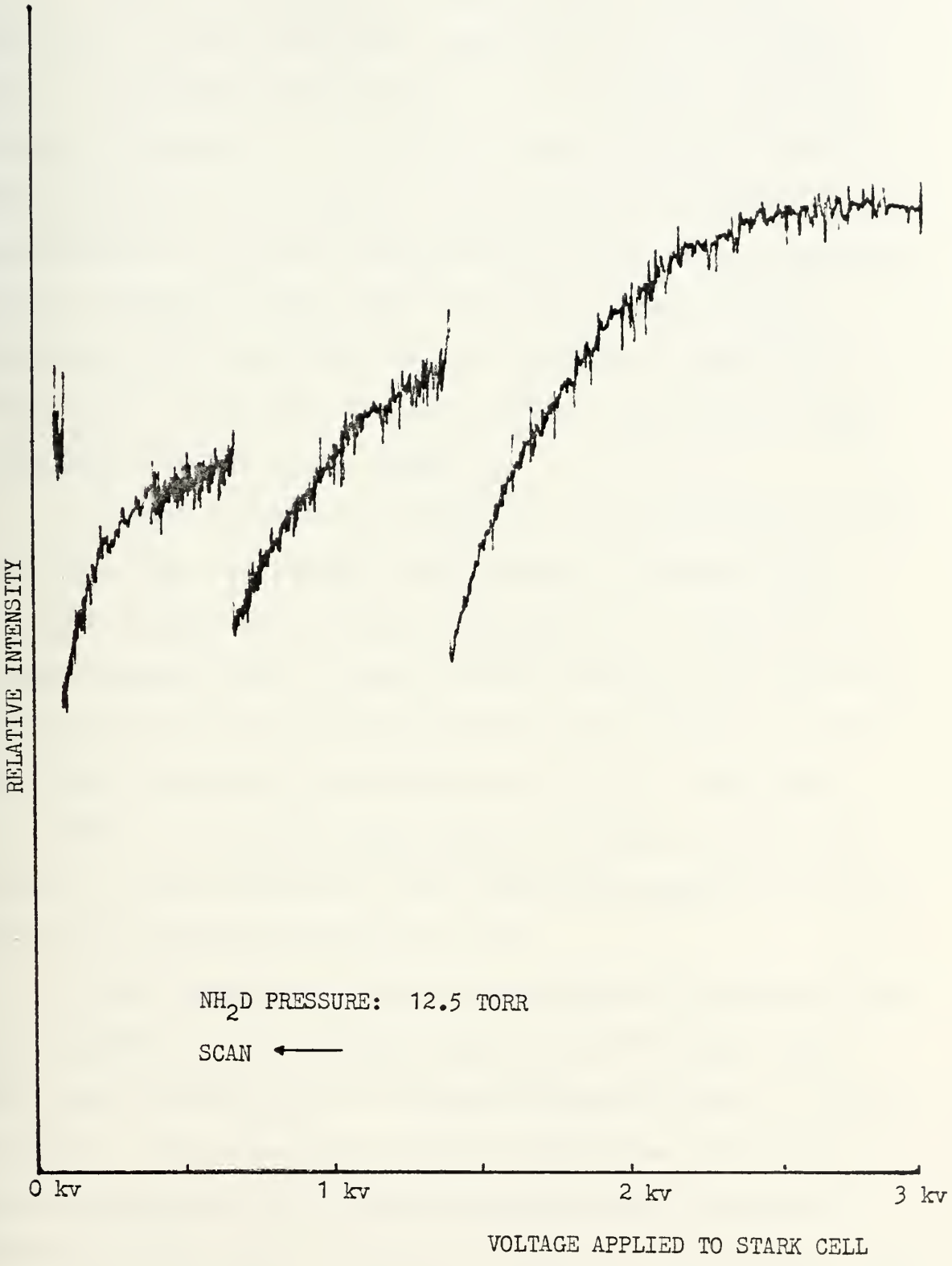
RELATIVE INTENSITY
NH_2D PRESSURE: 12.5 TORR
SCAN ←
0 kv
1 kv
2 kv
3 kv
VOLTAGE APPLIED TO STARK CELL

FIGURE 34

pressures above 5 torr. This abrupt change in the modulation of the laser made frequency stabilization impossible. Repetition of the experiment resulted in similar curves with no significant differences. It is evident from the curves in Figures 29 - 34 that the scan direction significantly effected the shape of the curve and location of the discontinuity, that the discontinuity occurred at different applied voltages to the Stark cell for different NH_2D pressures in the cell and that a substantial amount of modulation of the beam (as much as 50%) could be achieved using NH_2D and the Stark effect.

Closer inspection of Figures 29 - 34 indicated that the curve began to repeat itself after a discontinuity occurred independent of the scan direction. Figure 35 is an experimental plot of the relative intensity of the P(20) laser transition vs voltage applied to the Stark cell with the curves for both scan directions (a $\rightarrow$ 0 - 3000v and b $\rightarrow$ 3000 - 0v) on the same graph. It shows clearly the effect of scan direction on the plot and repetition of the curve shape after the discontinuity.

This repetition effect was studied by reversing the scan direction of the voltage applied to the Stark cell after each discontinuity yielding the plots shown in Figures 36 and 37. The curves did repeat themselves with basically the same shape and with the discontinuities occurring at different Stark cell voltages and relative intensities. The curves of Figures 36 and 37 could be retraced for both

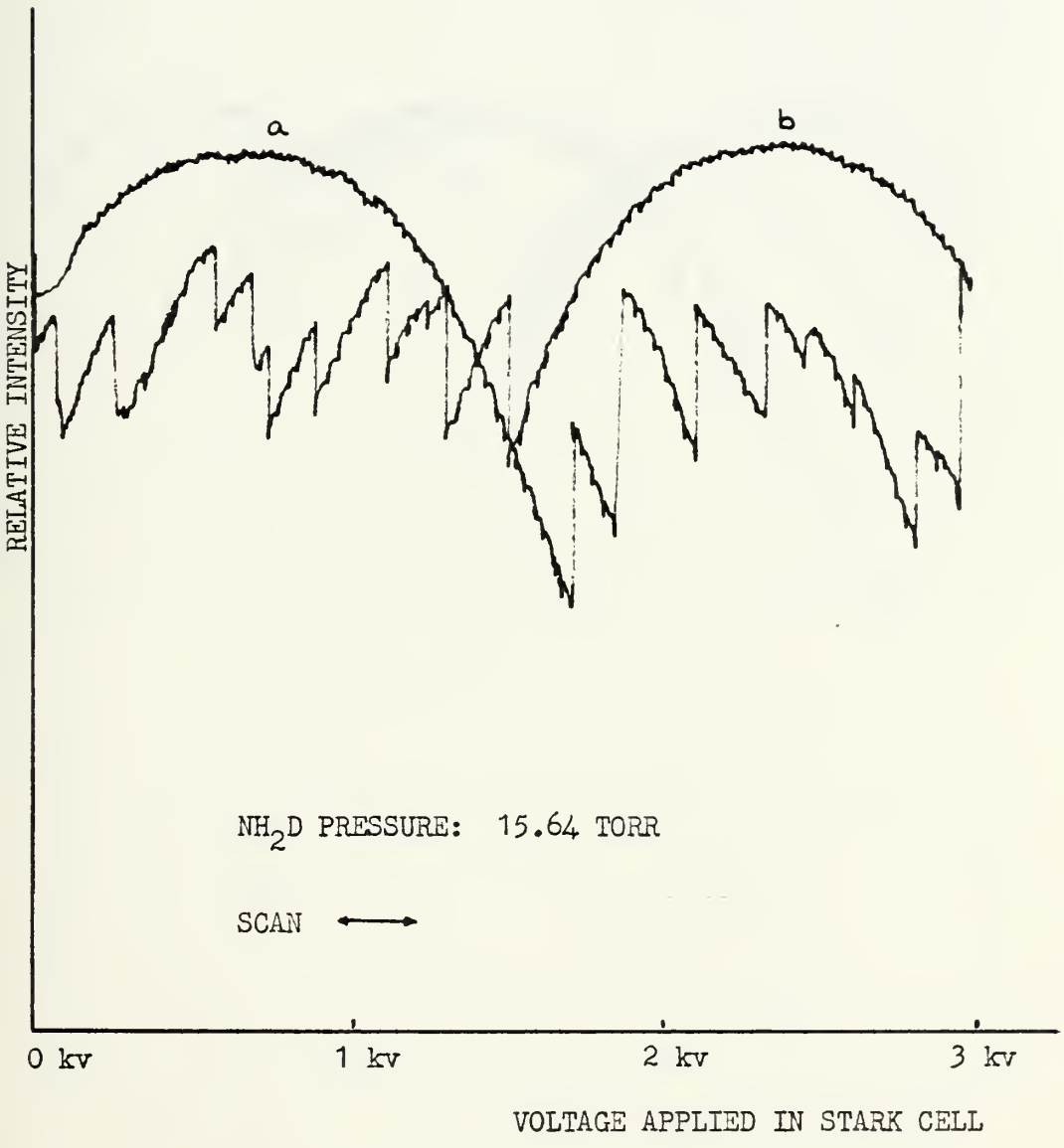
a
b
RELATIVE INTENSITY
NH2D PRESSURE: 15.64 TORR
SCAN
0 kv
1 kv
2 kv
3 kv
VOLTAGE APPLIED IN STARK CELL

FIGURE 35

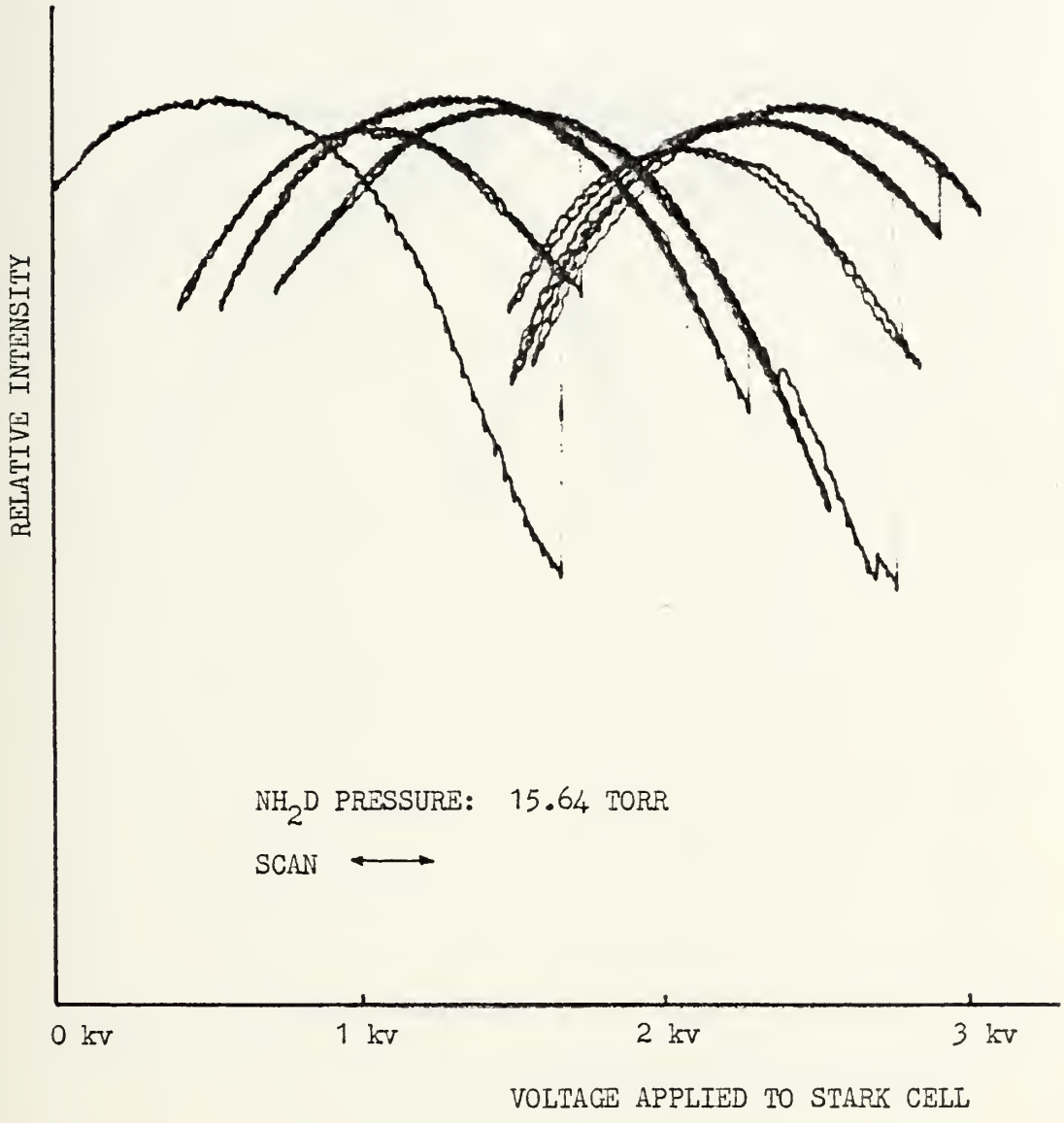
RELATIVE INTENSITY
NH_2D PRESSURE: 15.64 TORR
SCAN ⟷
0 kv
1 kv
2 kv
3 kv
VOLTAGE APPLIED TO STARK CELL

FIGURE 36

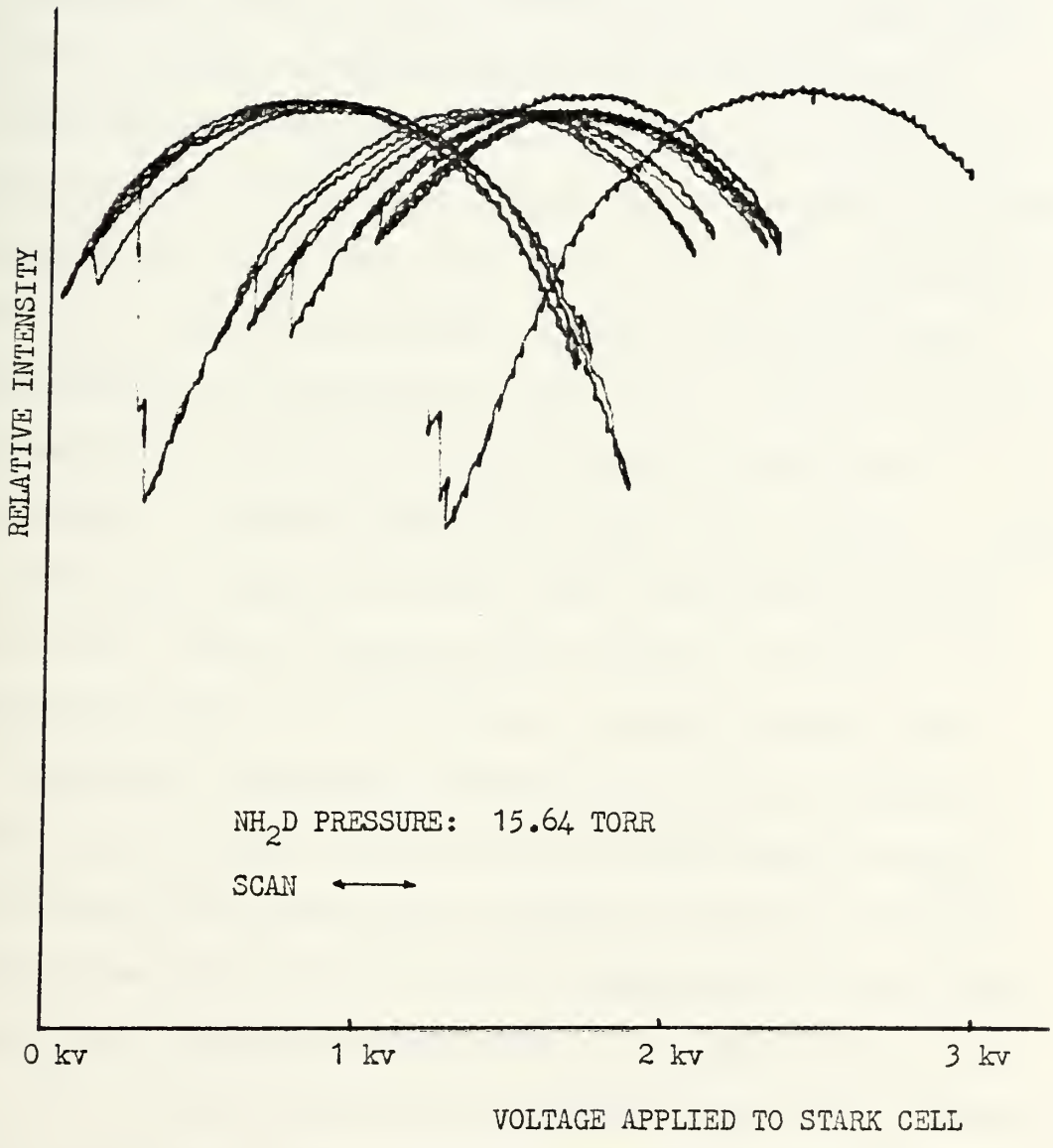
RELATIVE INTENSITY
NH_2D PRESSURE: 15.64 TORR
SCAN
0 kv
1 kv
2 kv
3 kv
VOLTAGE APPLIED TO STARK CELL

FIGURE 37

directions of scan provided the voltages corresponding to the discontinuity were not reached. Thus the shape of the irradiance is independent of scan direction.

In order to observe the operation of the dither mechanism an A.C. voltage was applied to one plate while the D.C. voltage on the cell was maintained at a voltage where sufficient modulation was observed but below the point where the discontinuity occurred. A 200Hz A.C. signal was supplied to one of the Stark plates from an audio oscillator amplified to 60 volts vms. The laser was set to oscillate on the P(20) transition and the chopper was removed from the experimental arrangement in Figure 25. The signal from the pyroelectric detector was fed directly into the oscilloscope. A 200Hz sinusoidal signal was observed. This 200Hz sinusoidal signal was lost when the laser was tuned off the P(20) line by changing the applied voltage to the piezoelectric driver in the laser. A scan through the laser's spectral signature revealed the expected results of modulation of the P(20) and P(14) laser lines by NH_2D. A 200Hz sinusoidal signal was evident on the oscilloscope for both these transitions with the amplitude of the signal for the P(14) line being about 50% of the amplitude of the signal for the P(20) line for the preset Stark cell voltage. Thus the Stark cell was actually modulating the laser beam and could produce a suitable signal for phase detection if the discontinuity could be corrected.

Attempts to determine the cause of the discontinuity were unsuccessful. The voltage across the cell was equal

to the supply voltage (0 - 3000VDC) with no detectable voltage drop existing that might have caused a discontinuity. No current could be detected through the cell which would have indicated ionization of the gas or cell breakdown. In order to determine if perhaps the beam was being steered off the detector by a refractive index gradient in the cell, rather than the gas modulating the beam, a detector was scanned across the output of the cell when the applied voltage on the cell was at a point where it was able to modulate the P(20) line. The pyroelectric detector was mounted on a moveable table and scanned across the Stark cell output signal giving a relative plot of intensity vs position. The signal from the detector was amplified, filtered and rectified and then fed into the y channel of a time base plotter. The scan rate of the detector was fixed so that the time base could be translated into a position measurement. Figure 38(a) shows the beam shape out of the cell as a function of position for zero voltage applied to the cell and Figure 38(b) the beam shape out of the cell when the beam was being modulated with an applied Stark cell voltage. The intensity of the beam is reduced with no noticable shift in position of the beam. The detector was positioned at the point of maximum intensity and a D.C. bias voltage was applied to modulate the base. The detector then moved to determine if the beam was being steered to the left or right, up or down. Figure 39 is a graph of intensity vs time and shows that the beam was not

EXPERIMENTAL PLOT TO DETERMINE IF A REFRACTIVE INDEX GRADIENT EXISTED IN THE STARK CELL.

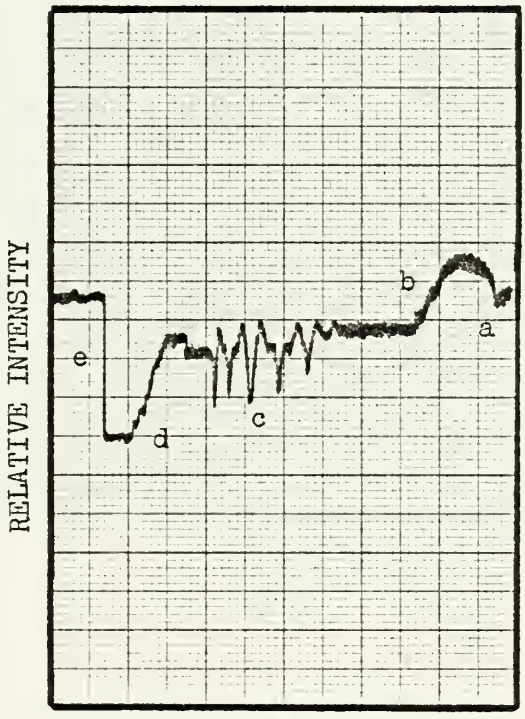

POINT ON GRAPH	EXPLANATION
a	Stark Cell Voltage Equals Zero
b	Stark Cell Coltage Increased to Modulate Laser Beam (Intensity Decreased)
c	Detector Moved to Determine if Beam was being Steered
d	Stark Cell Voltage Increased to Point of Discontinuity
e	Discontinuity (Intensity Jumps to a Zero Modulation Condition)

FIGURE 39

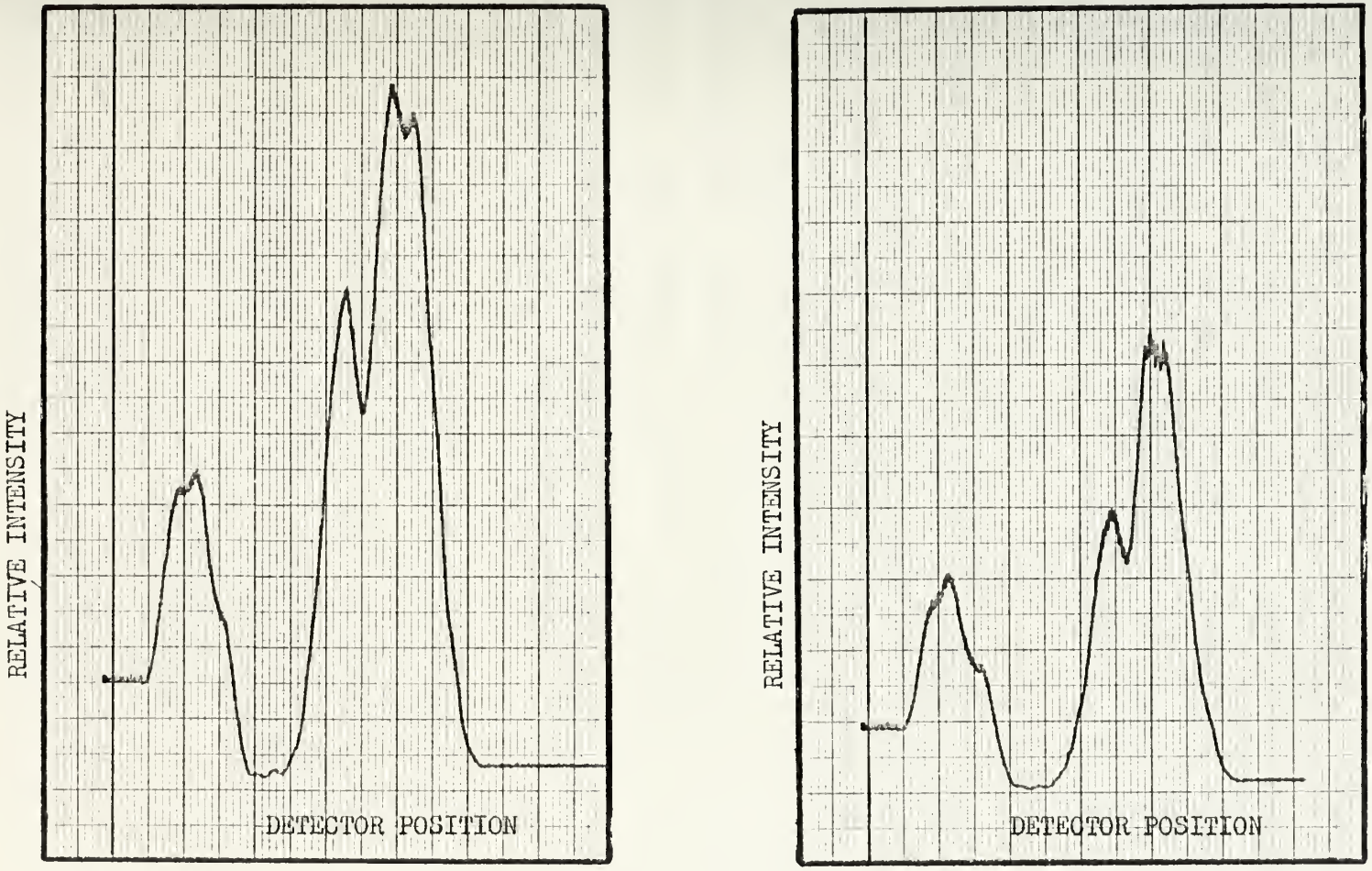
RELATIVE INTENSITY
DETECTOR POSITION
(a)
RELATIVE INTENSITY
DETECTOR POSITION
(b)

FIGURE 38

being steered. The intensity as the detector was moved did not exceed the modulated intensity. Again the discontinuity is evident as the applied voltage was increased.

The movable detector was placed at various positions in Figure 22 to determine if the beam shape was due to reflections in the cell or prior to the cell itself. Figure 40 shows the relative intensity beam profile of the laser at three positions prior to the cell: 40(a) directly out of the laser prior to beam splitter No. 1, 40(b) between beam splitters No. 1 and No. 2 and 40(c) between beam splitter No. 2 and the cell. It appears that the germanium beam splitters cause some distortion of the beam and contribute to the distorted shape of the beam out of the Stark cell. The profile to the left of the main profile in Figures 38(a) and 38(b) was probably caused by reflection from back surface of the parallel sided Ge beam splitter since it appears to be a mirror image of the main profile.

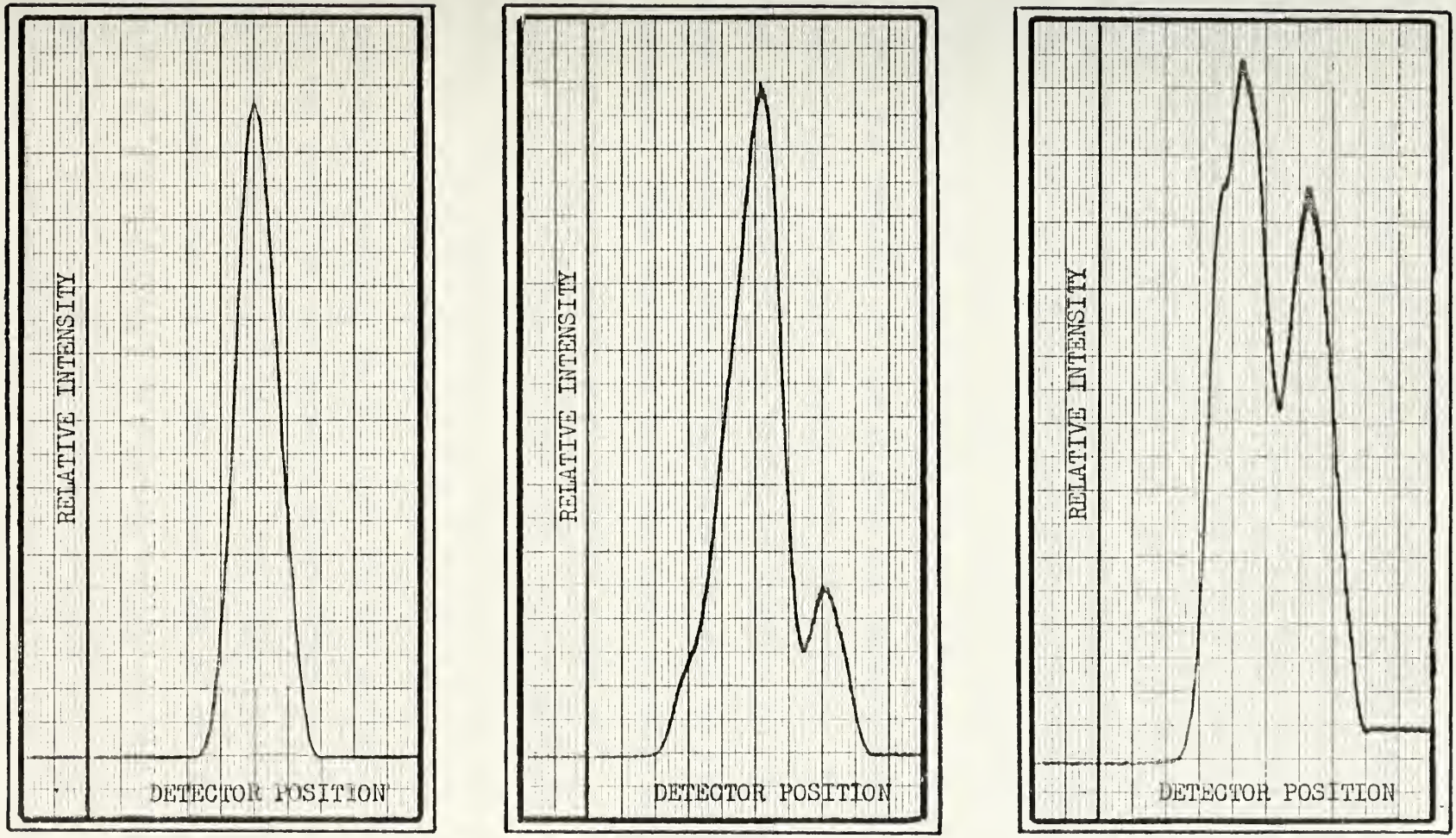
RELATIVE INTENSITY
DETECTOR POSITION
(a)
RELATIVE INTENSITY
DETECTOR POSITION
(b)
RELATIVE INTENSITY
DETECTOR POSITION
(c)

FIGURE 40

3. New Stark Cell Design

In order to determine if the discontinuity was due to the nonuniformity of Stark cell plate spacing in the cell or the cell design itself, another Stark cell patterned after one described in Reference 31 was built. The new Stark cell design with its specifications is shown in Figure 41. Its design was an attempt to reduce the applied voltage requirements by reducing the plate spacing to 3mm and eliminating the need for spacers to keep the plates parallel by attaching the plates to plexiglas holders with screws. This design allows for removal of the plates for modification, cleaning or substitution of a new design for the plates. The plate thickness can be used to vary their separation in the cell. The edges and ends of the plates were rounded to help prevent breakdown. The end caps hold the NaCl windows and simplify holding of the windows when modifying the cell. The cell held a good vacuum. The cell was filled with approximately 2 torr of NH_2D with breakdown and ionization of the gas occurring at 1000 volts. The breakdown was observed to occur along the edges and especially at the ends of the plates. It is believed that the inability to machine round edges is the primary cause for breakdown. Investigations into fabrication of plates with round edges, insulating the edges, use of geometrics other than strictly flat plates and electroplating of the plates on an insulator need to be conducted to produce a viable cell for frequency stabilization using Stark cell techniques. The present cell can be used to test plate designs and fabrication techniques without having to build a new cell each time.

NEW STARK CELL DESIGN WITH INTERCHANGEABLE PLATES

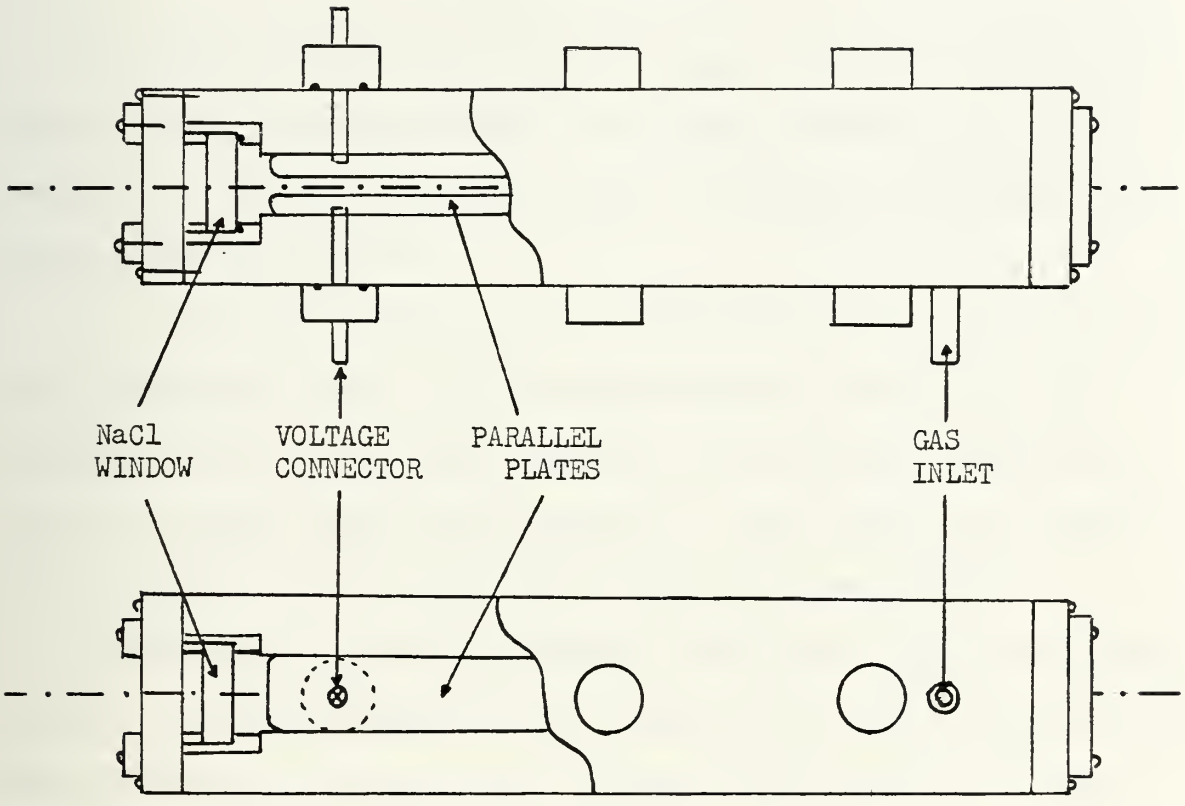

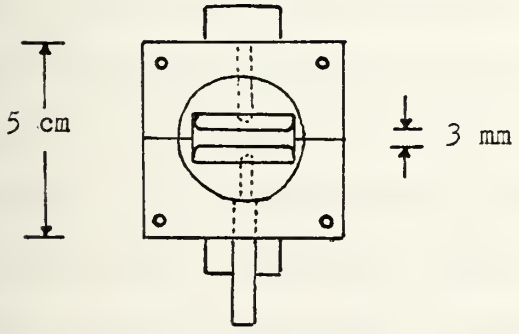

SPECIFICATIONS

PLATE:

MATERIAL	ALUMINUM
LENGTH	15.0 cm
WIDTH	2.5 cm
SEPARATION	3.0 mm

CELL:

MATERIAL	PLEXIGLAS

FIGURE 41

IV. CONCLUSIONS

A stable high voltage power supply (Sylvania 941S) run from a stable line regulator was found suitable as a power source for the Sylvania CO_2 Model 941 Laser in a Stark cell stabilization system.

A servo loop integrator was designed and built allowing the correction signal to the piezoelectric driver to be proportional to the time integral of the error signal produced by phase sensitive detection. The integrator used in the feedback system should provide increased stability.

A method for scanning through the laser's spectral signature to find the required P(20) transition incorporating the same integrator used in the feedback stabilization system was demonstrated and discussed.

A Stark cell was tested to determine its characteristics for use in the stabilization system. It was found that a discontinuity existed in the cell's lineshape function which made it unsuitable for use in a phase detection stabilization scheme. The cause of the discontinuity could not be determined. A voltage drop across the cell, ionization of the NH_2D gas, and beam steering caused by an index gradient being created in the cell were eliminated as possible causes.

A second new Stark cell with the capability of modifying or changing the cell plates was designed and built to determine if the discontinuity found in the first cell was inherent

in the cell design or caused by a factor outside the cell. Breakdown occurred in the second cell prior to the field strength required for modulation making the second cell unsuitable for use in the system. The fabrication of the plates in the new cell was the major cause for breakdown. Further investigation needs to be conducted in the Stark cell plate design and fabrication to prevent breakdown inside the cell.

Production of an error signal using a pyroelectric detector was demonstrated using the first Stark cell but was unsuitable for phase sensitive detection due to the discontinuity in the lineshape. It is expected that the successful fabrication and test of a Stark cell will produce a Stark stabilized CO_2 laser in the assembled system. This system frequency stabilized on the P(20) transition is expected to be operational in both the laboratory and the field.

APPENDIX A

MODEL 941 SYLVANIA LASER SPECIFICATIONS

Output wavelength: 10.6 μm

Power output: 3 watts

Beam divergence: 4 mrad

Beam diameter to 1/e point: 4 mm

Beam polarization: vertical

Cavity length: 45 cm

Bore diameter: 6 mm

Cooling requirements: tap water @ 15 to 30 ml/s

Output mirror: 70% reflecting, dielectric flat

Piezoelectric mirror: 100% reflecting, 300 cm radius of curvature

Piezoelectric $\frac{\Delta L}{\Delta V}$ parameter as given by

Sylvania: -4×10^{-3} m/volt

Laser voltage: 14 kV @ 7.6 ma

Tube voltage: 9.5 kV @ 7.6 ma

Series ballast resistance: 600 kΩ

Equivalent tube resistance @ 7.6 ma: 1.27 M

Pressure broadened linewidth: 100 MHz

Doppler broadened linewidth: 50 MHz

$\frac{c}{2L}$ mode separation: 333 MHz

Cavity linewidth: 19 MHz

APPENDIX B

OPTICAL ENGINEERING CO_2 LASER SPECTRUM ANALYZER

The CO_2 Laser Spectrum Analyzer is an infrared grating spectroscope designed simultaneously to monitor and visually display through the use of a calibrated thermal sensitive screen which darkens at points corresponding to the wavelength at which the laser is operating. The optical design of the instrument is basically an Ebert Mount using a plane grating and a spherical mirror. Folding mirrors are used to reduce the length and the design modified so that the display screen can be located near the top of the instrument. Incorrect positioning of the instrument so that the laser light does not enter within the acceptance cone, will not create incorrect readings but simply cause the light to miss some element in the optical path and not reach the display screen.

Figure 1B is a side-view of the spectrum analyzer showing its essential components. In normal operation the portion of the laser beam which passes through the slit will strike a flat mirror which folds the optical beam and introduces a slight vertical angular component to the direction of the beam. The light then strikes a concave mirror which collimates the divergence introduced by the diffraction of the slit. The light then is reflected to

the diffraction grating. The grating is rigidly mounted on the flat mirror and held at a fixed angle. Only the light which is diffracted into the first order of the diffraction grating continues on to strike the curved mirror for a second time which focuses the image on the display screen. Each laser wavelength leaves the grating at a unique angle and is imaged at a different point on the calibrated scale.

The specifications for the spectrum analyzer are given in Table I-B.

Side View of Spectrum Analyzer

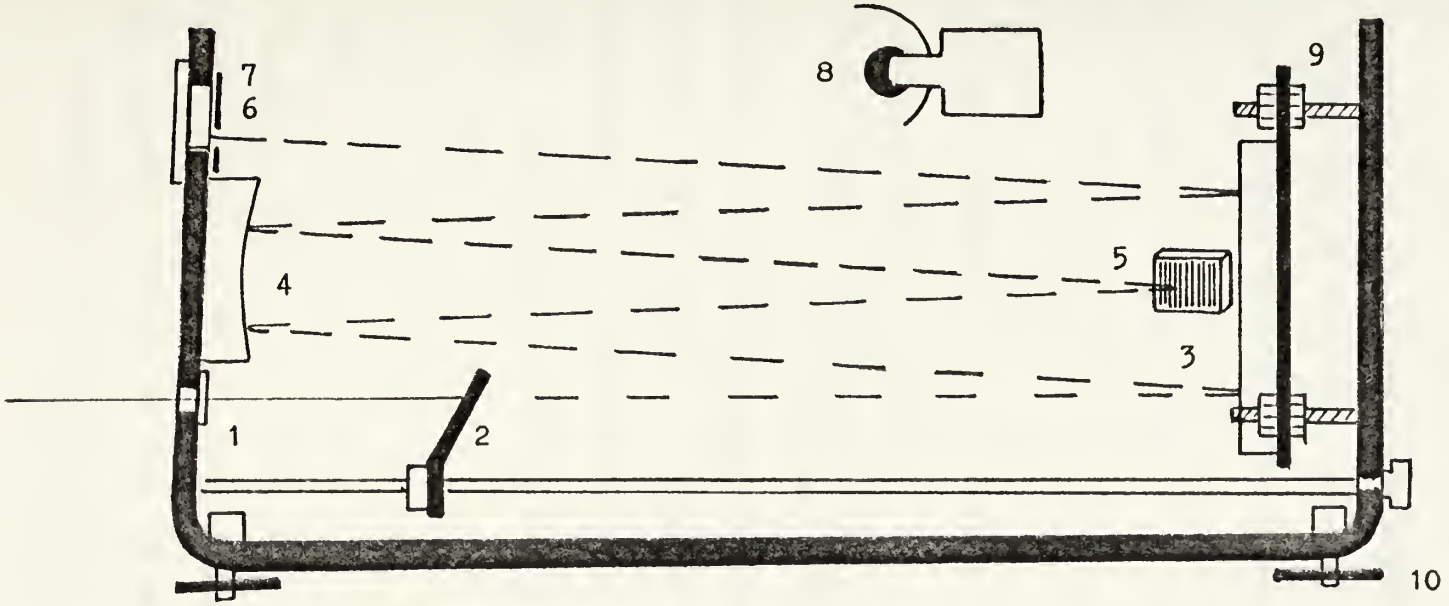

(1) Variable slit, (2) Beam Monitor, (3) Flat Mirror, (4) Concave mirror, (5) Diffraction grating, (6) Thermal Sensitive Display Screen, (7) Calibrated scale, (8) Ultraviolet lamp, (9) Calibration adjustment screws, (10) Adjustable legs.

FIGURE B-1

TABLE I-B

SPECIFICATIONS

The following is a list of the specifications for the Model 16A CO_2 Laser Spectrum Analyzer.

Wavelength range: 9.1 to 11.3

Resolution: .003 (0.3 cm^{-1})

Maximum power: 75 watts

Minimum power (focused): 0.01 watts

Screen responce time: ¼ second

Grating efficiency: 90% horizontal polarization
30% vertical polarization

Optical design: 3/4 meter modified Ebert

Total optical path length: 2.3 meters

Acceptance angle: 2.5° horizontal, 1.5° vertical

Slit width: adjustable - closed to 0.6 mm

Weight: 12 lbs.

Length: 18"

Width: 9.9"

Minimum height: 6.5"

Elevation of slit: 2.5" to 3.8" (adjustable)

Electrical power: 115 V, 60 Hz, 10 watts

$^{12}C^{16}O_2$ vibrational-rotational lines identified:

$00^{\circ}1 - 02^{\circ}0$
P2 to P62 and R2 to R60
$00^{\circ}1 - 10^{\circ}0$
P2 to P56 and R2 to R60
$01^{1}1 - 11^{1}0$
P19 to P45

APPENDIX C

SERVO LOOP INTEGRATOR

The output of an ideal integrator is a voltage proportional to the integral of the input voltage; or in other words, the output is proportional to the product of the amplitude and duration of the input. The integrator performs this mathematical operation on an instantaneous basis. The result is an output exactly proportional to the area under a wave form.

The circuit in Figure B-1 performs integration using a μA 747 dual frequency compensated operational amplifier to force the same current through both R_1 and C_f. The voltage across the feedback capacitor is related to capacitor current by

$$V_c = - \frac{1}{C_f} \int i_f \, dt \qquad (1C)$$

Since the circuit causes i_f to equal the input current ($i_i = {}^{v_i}/R_1$)

$$V_c = V_o = - \frac{1}{R_1 C_f} \int v_i \, dt \qquad (2C)$$

The gain of the circuit is given by ${}^{1}/R_1 C_f$. Thus the output voltage will change by $-{}^{1}/C_f R_1$ volts/sec for each volt of output.

The bias voltage, V_b, and variable voltage offset null resistor, R_V, the drift inherent in the integrator. The switch, S_r, will reset the integrator to zero.

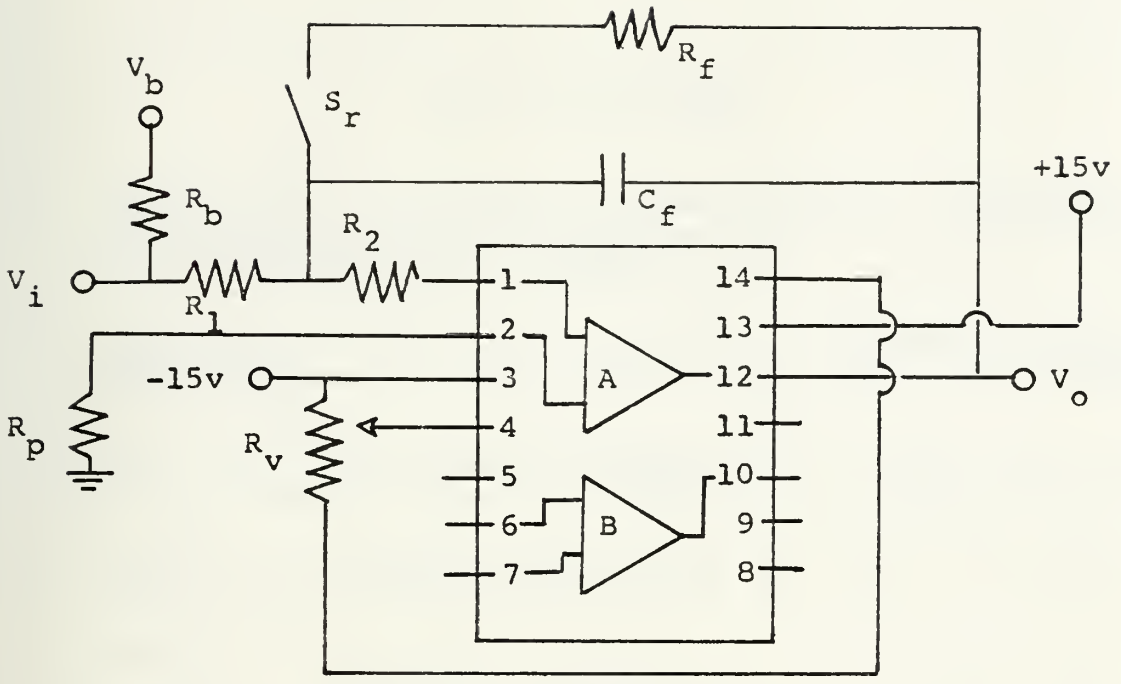

SERVO LOOP INTEGRATOR CIRCUIT

SPECIFICATIONS:

OPERATIONAL AMPLIFIER: μA 747 DUAL FREQUENCY COMPENSATED

$R_1 = R_p = R_b = 1\ M\Omega$
$R_2 = 10\ k\Omega$
$R_f = 1\ k\Omega$
$C_f = 1\ \mu f$
$R_v = 10\ k\Omega$ (variable)
Gain = $^{-1}/R_1C_f = -1$
V_i = input voltage
V_o = output voltage
V_b = bias voltage
S_r = reset switch

FIGURE C-1

LIST OF REFERENCES

1. Herzberg, G., "Infrared and Raman Spectra", Molecular Spectra and Molecular Structure, Vol. 2, pp. 370 - 399, Van Nostrand Reinhold Company, 1945.

2. Tyte, D.C., "Carbon Dioxide Lasers", Advances in Quantum Electronics I, ed. D.W. Goodwin, pp. 131 - 135, Academic Press, 1970.

3. Cheo, P.K., "CO_2 Lasers", Lasers, Vol. 3, ed. A.K. Levine and A.J. DeMaria, pp. 127 - 129, Marcel Dekker, Inc., 1971.

4. Svelto, O., Principles of Lasers, pp. 83 - 87, Plenum Press, 1976.

5. Svelto, O., Principles of Lasers, p. 87, Plenum Press, 1976.

6. Cheo, P.K., "CO_2 Lasers", Lasers, Vol. 3, ed. A.K. Levine and A.J. DeMaria, p. 144, Marcel Dekker, Inc. 1971.

7. Cheo, P.K., "CO_2 Lasers", Lasers, Vol. 3, ed. A.K. Levine and A.J. DeMaria, p. 142, Marcel Dekker, Inc. 1971.

8. Ferrarid, A. and Sona, A., "Gaseous Laser", Lasers and Their Applications, ed. A. Sona, p. 201, Gordon and Breach, 1976.

9. Yariv, A., Introduction to Optical Electronics, 2nd Ed., p. 92, Holt Rinehart Winston, 1976.

10. Yariv, A., Introduction to Optical Electronics, 2nd Ed., p. 93, Holt Rinehart Winston, 1976.

11. Svelto, O., Principles of Lasers, pp. 46 - 55, Plenum Press, 1976.

12. Townes, C.H. and Schawlow, A.L., Microwave Spectroscopy, p. 375, McGraw-Hill, 1955.

13. Brown, D., Frequency Control of a CO_2 Laser Using Stark Cell Stabilization, M.S. Thesis, Naval Postgraduate School, Monterey, 1979.

14. Yariv, A., Introduction to Optical Electronics, 2nd Ed., pp. 75 - 94 and 113 - 118, Holt Rinehart Winston, 1976.

15. Freed, C., "Design and Short-Term Stability of Single Frequency CO_2 Lasers", IEEE Journal of Quantum Electronics, Vol. QE-4, No. 6, pp. 404 - 408, June, 1968.

16. Mocker, Hans W., "A 10.6 μm Optical Heterodyne Communication System", Applied Optics, Vol. 8, No. 3, pp. 677 - 684, March, 1969.

17. Cheo, P.K., "CO_2 Lasers", Lasers, Vol. 3, ed. A.K. Levine and A.J. DeMaria, pp. 201 - 202, Marcel Dekker, Inc., 1971.

18. Mocker, Hans W., "Rotational Level Competition in CO_2 Lasers", IEEE Journal of Quantum Electronics, Vol. QE-4, No. 11, pp. 769 - 776, November, 1968.

19. Townes, C.H. and Schawlow, A.L., Microwave Spectroscopy, pp. 248 - 250, McGraw-Hill, 1955.

20. Townes, C.H. and Schawlow, A.L., Microwave Spectroscopy, pp. 250 - 255, McGraw-Hill, 1955.

21. Landman, A., Marantz, H., Early, V., "Light Modulation by Means of the Stark Effect in Molecular Gases - Application to CO_2 Laser", Applied Physics Letters, Vol. 15, No. 11, pp. 357 - 360, December, 1969.

22. Jensen, R.E., Tobin, M.S., "An Investigation of Gases for Stark Modulating the CO_2 Laser", IEEE Journal of Quantum Electronics, Vol. QE-8, No. 2, pp. 34 - 38, February, 1972.

23. Martin, J.M., Corcoran, V.J., Smith, W.T., "Identification of Absorption Lines in Gases Used to Modulate the CO_2 Laser", IEEE Journal of Quantum Electronics, Vol. QE-10, pp. 191 - 195, February, 1974.

24. Brewer, R.G., Kelly, M.J., Javan, A.,"Precision Infrared Stark Spectra of NH_2D Using Lamp Dip", Physical Review Letters, Vol. 23, No. 11, pp. 559 - 563, September, 1969.

25. Kelly, M.J., Francke, R.E., and Feld, M.S., "Rotational-Vibrational Spectroscopy of NH_2D Using High-Resolution Laser Techniques", Journal of Chemical Physics, Vol. 53, pp. 2979 - 2980, 1970.

26. Nussmeier, T.A. and Abrams, R.L., "Stark Cell Stabilization of CO_2 Laser Lines", Applied Physics Letters, Vol. 19, pp. 503 - 506, December, 1971.

27. Plant, T.K., and Abrams, R.L., "Broadening and Absorption Coefficients in $N^{14}H_2D$", Journal of Applied Physics, Vol. 47, No. 9, pp. 4006 - 4008, September, 1976.

28. Claspy, P.C. and Pao, Yoh-Han, "Basic Characteristics of High-Frequency Stark-Effect Modulation of CO_2 Lasers", IEEE Journal of Quantum Electronics, Vol. QE-7, No. 11, pp. 512 - 519, November, 1971.

29. Hall, D.R., Jenkins, R.M., Gorton, E.K., "A Frequency-Stabilized CW Waveguide Carbon Dioxide Laser", Journal of Physics D: Applied Physics, Vol. 11, pp. 859 - 868, 1978.

30. Johnson, A.R., Melville, R.D.S., "Stark-Effect Modulation of a CO_2 Laser by NH_2D", Applied Physics Letters, Vol. 19, pp. 503 - 506, 15 December, 1971.

31. Boyd, W.J., Brannon, P.J., Gailar, N.M., "Higher Electric Fields for Stark Induced Infrared Spectra", Applied Physics Letters, Vol. 16, No. 3, pp. 135 - 137, 1 February, 1970.

INITIAL DISTRIBUTION LIST

		No. Copies
1.	Defense Documentation Center Cameron Station Alexandria, Virginia 22314	2
2.	Library, Code 0142 Naval Postgraduate School Monterey, California 93940	2
3.	Department Chairman, Code 61 Department of Physics and Chenistry Naval Postgraduate School Monterey, California 93940	2
4.	Professor Alfred W. Cooper, Code 61 Cr Department of Physics and Chemistry Naval Postgraduate School Monterey, California 93940	3
5.	Professor E. C. Crittenden, Jr., Code 61 Ct Department of Physics and Chemistry Naval Postgraduate School Monterey, California 93940	1
6.	Lt. Larry E. Knolhoff, USN 2612 Mariner Drive San Pedro, California 90732	2

Thesis 188629
K67 Knolhoff
c.1 Stark cell stabiliza-
tion of a CO_2 laser.